PICOSECOND SPECTROSCOPIC STUDIES OF EQUILIBRIUM STRUCTURAL FLUCTUATIONS OF NATIVE AND PARTIALLY UNFOLDED STATES OF ZN^{II} -SUBSTITUTED AND METAL-FREE CYTOCHROMES C

By

Jagnyaseni Tripathy

A DISSERTATION

Submitted to
Michigan State University
in partial fulfillment of the requirements
for the degree of

DOCTOR OF PHILOSOPHY

Physics

2011

ABSTRACT

PICOSECOND SPECTROSCOPIC STUDIES OF EQUILIBRIUM STRUCTURAL FLUCTUATIONS OF NATIVE AND PARTIALLY UNFOLDED STATES OF ZN^{II}-SUBSTITUTED AND METAL-FREE CYTOCHROMES *C*

By

Jagnyaseni Tripathy

Picosecond time-resolved fluorescence spectroscopy was employed to characterize the equilibrium and non-equilibrium protein structural fluctuations in Zn^{II}-substituted (ZnCytc) and metal-free (fbCytc) cytochromes *c* using dynamic fluorescence Stokes shift (FSS) and fluorescence anisotropy (FA) measurements. The intrinsic porphyrin chromophore is used as the probe for the structural fluctuations of the surrounding protein and solvent. The FSS experiments examine how the time scales detected from the dynamic solvation of a chromoprotein report changes in the character of motion. ZnCytc and fbCytc serve as limited, single-chromophore models for photosynthetic reaction center and light-harvesting proteins. The dynamic solvation of redox and light-harvesting chromophores in photosynthesis plays an important role in the quantum efficiency of electron transfer and energy transfer performed by these systems, respectively.

The FSS response function of fbCytc in water is biexponential over the 100-ps-50-ns regime and the two time constants are 1.4 ns and 9.1 ns. ZnCytc under similar solution conditions shows a biexponential FSS response but with time constants of 0.2 ns and 1.5 ns. The two correlation times from the FSS response function correspond to motions of the hydrophobic core and the solvent-contact layer, respectively.

Both FSS correlation times were lengthened and the solvation reorganization energy was reduced from $43~\rm cm^{-1}$ to $33~\rm cm^{-1}$ in the presence of 50~% (v/v) glycerol. A Brownian diffusion model with thermally activated barrier crossings on the protein-folding energy landscape is used to interpret these results. The conclusion is that the mean-squared deviations of the fluctuations exhibited by fbCytc are perhaps a factor of ten larger than those in ZnCytc, which is consistent with the suggestion that fbCytc assumes a dynamic, partially unfolded structure with some of the characteristics of a molten globule.

The nature of the motion associated with the unfolding reaction coordinate was then studied in ZnCytc using the FA response of the Zn^{II} -porphyrin probe as guanidinium ion (Gdm⁺) is added to the solution. An unfolding transition-state-like intermediate is formed at ~ 1.0 M Gdm⁺, well below the unfolding transition concentration at ~ 2.0 M. The intermediate is characterized by an enhanced angular fluctuation of the porphyrin compared to the native and the denatured structures. The correlation time for internal angular motion returned by the FA response for the 1.0 M intermediate is similar to those observed for the FSS response of fbCytc, which suggests that the axial ligands for the Zn^{II} porphyrin have been lost.

The FSS response was then obtained as ZnCytc is titrated with Gdm⁺ using the same data sets as the FA studies. The FSS results show that even at the lowest concentrations of Gdm⁺, the native fold is destabilized so that the optical excitation of the Zn^{II} porphyrin chromophore perturbs the motions of the surrounding protein and solvent so that they depart from the linear-response regime. This conclusion is supported by the observation of an unusual bidirectional FSS response. This action of Gdm⁺ appears to saturate well prior to the formation of the 1-M intermediate structure noted in the FA studies. The main implication of these results is that structural changes in the hydration layer surrounding the folded protein are the origin of the dynamical changes reported in the FSS response in the presence of Gdm⁺.

To my parents and in laws

ACKNOWLEDGMENTS

The research presented in this dissertation could not have been performed without the help and support of many other individuals who has been there for me all these years. First and foremost, I would like to thank my advisor, Professor Warren Beck for providing me the opportunity to be a part of his research group. Without his invaluable guidance, mentorship and endless support, I would never be in a position to present this thesis. I am especially thankful to my committee members, Prof. Lisa Lapidus, Prof. Stuart Tessmer, Prof. C. W. Lai, Prof. Filomena Nunes and Prof. Lynmarie Posey for their valuable time and input.

I thank Professor Gary Blanchard and Dr. Sanela Lampa-Pastirk for their patience and instruction. They taught me almost everything I know about how to perform picosecond spectroscopy. I thank Dr. Kevin Dillman for his help. I also owe big thanks to my fellow graduate students Michael Bishop and Jenny Jo Mueller. Their curiosity and questions have led me to a better understanding of my own work. I have been fortunate to work with several talented undergraduate students, and I particularly wish to acknowledge Kenneth Barnes, Ryan Hendericks and Steven Miller. I wish to thank Navneet and all my Indian friends at Michigan State University for helping me to get through the difficult times and making my stay homely.

I also owe large thanks to my family for their endless support and love throughout my education and for encouraging me to pursue my dreams and aspirations.

Finally I convey special acknowledgement to the Department of Physics at Michigan State University for a Teaching Assistantship (2005–2009), to the National Science Foundation Biomolecular Systems Cluster/Molecular Biophysics program for stipend support under grants MCB-009120 and MCB-0520002 for their financial support. Additional support for instrumentation was provided by the Michigan Struc-

tural Biology Center at Michigan State University, which is supported by the Michigan Life Sciences Corridor.

TABLE OF CONTENTS

LIST OF TABLES				
LI	ST O	F FIGURES	X	
LIST OF ABBREVIATIONS				
1	Intr	oduction	1	
	1.1	Reaction Centers and Light-Harvesting Proteins	2	
		1.1.1 Reaction Centers	2	
		1.1.2 Light-Harvesting Proteins	5	
	1.2	Dynamic Solvation in Liquids and Proteins	7	
	1.3	Zn^{II} -substituted Cytochrome c	11	
	1.4	Aims and Summary of Results	14	
2	Fluc	ctuations in fbCytc from the Fluorescence Stokes Shift Response	17	
	2.1	Introduction	18	
	2.2	Experimental	21	
		2.2.1 Sample Preparation	21	
		2.2.2 Absorption and Fluorescence Spectroscopy	22	
		2.2.3 Picosecond Time-resolved Fluorescence Spectroscopy	22	
	2.3	Results	23	
		2.3.1 Absorption and Fluorescence Emission Spectra	23	
		2.3.2 Picosecond Time-resolved Fluorescence Spectroscopy	29	
	2.4	Discussion	37	
		2.4.1 Solvent-Response Functions in Liquids and Proteins	37	
		2.4.2 Activated Barrier-Crossing Model for Protein Fluctuations	41	
		2.4.3 Comparison of the Solvation Response in fbCytc and ZnCytc	45	
3	Pico	osecond Fluorescence Anisotropy Decays from ZnCytc in the Presence	<u>.</u>	
	of G	Gdm ⁺	50	
	3.1	Introduction	51	
	3.2	Experimental	53	
		3.2.1 Sample Preparation	53	
		3.2.2 Absorption and Fluorescence Spectroscopy	54	
		3.2.3 Time-Resolved Fluorescence Measurements	54	
	3.3	Results	56	
		3.3.1 Absorption and Fluorescence Emission Spectra	56	
		3.3.2 Picosecond Fluorescence Anisotropy Decays	67	

		3.3.3 Wobbling-in-Cone Mechanical Model	76
	3.4	Discussion	85
4	Fluc	orescence Stokes Shift Response Functions from ZnCytc in the Presence	
	of C	Gdm ⁺	89
	4.1	Introduction	90
	4.2	Experimental	92
		4.2.1 Sample Preparation	92
		4.2.2 Absorption and Fluorescence Spectroscopy	93
		4.2.3 Time-Resolved Fluorescence Measurements	93
	4.3	Results	94
		4.3.1 Absorption and Fluorescence Emission Spectra	94
		4.3.2 Picosecond Time-Resolved Fluorescence Spectroscopy	98
	4.4	Discussion	115
5	Con	nclusion	122
	5.1	Overview	122
	5.2	Comparison to Other Studies	124
	5.3	Conclusions and Next Steps	125
RI	BLIO	GRAPHY 1	128

LIST OF TABLES

2.1	Lognormal and Gaussian lineshape models for the 0–0 peak in the absorption (A) and fluorescence (F) spectra from fbCytc in water and in 50% (v/v) glycerol (see Figures 2.1 and 2.2) and estimates for the solvation reorganization energy (λ)	26
2.2	Model parameters for the time evolution of the time-resolved fluorescence spectrum observed in water and 50% glycerol in metal-free (fb-Cytc) and Zn ^{II} -substituted (ZnCytc) cytochrome c at 22 °C	36
3.1	Absorption (Q) and fluorescence (F) lognormal lineshape parameters for the unfolding transition of ZnCytc in the presence of Gdm^+	64
3.2	Thermodynamic parameters for the equilibrium unfolding transition for ZnCytc and the transition midpoints	65
3.3	Fluorescence anisotropy decay parameters for ZnCytc in the presence of Gdm ⁺ at 22°C	72
3.4	Wobbling-in-cone model parameters and the apparent hydrodynamic radius, R_h , for ZnCytc in the presence of Gdm ⁺ at 22°C	80
4.1	Lognormal lineshape parameters for the 0-1 vibronic feature of the time-resolved fluorescence spectra from ZnCytc in water at 22°C	101
4.2	Lognormal lineshape parameters for the 0–1 vibronic feature of the time-resolved fluorescence spectra from ZnCytc in 2.0 M Gdm ⁺ at 22°C.	105
4.3	Model parameters for the time evolution of the Fluorescence Stokes shift for ZnCytc in the presence of Gdm ⁺ at 22°C	108

LIST OF FIGURES

1.1		4
1.2	Energy levels and generalized solvent coordinate to describe solvation	
	in molecular liquids	8
1.3	Structure of ferricytochrome c from horse heart (1hrc.pdb)	12
2.1	Continuous-wave absorption and fluorescence emission spectra from	
	metal-free cytochrome c (fbCytc) in water	24
2.2	Continuous-wave absorption and fluorescence emission spectra from	
	fbCytc in 50% (v/v) glycerol	25
2.3	Time-resolved fluorescence dipole strength spectra from fbcytc in water.	31
2.4	Time evolution of the mean frequency of the 0-1 fluorescence transi-	
	tion, $\langle v_{0-1} \rangle$, from fbCytc in water	32
2.5	Time-resolved fluorescence dipole strength spectra from fbcytc in	
	50% (v/v) glycerol	34
2.6	Time evolution of the mean frequency of the 0-1 fluorescence transi-	
	tion, $\langle v_{0-1} \rangle$, from fbCytc in 50% (v/v) glycerol	35
2.7	Model for equilibrium structural fluctuations in a protein involving	
	barrier-crossing events	43
3.1	Q-band region of the absorption and fluorescence spectra from ZnCytc	
	in water	57
3.2	Fluorescence spectra from ZnCytc in water and over a range of Gdm ⁺	
	concentrations	60
3.3	Gdm ⁺ fluorescence titration curves for ZnCytc	61
3.4	Gdm ⁺ absorption titration curves for ZnCytc	62
3.5	Simulation of the fluorescence spectral changes that accompany Gdm ⁺	
	unfolding of ZnCytc	63
3.6	Gdm ⁺ concentration dependence of the ratio of the fluorescence inten-	
	sity of the 0-1 and 0-0 vibronic peaks in ZnCytc	66
3.7	Polarized fluorescence emission transients from ZnCytc in water	68
3.8	Single-wavelength and integrated dichroism-free fluorescence intensity	
	transients from ZnCytc in water	70
3.9	Integrated fluorescence anisotropy transients for the 0-1 band from Zn-	
	Cytc	71
	Anisotropy decay amplitudes of ZnCytc at 22°C and pH 7.0	73
3.11	I Anisotropy decay correlation time constants of ZnCytc at 22° C and pH 7.0.	74

3.12	Gdm^+ concentration dependence of r_0 , the total anisotropy amplitude	
	of ZnCytc.	75
3.13	Wobbling-in-cone model for fluorescence depolarization arising from	
	protein dynamics.	77
3.14	Anisotropy decay correlation times of ZnCytc from the wobbling-in-cone	
	mechanical model	81
3.15	Gdm^+ concentration dependence in ZnCytc for S , the anisotropic order	
	parameter, and θ_c , the cone angle	82
3.16	Gdm ⁺ concentration dependence in ZnCytc for the effective hydrody-	
	namic radius, $R_{\rm h}$	84
4.1	<i>Q</i> -band region of the absorption and fluorescence spectra from ZnCytc	
	in water	96
4.2	Gdm ⁺ fluorescence titration curves for ZnCytc	97
4.3	Time-resolved fluorescence dipole strength spectra from ZnCytc in water.	100
4.4	Time evolution of the mean frequency of the 0–1 fluorescence emission,	
	$\langle v_{01} \rangle$, from ZnCytc in water	103
4.5	Time-resolved fluorescence dipole strength spectra from ZnCytc in	
	2.0 M Gdm ⁺	104
4.6	Time evolution of the mean frequency of the 0–1 fluorescence emission,	
	$\langle v_{01} \rangle$, from ZnCytc over a range of Gdm ⁺ concentrations	107
4.7	Fluorescence Stokes shift time constants for ZnCytc as a function of the	
	Gdm ⁺ concentration	109
4.8	Fluorescence Stokes shift amplitudes for ZnCytc as a function of the	
	Gdm ⁺ concentration	110
4.9	Viscosity of aqueous solutions of guanidinium hydrochloride at room	
	temperature	113
4.10	Gdm ⁺ concentration dependence in ZnCytc of the total fluorescence	
		114
4.11	Gdm $^+$ concentration dependence of $ au_{ ext{int}}$, the correlation time for in-	
	ternal motion, and θ_c , the wobbling cone angle, from the picosecond	
	anisotropy decays from ZnCytc.	118

LIST OF ABBREVIATIONS

BChl, bacteriochlorophyll

BPheL, bacteriopheophytin electron acceptor

FA, fluorescence anisotropy

FSS, fluorescence Stokes shift

fbCytc, metal-free (or free-base) cytochrome *c*

FeCytc, Fe^{III} cytochrome c

fwhm, full width at half maximum

K, lysene

Mb, myoglobin

P, primary electron donor in the photosynthetic reaction center

Qa, primary quinone electron acceptor

Q_b, secondary quinone electron acceptor

TCSPC, time-correlated single photon counting ZnCytc, $\mathrm{Zn^{II}}$ -substituted cytochrome c

 ${\tt ZnTMPyP,\,Zn^{II}}\ \textit{meso-} {\tt tetrakis(N-methylpyridyl)porphyrin}$

ZnTPP, Zn^{II} tetraphenylporphyrin

CHAPTER 1

Introduction

Summary

This dissertation presents a time-resolved picosecond spectroscopic study of the dynamic fluorescence Stokes shift (FSS) and fluorescence anisotropy (FA) response functions of Zn^{II} -substituted cytochrome c (ZnCytc). ZnCytc was a chosen as a limited model for a single-chlorophyll-containing protein system with some of the features of a photosynthetic light-harvesting or reaction-center protein. The goal of this work was to determine how the equilibrium structural fluctuations of the protein and solvent are sensed by the intrinsic Zn^{II} porphyrin in ZnCytc. The significance of this question relates to the longstanding issue of how the protein structure controls the directionality and quantum efficiency of electron-transfer reactions in reaction centers and the directionality and yield of energy transport in light-harvesting proteins. The results establish for the first time a connection between the correlation time scales in the FSS and FA response functions to those for diffusive motion on the protein-folding energy landscape.

1.1 Reaction Centers and Light-Harvesting Proteins

Photosynthesis is one of most important yet complex processes found in plants, certain bacteria and algae in which light is converted into chemical energy. Photons are initially absorbed by light-harvesting or antenna proteins. The absorbed energy is rapidly (<100 ps) and efficiently transferred to a photosynthetic reaction center, where the photon's energy is trapped and drives transmembrane electron-transfer reactions. The result is storage of energy as a transmembrane electrochemical gradient. This stored energy is used by other membrane proteins to drive the synthesis of ATP and to make reducing agents that are used in the chemical reactions of the organism. The processes of absorption, transfer and trapping of excitation energy as well as electron transfer in photosynthesis are highly directional and quantum efficient. The high efficiency likely arises from the microscopic details of the chromophore-chromophore interactions that are organized within the well-defined chromophore-protein structures of the light-harvesting units and reaction centers. I

1.1.1 Reaction Centers

Figure 1.1 shows the X-ray crystal structure for the reaction center from a purple photosynthetic bacterium called $Rhodopseudomonas\ viridis$ in two different representations.² The original crystal structure was described by Deisenhofer $et\ al.^{3,4}$ and consists of four subunits as shown in Figure 1.1. The ribbon structure of the chromophore-protein complex shows the cytochrome c subunit attached to the periplasmic side of the lipid-bilayer membrane in green with the heme centers embeded in it. The two symmetrical subunits of the reaction center, L and M, are shown labelled by their components in the stick representation; these are shown as the magenta and purple units in the ribbon structure. Each of these two units L and M contain a bacteriochlorophyll (BChl) molecule and together make up the primary

electron donor (P), an additional bacteriochlorophyll molecule, a bacteriopheophytin (BPh) molecule, and a quinone (Q_A or Q_B). Note that the structure of the bacterial reaction center is structurally comparable to the photosystem reaction center although little structural homology is observed.⁵

The primary electron donor P is often called the "special pair" because it consists of a pair of strongly coupled BChl molecules. Absorption of a photon by P, either directly or via long-distance energy transfer from a light-harvesting protein, initiates the electron-transfer process across the membrane. The initial charge separation occurs in \sim 3 ps resulting in a ground-state radical cation-anion pair, P⁺ and BPh⁻. An electron is subsequently transferred to a quinone molecule Q_A in \sim 200 ps and later to a second quinone Q_B in \sim 100 μ s. This charge separation process is repeated but prior to the second charge separation event, P⁺ must be reduced by a nearby cytochrome c_2 , as shown in Figure 1.1.

The electron-transfer processes in a photosynthetic reaction center are highly directional. Though the molecular-orbital overlap between the participating chromophores is the major factor that determines the rate of electron transfer, small changes in the surrounding structure can also impact the electron transfer rates; slight differences in binding of the cofactors to the protein and in the surrounding protein environment has been shown to enhance the rate of electron transfer.⁷ It has long been proposed that the forward electron-transfer reaction is favored over the back reaction due to the reorganizational, protein conformational changes that occur during the formation of the charge-separated intermediates.⁸

The structural origin of the quantum efficiency of natural photosynthetic electron-transfer processes in reaction-center protein complexes has been heavily discussed. $^{3,4,9-14}$ Over the last twenty years, covalently linked donor-acceptor supramolecular assemblies $^{15-18}$ have been synthesized with the intention of emulating some of the photochemical properties of natural photosynthetic reaction cen-

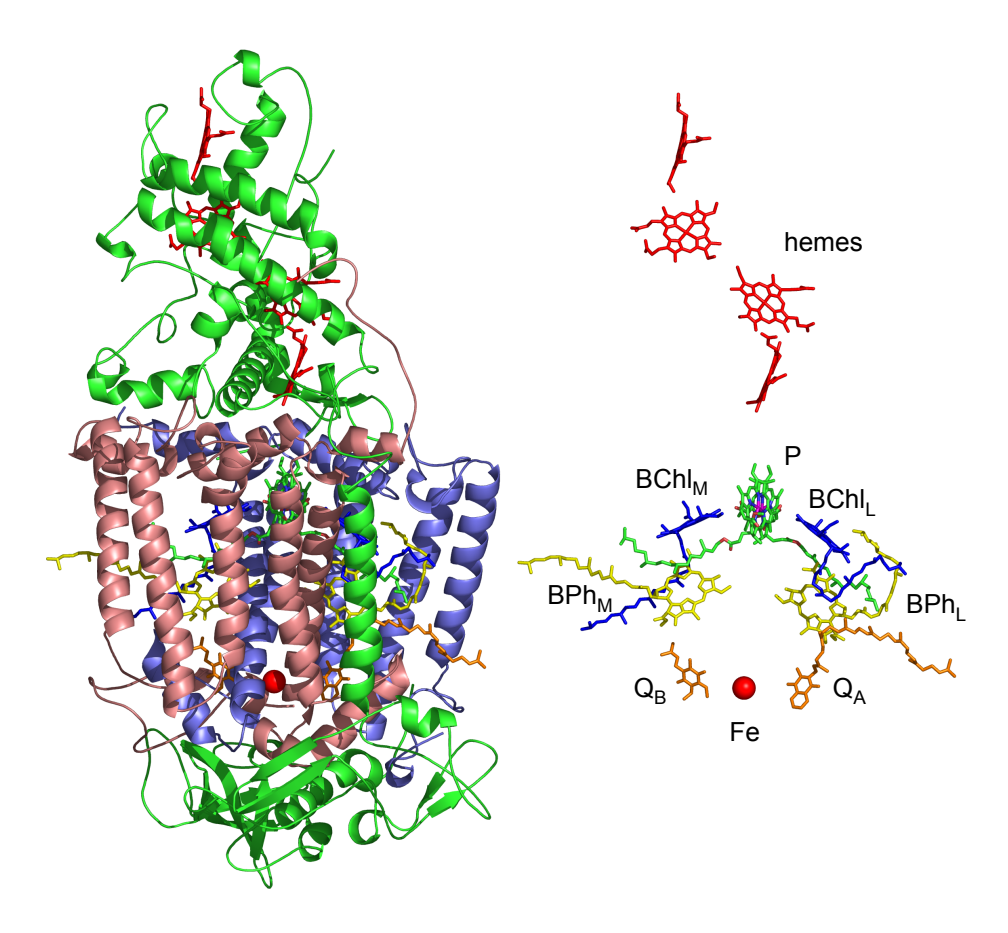


Figure 1.1. Structure of the *Rhodopseudomonas viridis* reaction center (1PRC.pdb), as shown in a ribbon representation on the left and a stick representation for the chromophores on the right. The ribbon diagram shows: the L and M subunits in magenta and purple, respectively, the cytochrome c subunit in green shown at the top over the L and M subunits, and the H subunit is shown in green at the bottom of the complex. The stick diagram shows the chromophores in the L, M and the cytochrome c subunits: the primary electron donor, P, the monomeric bacteriochlorophylls (BChl), the bacteriopheophytins (BPh), and the quinones c0 and c0. A non-heme Fe ion is shown between the L and M subunits as a red sphere. For interpretation of the references to color in this and all other figures, the reader is referred to the electronic version of this dissertation.

ters. Long-lived charge-separations with relatively high quantum yields have been achieved, 19-21 and some impressive progress has been made in connecting light-harvesting arrays 22-24 to charge-separation units to make artificial reaction centers that reproduce the essential features of bacterial photosynthesis. 25, 26 The artificial systems, however, do not yet match the quantum efficiency of the natural photosynthetic reaction center even though the same or similar redox-active chromophores have been employed in a wide range of constructs.

The unusually long lifetimes for the charge-separated states in the reaction center are likely to arise from two aspects of the dynamics of the protein medium that surrounds the redox-active chromophores:

- Protein-derived vibrational motions in the 100-cm⁻¹ regime²⁷ are coupled to the forward primary and secondary electron-transfer reactions in the purple-bacterial reaction center so that they occur in a nearly activationless manner.²⁸
- Formation of the charge-separated intermediates is followed by a solvation-like reorganization of the reaction-center protein that dissipates the energy of the transition state by displacing modes that are not directly along the reaction coordinate.²⁹

Thus, it will be important in future work to determine the timescales and structures associated with the solvation of the excited-state and charged chromophores involved in the energy-transfer and electron-transfer reactions in order to understand better how solvation plays a role in these processes.

1.1.2 Light-Harvesting Proteins

Light-harvesting proteins are the chromophore–protein systems that act as the medium through which light energy is transferred to a photosynthetic reaction center.^{30,31} The overall antenna for an organism contains several light-harvesting pro-

teins in a multisubunit complex that is arranged structurally in the membrane so that the excitation energy is funneled towards a centrally located reaction center. $^{31-34}$ Light-harvesting proteins are in general relatively small molecular weight (6–30 kDa) polypeptides. The chromophores are highly ordered and typically arranged in clusters. As an example, the X-ray crystal structure of the light-harvesting system LH2 in purple bacteria consists of a cylinder of nine paired transmembrane α -helical protein subunits that carries nine pairs of overlapping BChl α (B850) molecules; the overall complex exhibits a nine-fold symmetry. The LH1 complex that surrounds the purple-bacterial reaction center has a ring-like structure similar to that of LH2 but contains sixteen subunits and carries 32 BChl α molecules.

Energy-transfer processes in light-harvesting complexes have been extensively studied using picosecond and femtosecond spectroscopy. 1,36,37 It takes less than 100 ps overall for the excitation energy absorbed by a light-harvesting protein subunit to be transferred and trapped by a reaction center, 1 but the energy transfer time scale between a given pair of chromophores is typically 200 fs or less. For example, the Fleming 38,39 and Wasielewski 40 groups have observed energy-transfer processes between chlorophyll molecules on the 200 fs time scale in the light-harvesting complexes of photosystem I (LHCI) and photosystem II (LHCII). Bradforth *et al.* 41 found a biphasic fluorescence anisotropy response in the purple bacterial light-harvesting system LHI with time constants of 110 and 400 fs; the components are attributed to the energy transfer between BChl *a* molecules. Jimenez *et al.* 42 found a biexponential fluorescence depolarization response from B850 in the purple bacterial LH2 complex, with the time constants of 50–90 and 400–500 fs.

The energy-transfer steps in light-harvesting complexes are radiationless processes mediated by dipolar interactions between adjacent chromophores. For weakly coupled chromophores, the excitation-energy is transferred through an inductive resonance mechanism that involves an incoherent hopping (Förster) mechanism. When

the electronic interactions between the excited singlet states of the chromophore are very strong, however, the energy-transfer process is said to be coherent and involves excited-state wavefunctions that are delocalized over more than just one chromophore. Fluctuations of the surrounding protein structure results in randomization of the ordering of the energy level in a given dimer or larger chromophore cluster, and localization of the initially coherent excited state onto a single chromophore is the result. Beck and coworkers have suggested that localization can play an important role in directing energy towards the reaction center. 45,46

1.2 Dynamic Solvation in Liquids and Proteins

Proteins undergo a wide range of motions on very short time scales.^{47,48} The protein dynamics that underly the functional motions that control energy-transfer pathways and electron-transfer rates in photosynthesis are probably the short-ranged fluctuations that accompany propagation on the protein-folding energy landscape near the native minimum.^{47–50} The individual energy-transfer steps in light-harvesting proteins are known to occur on the 20 fs–10 ps time scale or longer.¹ The time scale for solvation-like reorganizational dynamics and vibrational equilibration in these proteins are comparable to the energy-transfer time scales.

One approach at determining the relevant time scales in a chromoprotein is the method of dynamic solvation, which has been very widely used to study dynamics in liquids. The a chromophore in solution is optically excited, the excited state of the molecule has a significantly different charge distribution compared to the ground state. This causes the excited state molecule typically to have a larger permanent dipole moment. The reorientational response of the surrounding solvent to the change in charge distribution or dipole moment of the chromophore between the ground and excited states is called dynamic solvation. Figure 1.2 shows how the sol-

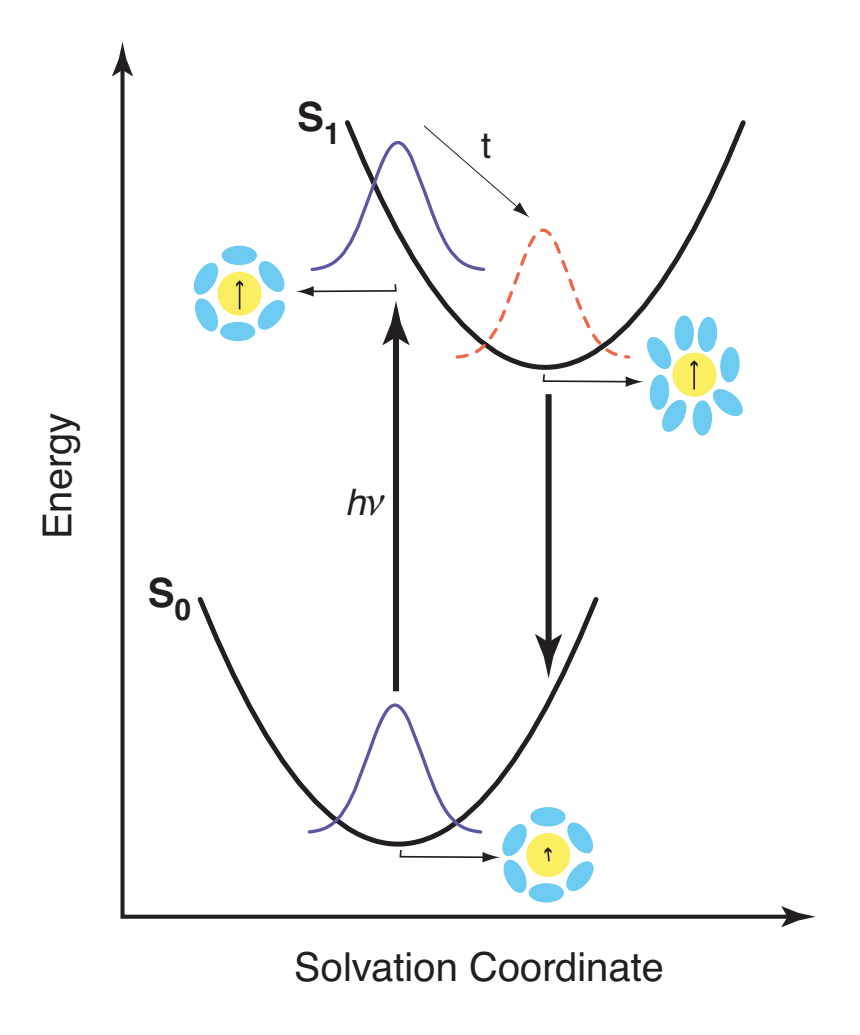


Figure 1.2. Energy levels and generalized solvent coordinate to describe solvation in molecular liquids. The potential energies of the ground and first-excited singlet states of a probe molecule (yellow circles), S_0 and S_1 , respectively, are shown with respect to a generalized solvation coordinate. After formation of the excited state, the surrounding solvent molecules (blue ovals) reorient so as to return to equilibrium with respect to the excited state's generally larger dipole moment (arrows). The resulting stabilization of the probe/solvent system makes the excited-to-ground-state energy gap decrease. The solvation process can be detected in terms of the shift of the time-resolved emission spectrum to lower energy as the solvation reorganization process proceeds. Adapted from reference 51.

vent's reorganizational response results in a dynamic Stokes shift, a time-dependent shift of the molecule's emission spectrum to the red. The solvent response is often described by a normalized response function, ⁵¹

$$S_{\mathcal{V}}(t) = \frac{v(t) - v(\infty)}{v(0) - v(\infty)} \tag{1.1}$$

where v(t) is the mean frequency of emission at time t. In this dissertation, experimentally measured $S_{v}(t)$ responses are called fluorescence Stokes shift (FSS) response functions.

The molecular character involved in the FSS response function is usually discussed in terms of the fluctuations of the local electric field that arise from the random motions of the solvent dipoles or charges around the probe chromophore. In the time domain, the probe's ground-to-excited state transition frequency $\omega = 2\pi v$ exhibits fluctuations due to the motions of the surrounding solvent. These fluctuations are characterized by a energy-gap time-correlation function,

$$M(t) = \frac{\langle \Delta \omega(0) \Delta \omega(t) \rangle}{\langle (\Delta \omega)^2 \rangle}$$
 (1.2)

which describes the associated loss of memory over time of the instantaneous transition frequency $\omega(0)$ that was present initially at some reference time t=0. At high temperatures and in the linear-response regime, where the fluctuation-dissipation relation holds, M(t) is equal to the solvent-response function $S_{\mathcal{V}}(t).^{54-56}$ The requirement for the linear-response regime is generally met in most probe/solvent systems because the optical excitation of the probe results only in a small change in the probe's dipole moment and accordingly presents a small perturbation to the motions and structure of the solvent. 57,58

The instantaneous normal-mode theory of liquids 51,59,60 provides some suggestions about the time scale and character of the solvation response in liquids. Three regions of solvation response have been identified in molecular dynamics simulations of liquids: an inertial or ballistic, free-rotor motion regime in the short-time

limit (\sim 100 fs or so), an intermediate-time regime in which oscillatory motions are observed, and then a long-time (>500 fs) regime in which the oscillatory motions are damped out and diffusive, random motions predominate. The ordering of these time scales effectively describes the onset of intermolecular forces; in the inertial regime, the molecules move independently, whereas the intermediate and long-time scales are associated with coherent and incoherent motions, respectively, under the action of the intermolecular forces. From the molecular dynamics trajectories, the instantaneous normal-mode theory projects the motions associated with these solvation time regimes into a spectrum of intermolecular frequencies that primarily involves hindered translational and hindered rotational (librational) motions. Fleming and coworkers 61 , 62 confirmed experimentally that the solvent response function of small molecular solvents is bimodal in character, with perhaps 50% of the solvation response of water 61 and acetonitrile 63 on the <100 fs time scale identified as an inertial response with a Gaussian shape, whereas the subsequent diffusive, exponential solvent response occurs on a slower (<1 ps) time scale.

The dynamics of folded proteins are arguably more like those of liquids than of crystalline solids, where long-range order is permanently organized, especially because internal diffusion of small molecules occurs in proteins.⁶⁴ The structural fluctuations occur over a wide range of time scales in proteins and are especially temperature dependent. In some landmark investigations, Frauenfelder *et al.* used the reaction rate of the photochemical dissociation of carbon monoxide from myoglobin to probe the underlying conformational timescales.^{47,48} The results suggested that proteins share a number of the structural and dynamical properties in common with glasses. It was found that protein conformational changes do not exhibit exponential time dependences or Arrhenius-type temperature dependences. These observations suggested that the protein motions involve sampling a rough energy landscape with a hierarchy of barrier heights.

1.3 Zn^{II} -substituted Cytochrome c

Applying the dynamic solvation approach directly to a characterization of protein fluctuations in photosynthetic reaction centers and light-harvesting proteins is not presently feasible owing to the presence typically of a large number of chromophores with overlapping spectra. In order to learn about the relevant time scales for protein motion in photosynthesis, then, we will need to use a model system that mimics aspects of how the chromophores are contained in a photosynthetic protein but has just a single chromophore.

McLendon and coworkers⁶⁵ and Pierce and Boxer⁶⁶ have investigated the solvation of *extrinsic* chromophore as probes for the dynamics in heme proteins. The time scale for the FSS response function obtained with various probes in these experiments was in the range of picoseconds to nanoseconds. The solvation time scales were strongly dependent on the probe used and also depended on the character of the bulk solvent. The use of extrinsic probe in these experiments added complexity to the experiments because their interaction with the heme binding site was not well understood. An ideal system for the measurement of solvation dynamics in a protein would employ an *intrinsic* probe chromophore tightly held in the binding pocket with a well defined structure.

In the late 1990's, the research group of Warren Beck began some studies at Vanderbilt University on bacteriochlorophyll-containing systems using the approach suggested by Boxer and coworkers, who synthetically modified bacteriochlorophyll a so that it could be installed into the heme-binding pocket in hemoglobin. Subsequently, after moving to Michigan State University, the Beck group chose to study ${\rm Zn^{II}}$ -substituted cytochrome c (ZnCytc) as the main target system for their protein solvation studies. By replacing the native Fe^{II} ion with ${\rm Zn^{II}}$ or by removing it entirely, an intrinsic fluorophore with good photophysical properties comparable to those of chlorophyll a is obtained.

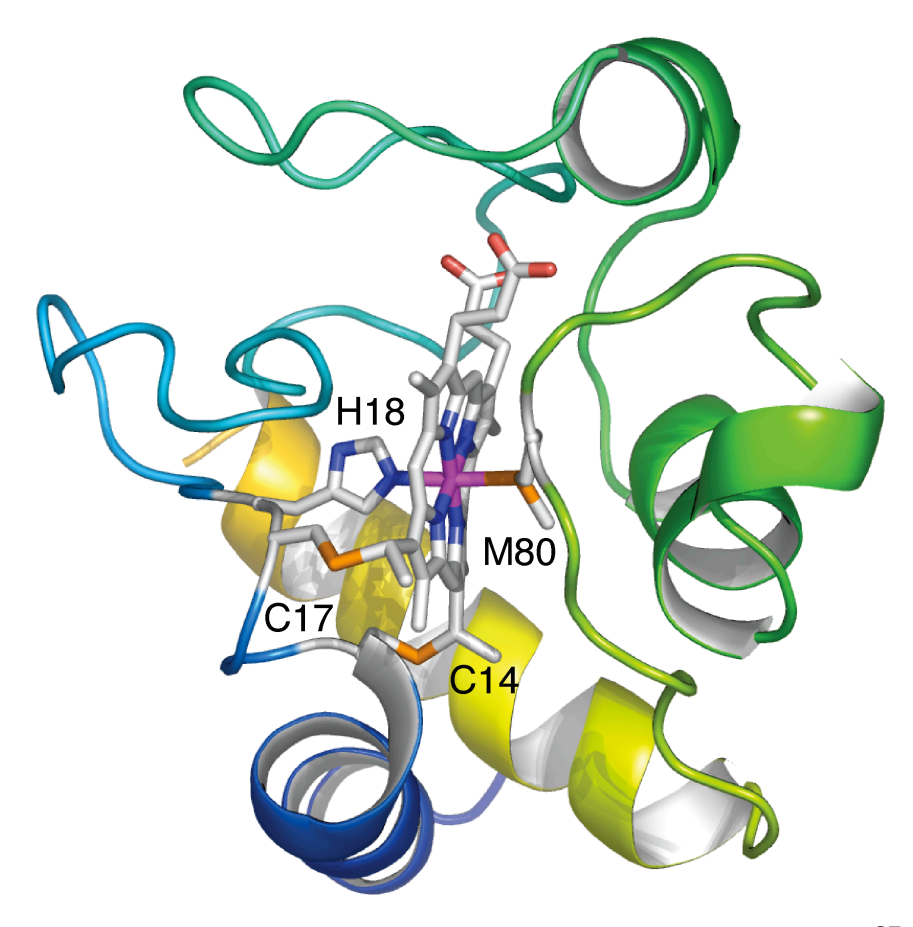


Figure 1.3. Structure of ferricytochrome c from horse heart (1hrc.pdb).⁶⁷ The porphyrin, its thioether linkages from cysteine ligands C14 and C17, and the axial ligands to the metal ion, from the histidine and methionine residues H18 and M80, respectively, are rendered as stick structures.

Figure 1.3 shows the X-ray crystal structure of horse-heart ferricytochrome c (FeCytc). 2D NMR studies have shown that the solution structure of ZnCytc is very similar to that of FeCytc, 72 , 73 and the structure of the ZnII-containing sites was not distinguishable from the FeIII-containing sites in Zn/Fe cocrystals of cytochrome c. The porphyrin in cytochrome c is attached to the protein by the two cysteine residues, C14 and C17, via thioether linkages, and the metal ion is axially ligated by the histidine and methionine residues, H18 and M80. Except for a small exposure of the edge of the porphyrin to the external medium via a cleft on the protein surface that constrains the porphyrin orthogonal to its plane, the porphyrin is largely confined to the hydrophobic core of the protein. This structural organization of the porphyrin in ZnCytc makes it well suited for the solvation dynamic studies. The porphyrin is positioned well to serve as an *intrinsic* probe that senses the internal motions of the protein, but owing to the slight exposure of the edges it is also capable of sensing the motion in the solvent-contact layer of the protein.

The initial studies of dynamic solvation in ZnCytc were conducted in the Beck laboratory by Sanela Lampa-Pastirk.⁷⁵ She characterized the time-resolved fluorescence spectrum from ZnCytc over the 100-ps-25-ns timescale using the time-correlated, single-photon counting approach.⁷⁶⁻⁷⁸ The findings from this work are extensively reviewed and discussed in the following chapters, but the main points are as follows. Lampa-Pastirk found that the FSS response function from ZnCytc had two exponential components with time constants of 200 ps and 1.5 ns in water. That the slower of these two components was sensitive to the presence of added glycerol in the surrounding solvent suggested an assignment to characteristic motions of the solvent-contact layer of the protein. The faster of the two components was accordingly assigned to the hydrophobic core of the protein.⁷⁶ When the excitation laser was tuned to the Soret absorption band in the blue (420-nm) part of the spectrum, however, an unprecedented bidirectional FSS response function was observed that

was terminated with a sustained blue shift that lasted throughout the fluorescence timescale, out to >20 ns. This result was interpreted as showing that the protein had absorbed the blue photon's excess vibrational energy above the S₁ state's energy and had been vibrationally excited over the activation barriers that separate the native state from a partially unfolded state along the protein unfolding/refolding reaction coordinate.^{78,79}

1.4 Aims and Summary of Results

The work by Lampa-Pastirk provides the primary motivation for the experiments discussed in this dissertation. Although the glycerol dependence in the FSS response of ZnCytc provides the very first structural information in any protein solvation study, it does not account for the different timescales in a manner that affords any structural insight about the types of motions that are detected. Further, that the FSS response would depend so sensitively on the amount of excess vibrational energy used to prepare the S_1 state is unprecedented by any study in a molecular liquid, so its bidirectional character is uniquely that from a protein. The following chapters describe an effort to obtain chiefly a better structural picture for the motions that contribute to the FSS response in ZnCytc. The following aims were addressed:

- Obtain the relationship between the time scales and the amplitudes of the equilibrium structural fluctuations that contribute to the FSS response in ZnCytc.
- Determine how motions associated with the unfolding reaction coordinate contribute to the FSS response in ZnCytc.
- Compare the timescales returned by the FSS response with the timescales detected in the fluorescence anisotropy (FA) response, which is a direct measure of internal motion in ZnCytc.

Here is an overview of the experimental work described in the following chapters of this dissertation:

In Chapter 2, we discuss the dynamic solvation response in fbCytc cytochrome c using FSS measurements. This system was chosen as an analogue of a partially unfolded form of ZnCytc or FeCytc. The time scales of the FSS response function for fbCytc were determined to be 1.4 ns and 9.1 ns compared to the time scales obtained for ZnCytc under similar solution conditions which are 250 ps and 1.45 ns, respectively. A comparison of the results from the Zn^{II}-substituted and metal-free forms of cytochrome c suggests that the mean-squared deviations of the structural fluctuations exhibited by fbCytc are ~ 10 times larger than that of ZnCytc. This is consistent with the idea that loss of metal ion in fbCytc allows the native state to adopt a partially unfolded conformation with some of the characteristics of a molten globule.⁷⁹ Unlike ZnCytc where only the slower of the two time components of FSS response function shows a solvent viscosity dependence⁷⁷ both components in fbCytc show a lengthening on changing the solvent from water to a 50% (v/v) glycerol mixture. The results establish a connection between the time scales and amplitudes of fluctuations for motions along the energy surface. The results lead to a structural interpretation of the motion using a model for Brownian diffusion with thermally activated barrier crossings on the folding energy landscape.

In Chapter 3, the structural fluctuations that occur when ZnCytc is driven through an unfolding transition in the presence of guanidinium ion concentration (Gdm⁺), a chemical denaturant, is probed using the FA response. The mechanism of Gdm⁺'s action involves an interaction with the hydration layer of water that surrounds and stabilizes the native fold of the protein.⁸⁰ The goal of this study was to establish a relation between the protein dynamics detected by the FSS response and the thermodynamic stability of the protein. The fluorescence anisotropy gives a direct measure of the motions of the protein that immediate surround the Zn^{II} porphyrin. The

results indicate that the unfolding transition is accompanied by the formation of intermediates at low denaturant concentrations that are characterized by porphyrin motions of intermediate amplitude and angular range relative to those in the native and unfolded states.

Chapter 4 discusses how the fluorescence Stokes shift (FSS) reports the changes in protein dynamics that occur during the unfolding titration of ZnCytc with Gdm⁺. The results are compared to those obtained using the FA response. The results show that the presence of Gdm⁺ destabilizes the native fold enough even at very low concentrations that the optical transition of the Zn^{II}-porphyrin chromophore departs from the linear-response regime; the FSS response changes from the monotonic response expected from a pure solvation response to a biphasic, blue/red response that reports the transient production of a structure that is displaced significantly from the equlibrium structure present prior to the optical excitation. These observations strongly implicate structural changes in the hydration layer as the origin of the dynamical changes reported in the FSS response as the protein approaches the unfolded state.

The work described in this dissertation provides arguably the first direct studies of the relationship between the timescales of fluctuations and the amplitudes of motions over the timescales that are relevant to understanding energy-transfer processes in photosynthetic light-harvesting proteins. The results obtained suggest strongly that the dynamics in the hydration layer play a dominant role in controlling the stability of a folded protein, so studies have already been initiated in the Beck laboratory to employ fluorescent probes covalently mounted on the surface of ZnCytc to measure directly how the hydration layer is affected as denaturants are added. The next logical step is to perform analogous experiments on folded proteins in situ in a membrane to understand how the membrane controls the dynamics in a photosynthetic protein.

CHAPTER 2

Fluctuations in fbCytc from the Fluorescence Stokes Shift Response

Summary

We used picosecond time-resolved fluorescence spectroscopy to characterize the fluorescence Stokes shift (FSS) response function of metal-free (or free-base, fbCytc) cytochrome c under the solution conditions that favor the native states of ferricytochrome c (FeCytc) and Zn^{II} -substituted cytochrome c (ZnCytc). The intrinsic porphyrin chromophore serves in these experiments as a fluorescent probe of the structural fluctuations of the surrounding protein and solvent. Demetalation of the porphyrin destabilizes the folded structure of cytochrome c owing to the loss of the axial metal-histidine and metal-methionine bonds. Thus, these experiments examine how the timescales detected in a dynamic solvation experiment in a chromoprotein report changes in the character of the motion. The FSS response function in fbCytc in water and pH 7 is well described by a biexponential response over the 100-ps-50-ns regime with time constants of 1.4 ns and 9.1 ns; under similar conditions, ZnCytc exhibits a biexponential FSS response with time constants of 250 ps and 1.5 ns. 77 These

time constants correspond, respectively, to the correlation timescales for motions of the hydrophobic core and the solvent-contact layer of the protein. Both of the time constants observed in fbCytc are further lengthened upon addition of glycerol to the external solvent so that a significant fraction of the protein dynamics is rendered effectively static on the fluorescence timescale. The solvation reorganization energy, the time-integrated Stokes shift of the fluorescence spectrum, is reduced by about a third to 33 cm⁻¹ in 50% glycerol from 43 cm⁻¹ in water. These results are interpreted structurally using a model for Brownian diffusive motion with thermally activated barrier crossings on the protein-folding energy landscape. The results suggest that the mean-squared deviations of the structural fluctuations exhibited by fbCytc are nearly a factor of ten larger than those of ZnCytc. This conclusion is consistent with the suggestion that fbCytc assumes a dynamic, partially unfolded structure with the characteristics of a molten globule.

2.1 Introduction

The energy landscape paradigm accounts for the molecular dynamics of folded proteins in terms of a hierarchy of conformational states sorted by tiers of intervening activation-energy barriers of increasing magnitude. 47,81,82 On the single-molecule level, a protein makes a diffusive search of the potential energy surface near the native structure by hopping from minimum to minimum over the barriers that are thermally accessible. 83,84 These motions correspond to what Frauenfelder calls *equilibrium fluctuations*. 47 Similar dynamics are expected to accompany the folding of a protein as it descends the funnel-shaped Gibbs free-energy gradient and approaches the native structure, 85 but the details of the motions that a protein makes as it searches for the native structure or when the structure is displaced from that at

equilibrium by a perturbation deserve additional experimental and theoretical attention.

In recent work from this laboratory, we showed how Zn^{II}-substituted cytochrome c (ZnCytc) can be driven from the native fold to a series of partially unfolded structures by the intramolecular vibrational excitation generated by the radiationless decay of the intrinsic Zn^{II}-porphyrin chromophore. ^{78,79} When the 0-0 vibronic transition in the Q absorption band is pumped, so that the S_1 electronic state is prepared with very little excess vibrational energy, the time-resolved fluorescence spectrum exhibits a conventional, unidirectional dynamic fluorescence Stokes shift (FSS) response 51,54 to the red with two characteristic timescales, 250 ps and 1.45 ns. This response is assigned in analogy to that in polar liquids to a polar solvation response of the surrounding protein to the ground-to-excited-state change in the Zn^{II}-porphyrin's dipole moment. The two timescales were assigned to motions of the hydrophobic core and solvent-contact layers of the protein, respectively, because addition of glycerol to the external solvent medium slowed only the latter component. When the excitation wavelength was set at 420 nm in the Soret band, so that that the S₁ state is prepared with ~ 7000 -cm⁻¹ excess vibrational energy, the Zn^{II}-porphyrin in ZnCytc exhibits an unusual bidirectional FSS response that directly reports a change in the surrounding protein structure. The time-resolved fluorescence spectrum shifts initially to the red with a 125-ps time constant; after the 180-ps delay point, however, the spectrum begins a slower, biexponential shift to the blue that persists to the end of the fluorescence timescale (>12 ns). The blue-shifted fluorescence spectrum is assigned to a partially unfolded state of the protein that transiently resembles that of the molten-globule state observed under acid conditions; 86,87 the heat-denatured state of ZnCytc also exhibits a blue-shifted fluorescence spectrum.⁸⁸

Subsequent work⁷⁹ showed that the continuous-wave fluorescence spectrum from ZnCytc reports the activation-enthalpy thresholds to at least three partially

unfolded states in terms of step-like transitions of the solvation reorganization energy, 89 the time-integrated Stokes shift of the fluorescence spectrum. The corresponding barriers in metal-free (or free-base, fbCytc) cytochrome c occur at relatively low enthalpies, perhaps one-third of those in ZnCytc. This finding shows that the axial metal-histidine (H18) and metal-methionine (M80) bonds in cytochrome c play an important structural role (see Figure 1.3). Under the solution conditions that favor the native state of ferricytochrome c (FeCytc) or ZnCytc, it is likely that fbCytc exists as a partially unfolded, molten-globule-like structure that retains a well-defined hydrophobic core like that of ZnCytc. 79

In this chapter, we discuss the FSS response obtained from fbCytc with the excitation laser tuned close to the 0-0 vibronic transition. This work allows a direct comparison to the previously reported FSS response observed in the native state of ZnCytc.⁷⁷ These experiments provide a unique opportunity to determine how the timescales detected in a dynamic solvation experiment in a chromoprotein report changes arising from a structural perturbation. The results show that the two exponential time constants observed in the FSS from fbCytc are lengthened by almost a factor of ten from those of ZnCytc and that both components are sensitive to the presence of glycerol in the external solvent medium. By applying a model for the structural fluctuations that arise from Brownian diffusion on the protein-folding energy landscape,⁹⁰ we infer that the increased polar solvation timescales observed in fbCytc correspond to significantly enhanced fluctuation amplitudes compared to those in ZnCytc under similar solvent conditions.

2.2 Experimental

2.2.1 Sample Preparation

The procedure established by Vanderkooi and coworkers^{69,91} was used to prepare fbCytc using horse-heart ferricytochrome c (FeCytc, Sigma) as the starting material. The free-base porphyrin is obtained *in situ* using liquid anhydrous hydrogen fluoride (HF) as the demetalating agent. The reaction of FeCytc with HF was run on a homebuilt gas-handling system that employs tubing, valves, and reaction vessels all made of Teflon. The extent of the demetalation reaction was monitored spectrophotometrically using the vibronic structure of the Q-band region of the absorption spectrum. The fbCytc product was worked up using methods adapted from those employed by Winkler and coworkers⁹² and Kostić and coworkers.⁹³ After desalting, the protein was isolated by cation-exchange chromatography first on a Whatman CM-52 column and optionally then on a Mono-S 4.6/100 PE FPLC column (GE Healthcare Life Sciences). Fractions corresponding to fbCytc were combined and then were equilibrated with a 25 mM sodium phosphate buffer solution at pH 7.0 by repeated concentration using an Millipore YM10 ultrafilter and dilution with the buffer solution. After a final ultrafiltration step, the product was analyzed on a Superdex 75 FPLC gel-filtration column (GE Healthcare Life Sciences). This procedure yields fbCytc free of the low molecular-weight polypeptide contaminants that are typically observed directly from the HF demetalation reaction. The concentrated fbCytc solution obtained from the final ultrafiltration step was divided into small aliquots and then flash-frozen in liquid nitrogen. The frozen samples were stored in a -85 °C freezer for up to a year.

For use in fluorescence spectroscopy, one of the frozen samples was thawed and then diluted with 25 mM phosphate buffer solution at pH 7.0 or with a glycerol-buffer solution mixture (50% glycerol by volume). The final protein solution was then passed through a 0.22 μ M microfilter to remove any large debris. The sample's concentration

was then adjusted by adding additional diluent solution so that the absorption at the peak of the $Q_{\mathcal{Y}}$ absorption band for a path length of 1.0 cm ranged from 0.1-0.2. The sample was held in quartz cuvettes with the headspace purged with dry nitrogen gas prior to an experiment.

2.2.2 Absorption and Fluorescence Spectroscopy

Absorption spectra were acquired with a Hitachi U-2000 spectrophotometer (2-nm band pass). Fluorescence spectra were obtained with a home-built spectrofluorimeter 79 consisting of an Jobin-Yvon AH10 100-W tungsten-halogen light source, a Jobin-Yvon H10 excitation monochromator (4-nm bandpass), an Acton Research SP-150 emission spectrograph (2-nm bandpass), and a Jobin-Yvon Symphony charge-coupled device (CCD) detector. The CCD detector employs a liquid nitrogen cooled, backilluminated, 2000×800 pixel silicon detector chip (EEV corporation). The sample cuvette was held in a Quantum Northwest TLC50F Peltier-effect temperature controller. As presented as a function of wavenumber, the fluorescence intensities are multiplied by the square of the wavelength in order to compensate for the fixed (in wavelength units) spectral bandpass of the emission spectrograph. The absorption and fluorescence instruments were controlled by LabVIEW (National Instruments) programs.

2.2.3 Picosecond Time-resolved Fluorescence Spectroscopy

Single-wavelength fluorescence transients were acquired with a time-correlated, single photon counting (TCSPC) system operated in the reverse triggered mode. This instrument was described in detail in an earlier contribution.⁷⁶ Excitation pulses were obtained from a synchronously pumped, cavity-dumped rhodamine-6G dye laser (Coherent 702-1), which was pumped by the 532-nm second-harmonic output of a modelocked Nd^{III}-YAG laser (Coherent Antares 76-S). The cavity dumper on the dye laser

was operated at 4 MHz, so the excitation interpulse period was 250 ns. The zerobackground autocorrelation width of the excitation pulses was 5 ps, as measured using an Inrad 5-14A autocorrelator. The fluorescence emission was collected at 90° from the excitation laser beam and was analyzed by a calcite polarizer set to the magic angle with respect to the plane of the excitation laser so that dichroismfree transients were acquired. The emission was then detected using a double subtractive monochromator (CVI CM112) and a microchannel-plate photomultiplier tube (Hamamatsu R3809U-51), the output of which was analyzed using a NIM-based TC-SPC setup as previously described. The instrument-response function obtained with a dilute scattering solution at the sample position had a width (fwhm) of approximately 100 ps in these experiments. A LabVIEW (National Instruments) program controlled the emission monochromator and the photon-counting hardware so that a set of single-wavelength fluorescence transients over a range of emission wavelengths across the fluorescence spectrum could be automatically acquired. The sample was held in a water-cooled mount, which was maintained at 22 °C with a Neslab 221 water circulator.

2.3 Results

2.3.1 Absorption and Fluorescence Emission Spectra

Figures 2.1 and 2.2 show the absorption (A(v)) and fluorescence (F(v)) spectra obtained at 22 °C from fbCytc at pH 7.0 in water and 50% (v/v) glycerol, respectively. The spectra are plotted with respect to wavenumber v as relative dipole strengths, $A_D(v) = A(v)/v$ and $F_D(v) = F(v)/v^3$, respectively. The plotted region shows the Q band, which consists of a pair of partially resolved vibronic bands from the x and y polarized transition-dipole moments in the plane of the z^{II} porphyrin. The fluorescence spectrum's 0-0 and 0-1 peaks exhibit an approximate mirror-symmetry

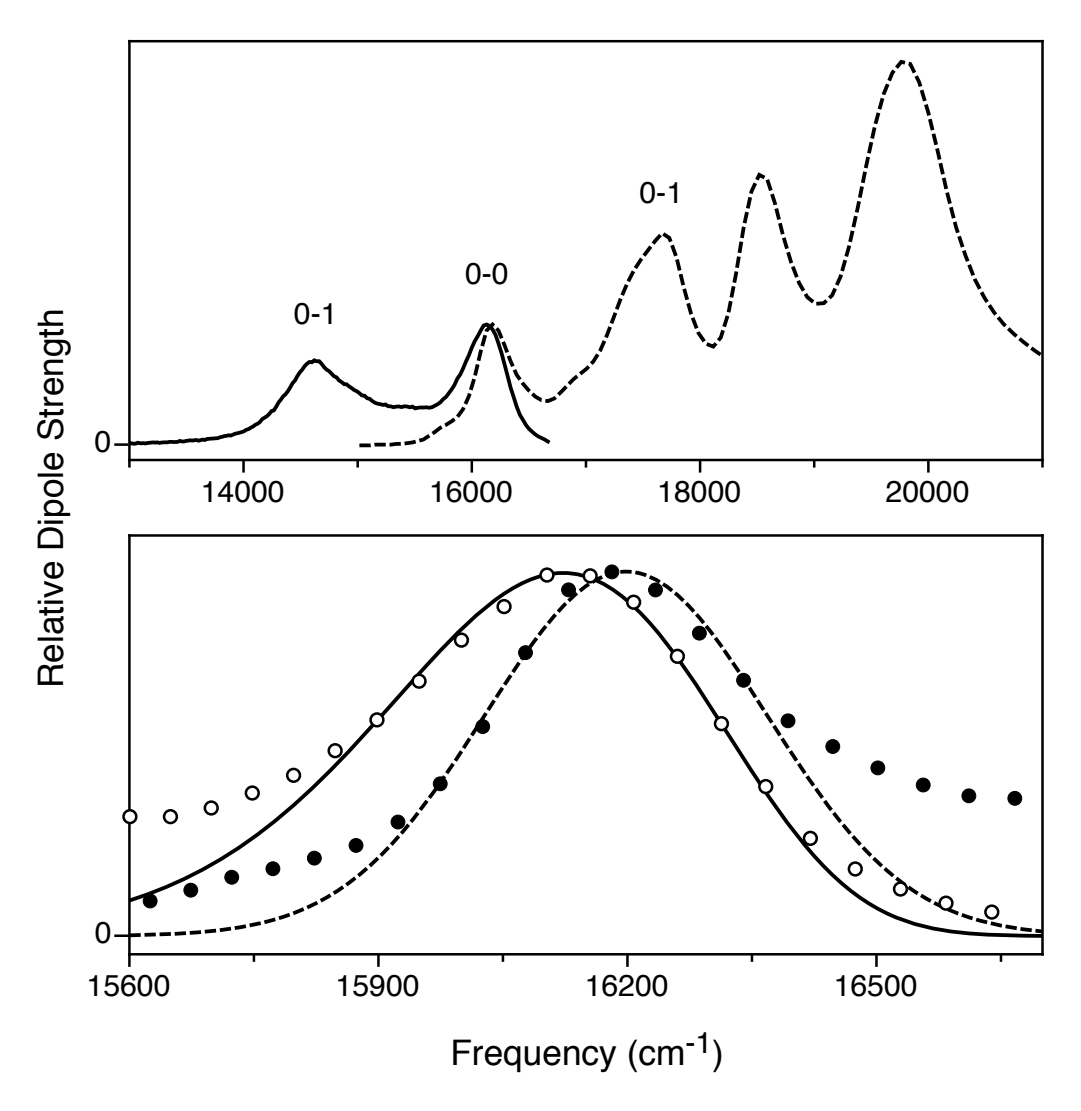


Figure 2.1. *Top panel:* Continuous-wave absorption (dashed) and fluorescence emission (solid) spectra from metal-free cytochrome c (fbCytc) in water at 22 °C and pH 7, plotted as relative dipole strengths, A(v)/v and $F(v)/v^3$, respectively. The fluorescence spectrum was obtained with the excitation light source tuned to 16130 cm⁻¹ (620 nm). *Bottom panel*: Detailed view of the 0–0 region, with the data points shown superimposed with log-normal line shapes (see Table 1 for the fit parameters).

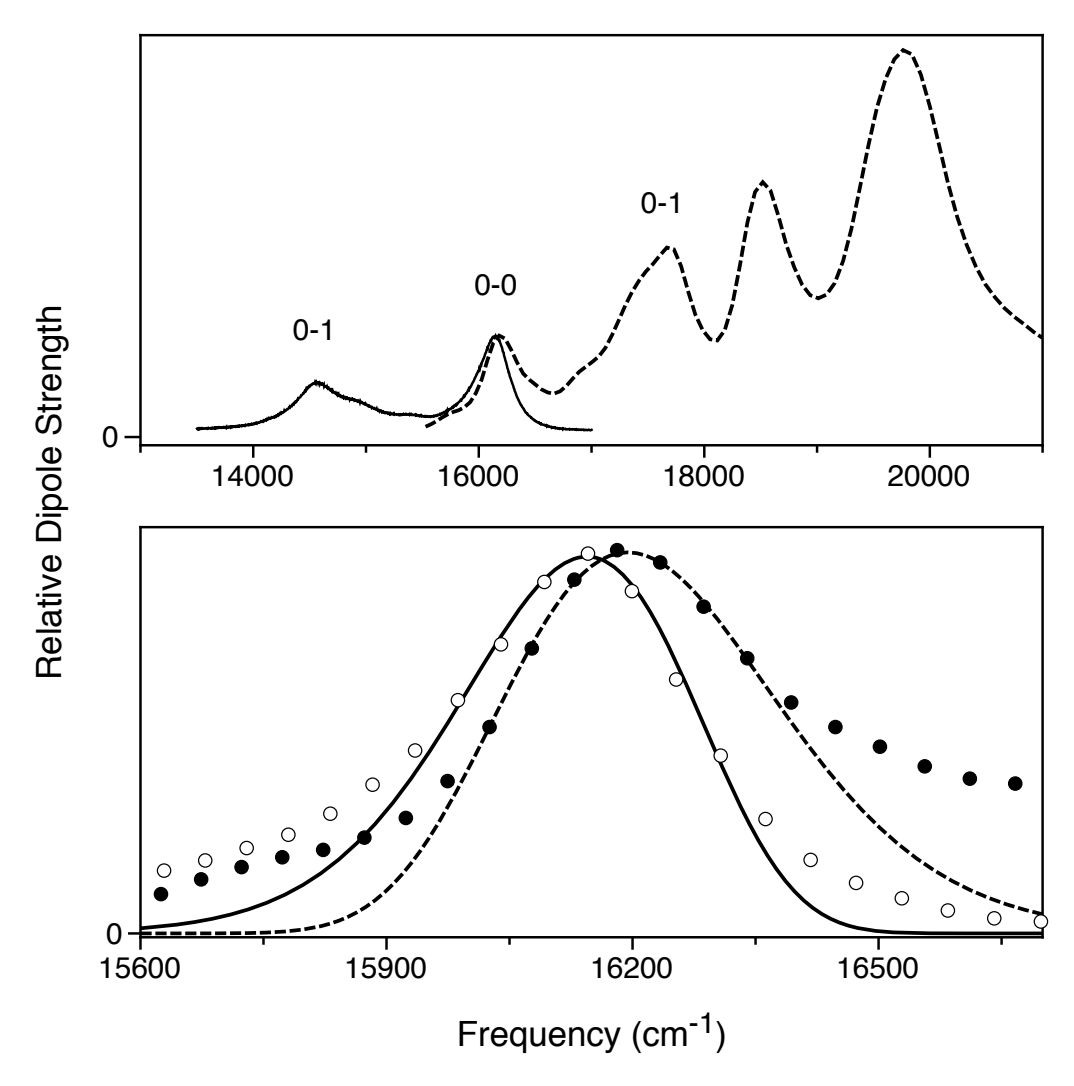


Figure 2.2. *Top panel:* Continuous-wave absorption (dashed) and fluorescence emission (solid) spectra from fbCytc in 50% (v/v) glycerol at 22 °C and pH 7, plotted as relative dipole strengths, A(v)/v and $F(v)/v^3$, respectively. The fluorescence spectrum was obtained with the excitation light source tuned to 16130 cm⁻¹ (620 nm). *Bottom panel:* Detailed view of the 0–0 region, with the data points shown superimposed with log-normal line shapes (see Table 2.1 for the fit parameters).

Table 2.1. Lognormal and Gaussian lineshape models for the 0–0 peak in the absorption (*A*) and fluorescence (*F*) spectra from fbCytc in water and in 50% (ν/ν) glycerol (see Figures 2.1 and 2.2) and estimates for the solvation reorganization energy (λ).

	W	ater	50% (v/v) Glycerol		
Parameter ^a	Lognormal	Gaussian	Lognormal	Gaussian	
$ \begin{array}{c} \nu_{0-0,A} \\ \Delta\nu_{0-0,A} \\ \rho_{0-0,A} \end{array} $	16198 cm ⁻¹ 426 cm ⁻¹ 1.13	16199 cm ⁻¹ 408 cm ⁻¹ —	16194 cm^{-1} 396 cm^{-1} 1.22	16201 cm ⁻¹ 370 cm ⁻¹	
$ v_{0-0,F} $ $ \Delta v_{0-0,F} $ $ \rho_{0-0,F} $	16122 cm ⁻¹ 476 cm ⁻¹ 1.22	16133 cm ⁻¹ 465 cm ⁻¹ —	$16144~{ m cm}^{-1} \ 396~{ m cm}^{-1} \ 1.22$	16135 cm ⁻¹ 337 cm ⁻¹	
λ	38 cm^{-1}	43 cm^{-1}	25 cm ⁻¹	33 cm^{-1}	

^a See Equation 2.1 and the text.

with respect to the two lowest wavenumber features, the 0–0 and 0–1 peaks from the $Q_{\mathcal{Y}}$ transition. The relative scaling of the absorption and fluorescence spectra in Figures 2.1 and 2.2 was set so that the 0–0 peaks have the same intensities.

In order to determine the changes in spectral lineshape and position that are induced by the change of solvent from water to 50% glycerol, we fit the the 0-0 peaks of the absorption and fluorescence dipole-strength spectra to Gaussian and lognormal⁹⁷ lineshapes. The lower panels of Figures 2.1 and 2.2 show the lognormal lineshapes superimposed on an expanded view of the 0-0 peaks. The fit parameters listed in Table 2.1 include the center frequencies (ν_{0-0}), the widths (fwhm, $\Delta\nu_{0-0}$) and for the log-normal lineshapes, the asymmetry (or skew) parameter, ρ_{0-0} . Estimates for the solvation reorganization energy, λ , were then obtained as one-half the difference between the center frequencies of the absorption (A) and fluorescence (F) 0-0 peaks,

$$\lambda = (\nu_{0-0,A} - \nu_{0-0,F})/2. \tag{2.1}$$

Using the ν_{0-0} parameters from the fitted lognormal lineshapes, this equation returns values for λ of 38 cm⁻¹ in water and 25 cm⁻¹ in 50% glycerol. These estimates are valid if the ground-state and excited-state potential-energy surfaces are harmonic and have the same normal-mode frequencies, 98 , 99 which is the case if the absorption and fluorescence spectra exhibit an exact mirror symmetry with respect to frequency. An additional formal requirement for the applicability of Equation 2.1 is that the vibronic lineshapes are Gaussians. 100 The estimates for λ are somewhat larger in both solvents if Gaussian lineshapes are used to fit the 0-0 peaks (43 cm⁻¹ and 33 cm⁻¹, respectively). Still, these peak-shift estimates for λ should be regarded as lower limits. Because the 0-0 peaks are only partially resolved, it is not possible to apply rigorously the equation for λ introduced by Fleming and coworkers, 100

$$\lambda = \frac{\int_0^\infty d\nu \ \nu \left[\sigma_a(\nu) - \sigma_f(\nu)\right]}{\int_0^\infty d\nu \left[\sigma_a(\nu) + \sigma_f(\nu)\right]},\tag{2.2}$$

which integrates over the absorption (σ_a) and fluorescence (σ_f) spectra and avoids assumptions about the lineshapes. When applied to the spectra shown in Figures 2.1 and 2.2, Equation 2.2 obtains estimates for λ that are about a factor of two larger than those listed in Table 2.1. This scaling of estimates for λ using Equations 2.1 and 2.2 is similar to that obtained by Fleming and coworkers for eosin in water and for lysozyme labelled with eosin. 100

The reduction by at least a third of the solvation reorganization energy for fb-Cytc that accompanies the change from water to 50% glycerol (see Table 2.1) is too large to be explained only by the change in solvent. Using a dielectric continuum treatment of the solvent surrounding a probe chromophore, the Lippert-Mataga equation 94,101,102 relates the solvation reorganization energy to the dielectric constant, ϵ_0 , and the index of refraction, n, in a given solvent mixture:

$$\lambda = \frac{\Delta \mu_{\text{eg}}^2}{hca^3} \left[\frac{\epsilon_0 - 1}{2\epsilon_0 + 1} - \frac{n^2 - 1}{2n^2 + 1} \right]. \tag{2.3}$$

The first term in this equation depends on the probe; it indicates that λ depends on the ground-to-excited-state change in the probe's dipole moment, $\mu_{\rm eg}$, and the radius of the surrounding spherical solvent cavity, a. If these parameters are held constant, λ is reduced only by about ten percent by changing the parameters in the bracketed expression from those for water ($\epsilon_0 = 80.37$, n = 1.3326) to those for 50 % (v/v) (or 56 % (w/w)) glycerol/water ($\epsilon_0 = 64$, n = 1.4063) at 25 °C. 103,104 This estimate would be appropriate if the porphyrin chromophore in fbCytc is fully solvated by the external solvent, but it is probable that the porphyrin is almost fully solvated by the surrounding protein structure; Table 2.1 shows that the fluorescence spectrum is only shifted a few cm $^{-1}$ to the blue by the change from water to 50% glycerol. In contrast, the fluorescence spectrum from ZnCytc shifts 50 cm $^{-1}$ to the blue when water is replaced by 50% glycerol. Such a shift is consistent with the partial exposure to the external solvent of the edge of the porphyrin macrocycle that is indicated by the FeCytc crystal structure (see Figure 1.3). The change in solvent to 50% glycerol

has no effect, however, on λ for ZnCytc; the same value, $\lambda = 145 \text{ cm}^{-1}$, is observed in water and in 50% glycerol.⁷⁷

2.3.2 Picosecond Time-resolved Fluorescence Spectroscopy

Since the dielectric properties of the external solvent account only for a small fraction of the reduction of the solvation reorganization energy, λ , that accompanies changing the solvent from water to 50% glycerol, it is likely that the average timescale for the solvation response of the protein in fbCytc is lengthened enough in the presence of 50% glycerol so that some of the motions are slowed enough that they do not contribute to λ . These conclusions are supported by the measurements of the FSS response function that are described next.

Time-resolved fluorescence spectra from fbCytc in water and in 50% glycerol were obtained as slices from a time-wavelength-intensity (dipole-strength) surface $F_D(v,t)$ that spanned the 0-50-ns by 13500-16000-cm⁻¹ region. The excitation laser was fixed at 16130 cm^{-1} , which is near to the wavenumber of the 0-0 transition in water and 50% glycerol, respectively (see Figures 2.1 and 2.2). The surface was acquired as a set of single-wavelength transients spaced by 5.0 nm ($\sim 130~{\rm cm}^{-1}$ at 620 nm), the bandpass of the emission monochromator. The emission tuning range spans the 0-1 peak and continues nearly to the maximum of the 0-0 peak. Owing to the 5-nm bandpass of the emission monochromator and the relatively small value for λ , we were unable to work further to the red than the maximum of the 0-0 peak because of interference from scattering from the excitation laser. Because the transients were recorded over the 0-50-ns delay range, a span of 25 times the fluorescence lifetime under the chosen sample conditions, the time-wavelength-intensity surface was constructed by normalizing the integral of each transient to the fluorescence dipole strength observed in the continuous-wave spectrum at the emission wavenumber of the transient. The transients were then used directly, without deconvolution of the instrument-response function, and they were truncated so that the first data point employed in further analysis was that of the 100-ps delay, a full instrument-response width after the center of the excitation pulse.

Figure 2.3 shows a set of time-resolved fluorescence dipole-strength spectra from fbCytc in water at 22 °C. The spectra were obtained as slices from the $F_D(v,t)$ time-wavelength-intensity surface at four delay times t. Fitted lognormal lineshapes are shown superimposed on the data points. As the time delay increases, the spectra decay in intensity and the wavenumber of the peak maximum shifts to lower frequency. The time evolution of the mean fluorescence dipole strength for the 0-1 peak, $\langle v(t) \rangle$, was obtained by integrating over the time-resolved spectrum at a given time t:

$$\langle v(t) \rangle = \frac{\int_{v_1}^{v_2} dv \, v \, F_D(v, t)}{\int_{v_1}^{v_2} dv \, F_D(v, t)}.$$
 (2.4)

The $\langle v(t) \rangle$ response is used without normalization in the following as a direct measure of the FSS response function (Equation 2.5) over the 100-ps-50-ns regime. This practice avoids the need to estimate the mean fluorescence emission frequencies at zero time and at infinite time (see also the discussion on this issue in ref. 105). The response shown in Figure 2.4 is well described by a biexponential decay function. The limits for the integral, $v_1 = 14000~{\rm cm}^{-1}$ and $v_2 = 15500~{\rm cm}^{-1}$, were selected so that the range of integration spanned the 0-1 peak but avoided the onset of the 0-0 peak. The calculated $\langle v(t) \rangle$ response is essentially invariant with different choices of v_1 and v_2 , but the fitted $t = \infty$ asymptote varies over a few wavenumbers depending on how far the integration extends over the congested region between the 0-1 and 0-0 peaks. In the previous work on ZnCytc, ⁷⁷ $\langle v(t) \rangle$ was determined from the time evolution of the fluorescence 0-0 transition frequency, which was obtained from a fitted vibronic progression for the 0-0 and 0-1 peaks. The use of the mean-frequency calculation in the present work allows us to obtain a robust measurement of the FSS response function despite the smaller solvation reorganization energy and the poorer signal/noise ratio of the fbCytc data sets. A similar approach was used previously by

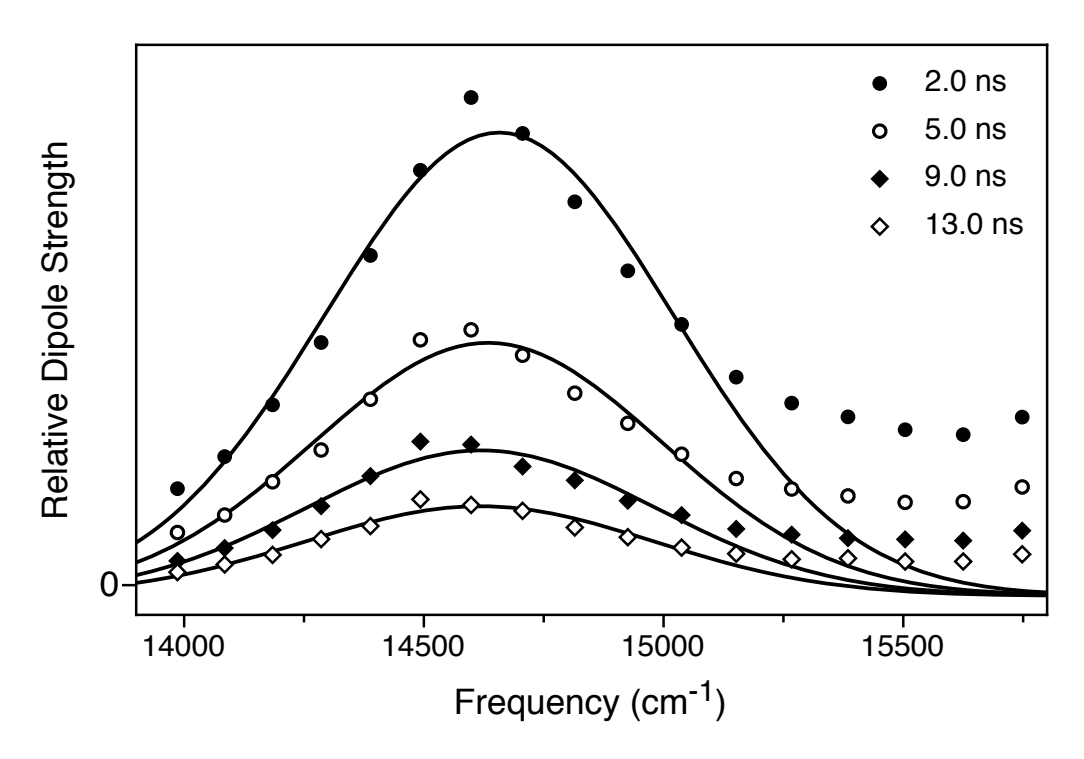


Figure 2.3. Time-resolved fluorescence dipole strength spectra from fbcytc in water at 22 °C at four time delays. The displayed spectral region corresponds to the 0–1 peak. The spectra are superimposed with fitted lognormal line shapes.

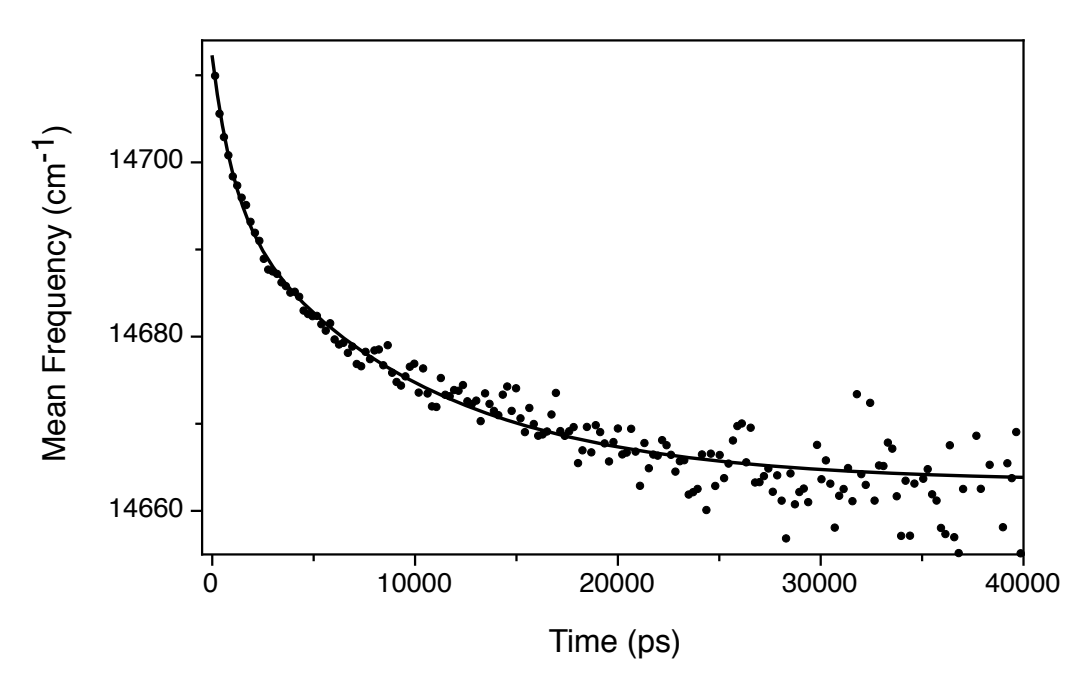


Figure 2.4. Time evolution of the mean emission frequency of the 0–1 fluorescence transition, $\langle \nu_{0-1} \rangle$, from fbCytc in water at 22 °C. The data points are superimposed on a fitted double-exponential model. The fit parameters are listed in Table 2.2.

Toptygin *et al.* in their study of dynamic solvation in single-tryptophan mutants of IIA^{Glc} protein.¹⁰⁶

The addition of glycerol to the fbCytc solution results in a significant slowing of the FSS response function. Two exponential components are observed, just as in water, but the total shift to the red is smaller than observed in water (see Figures 2.5 and 2.6). The time constants observed in 50% glycerol, 3.18 ns and 13.71 ns, are lengthened significantly compared to those observed in water, 1.37 ns and 9.06 ns, respectively (see Table 2.2). The reduction of λ indicated by the continuous-wave spectra (Figure 2.2) and by the $\langle v(t) \rangle$ response (Figure 2.6) further requires that a portion of the motion observed in water is rendered effectively static relative to the fluorescence timescale in 50% glycerol.

Table 2.2 also lists the parameters that describe the FSS response function observed previously from ZnCytc under similar conditions.⁷⁷ Both of the time constants observed in ZnCytc are almost ten times shorter than those of fbCytc. Note that only the slower of the two components observed from ZnCytc is affected significantly by the addition of glycerol to the external solvent medium (see Table 2.2). That the solvation reorganization energy for ZnCytc in water is the same as that in 50% glycerol⁷⁷ supports the conclusion that the addition of glycerol primarily acts on the FSS response by damping the motions of groups in the solvent-contact layer of the protein; the studies by Vincent *et al.*¹⁰⁷ suggest that this frictional action of glycerol involves changes of the structure and dynamics of water molecules in the hydration layer. The results observed here with fbCytc evidence a similar structural order of assignment for the two timescales in the FSS response but with an even larger effect of the solvent friction than observed with ZnCytc.

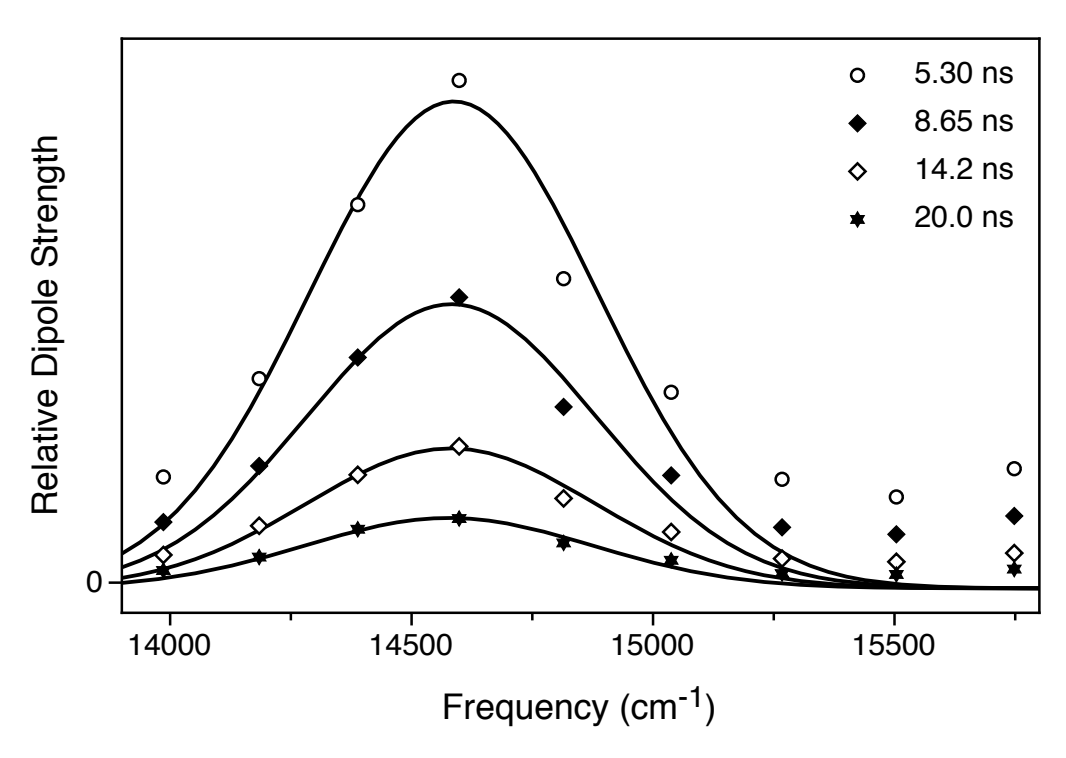


Figure 2.5. Time-resolved fluorescence dipole strength spectra from fbcytc in 50% (v/v) glycerol at 22 °C at four time delays. The displayed spectral region corresponds to the 0–1 peak. The spectra are superimposed with fitted lognormal line shapes.

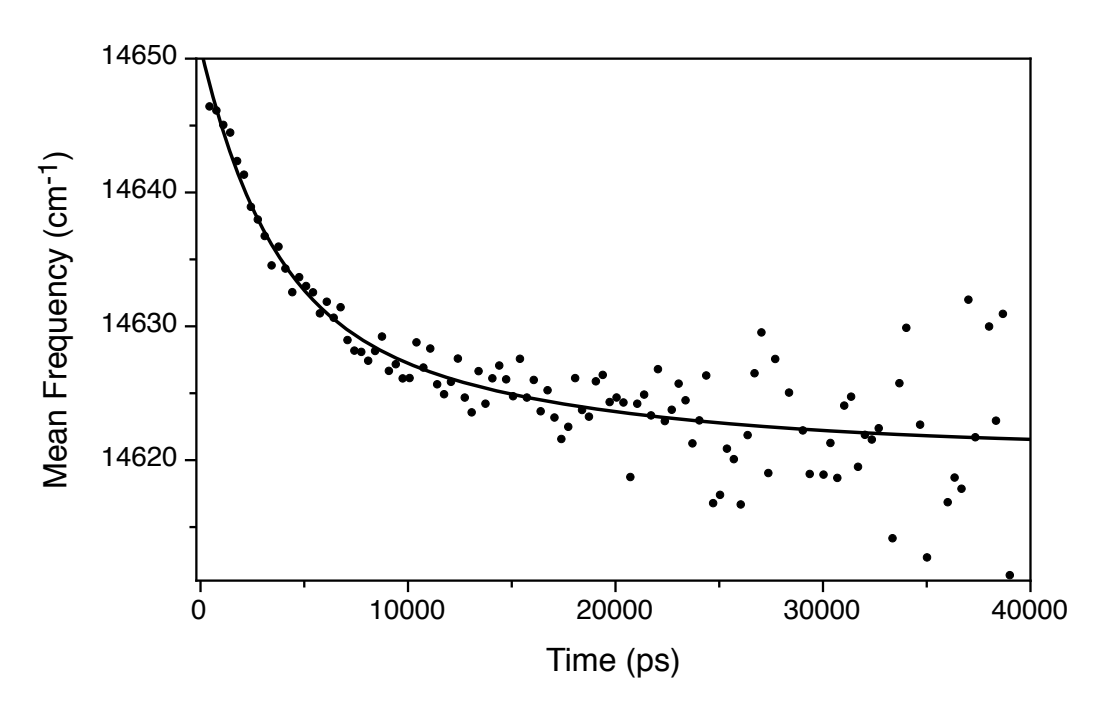


Figure 2.6. Time evolution of the mean emission frequency of the 0–1 fluorescence transition, $\langle v_{0-1} \rangle$, from fbCytc in 50% (v/v) glycerol at 22 °C. The data points are superimposed on a fitted double-exponential model. The fit parameters are listed in Table 2.2.

Table 2.2. Model parameters for the time evolution of the time-resolved fluorescence spectrum observed in water and 50% glycerol in metal-free (fbCytc) and $\rm Zn^{II}$ -substituted (ZnCytc) cytochrome $\it c$ at 22 °C

Protein	Solvent	A_1 , cm ⁻¹	$ au_1$, ns	A_2 , cm ⁻¹	$ au_2$, ns	v_{∞} , cm ⁻¹
fbCytc ^a	water	13.9	1.37	36.5	9.06	14663
	50% glycerol	18.4	3.18	11.4	13.7	14621
ZnCytc ^b	water	70	0.250	100	1.450	16940
	50% glycerol	60	0.260	90	2.200	17000

a $\langle \nu_{0-1}(t) \rangle = A_1 \, \mathrm{e}^{-t/\tau_1} + A_2 \, \mathrm{e}^{-t/\tau_2} + \nu_{\infty}$, see Equation 2.4 and the text. b From reference 16; $\langle \nu_{0-0}(t) \rangle = A_1 \, \mathrm{e}^{-t/\tau_1} + A_2 \, \mathrm{e}^{-t/\tau_2} + \nu_{\infty}$, from a fitted vi-

^b From reference 16; $\langle v_{0-0}(t) \rangle = A_1 e^{-t/\tau_1} + A_2 e^{-t/\tau_2} + v_{\infty}$, from a fitted vibronic progression over the 0–0 and 0–1 region of the fluorescence spectrum.

2.4 Discussion

The main finding is that the FSS response function measured for fbCytc over the 100-ps-50-ns timescale is significantly slower than that of ZnCytc under the solution conditions that favor the native folded state. The motions that are sensed by the intrinsic porphyrin chromophore in this timescale regime are predominantly from fluctuations of the surrounding protein structure. In the following, we review the current thinking about the origin of the FSS response in chromoproteins that supports this assignment, and then we consider how the correlation timescales observed in the FSS response function of fbCytc and ZnCytc can be interpreted structurally in terms of Brownian diffusive motion on the protein-folding energy landscape. The effect of external solvent friction is included by incorporating an Arrhenius expression relating the barrier heights that divide the minima on the energy landscape to the correlation timescales for the fluctuations. Overall, the analysis supports the conclusion that the slowing of the FSS response function in fbCytc arises from an increase in the mean-square displacements of the core and surface fluctuations compared to those in ZnCytc. These conclusions are consistent with the suggestion that the equilibrium structure of fbCytc is a partially unfolded, molten-globule-like state.

2.4.1 Solvent-Response Functions in Liquids and Proteins

The FSS or solvent-response function, $S_{\mathcal{V}}(t)$, 51,54,89,108 describes the reorganizational response triggered in a condensed phase medium by the ground-to-excited-state change in the probe's dipole moment that accompanies its optically driven absorption transition. It is usually defined in terms of the time evolution of the mean frequency of the time-resolved fluorescence spectrum, $\langle \mathcal{V}(t) \rangle$, as

$$S_{\mathcal{V}}(t) = \frac{\langle \nu(t) \rangle - \langle \nu(\infty) \rangle}{\langle \nu(0) \rangle - \langle \nu(\infty) \rangle}.$$
 (2.5)

In polar liquids, most of the properties of $S_{\nu}(t)$ observed experimentally can be calculated by treating the liquid medium as a dielectric continuum.^{54,102} Here the optical transition of the probe is treated as applying a step-function change in the electric field that is sensed by the surrounding solvent molecules. In the simplest picture, given the parameters from a description of the liquid's frequency dependent dielectric response, $\epsilon(\omega)$, using a single Debye dispersion,

$$\epsilon(\omega) = \epsilon_{\infty} + \frac{\epsilon_0 - \epsilon_{\infty}}{1 - i\omega\tau_D},\tag{2.6}$$

the calculated solvation response is a single exponential function with a time constant

$$\tau_F = \left(\frac{2\epsilon_\infty + \epsilon_C}{2\epsilon_0 + \epsilon_C}\right) \tau_D. \tag{2.7}$$

In these equations, ϵ_{∞} and ϵ_{0} are the infinite-frequency and zero-frequency (static) dielectric constants and τ_{D} is the dielectric (Debye) relaxation time. The parameter ϵ_{c} is the dielectric constant of the cavity in the solvent medium that surrounds the probe chromophore; it can be calculated knowing the structure of the probe and the polarizability of the solvent medium. Because usually $\epsilon_{0} \gg \epsilon_{\infty}$ and $\epsilon_{0} \gg \epsilon_{c}$, the solvation time constant τ_{F} is equal to the longitudinal relaxation time constant ϵ_{0}

$$\tau_L = (\epsilon_{\infty}/\epsilon_0)\tau_D. \tag{2.8}$$

This result indicates that $\tau_F \ll \tau_D$.⁶² In polar solvents, τ_F is predominantly determined by the timescale for rotational diffusion. At very short timescales, hindered rotations (librations)⁶² and inertial (free-rotor) motions^{59,61,63,109-111} make major contributions to the solvent-response function.

The molecular character of $S_{\mathcal{V}}(t)$ is usually discussed in terms of the fluctuations of the local electric field that arise from the random motions of the solvent dipoles around the probe chromophore. In the time domain, the probe's ground-to-excited state transition frequency $\omega = 2\pi v$ exhibits fluctuations

$$\Delta\omega(t) = \langle \omega \rangle - \omega(t) \tag{2.9}$$

from that averaged over time or averaged instantaneously over the ensemble. The fluctuations are characterized by a time-correlation function,

$$M(t) = \frac{\langle \Delta \omega(0) \Delta \omega(t) \rangle}{\langle (\Delta \omega)^2 \rangle},$$
(2.10)

which describes the associated loss of memory over time of the instantaneous transition frequency $\omega(0)$ that was present initially at some reference time t=0. At high temperatures and in the linear-response regime, where the fluctuation-dissipation relation holds, M(t) is equal to the solvent-response function $S_{\mathcal{V}}(t)$. The requirement for the linear-response regime is generally met in most probe/solvent systems because the optical excitation of the probe results only in a small change in the probe's dipole moment and accordingly presents a small perturbation to the motions and structure of the solvent.^{57,58} Note that the three-pulse stimulated photon-echo peak shift (3PEPS) response is usually taken as being a *direct* measure of M(t). 55,56 In several systems, however, the 3PEPS response includes components from intramolecular nonradiative electronic state dynamics in addition to those arising from solvation dynamics. 46,108,112 Given knowledge of M(t), or of the spectral density, $\rho(\omega)$, which is obtained as its Fourier transform, it is possible to calculate all of the spectroscopic observables for the probe/solvent system. For example, the solvation reorganization energy, λ , is equivalent to the mean frequency of the spectral density, 56,89

$$\lambda = \hbar \int_0^\infty d\omega \, \omega \, \rho(\omega). \tag{2.11}$$

The studies of dynamic solvation in small proteins using transient holeburning, time-resolved fluorescence, or stimulated photon-echo methods have targeted predominantly the <100-ps regime that is readily probed by femtosecond spectroscopy. Five when sensed by electronic probes located in the interior of a protein, the motions of water molecules in the bulk or in the hydration layer surrounding proteins still make dominant contributions to the detected response

function and especially at short times (<1 ps). 100,121 Because the effective dielectric constant in the interior of a protein is small, 122 the electric-field fluctuations sensed by the probe from water molecules in the surroundings are poorly screened by the protein medium. In liquid water, M(t) decays according to two phases, the inertial (<100 fs, Gaussian) and diffusive reorientational (<1 ps, exponential) responses.⁶¹ In a number of studies, components in the FSS response with time constants as long as 100 ps have been assigned to motions of water molecules as they exchange between sites on the surface of proteins and the hydration layer. 115-117, 123-125 In contrast, Nilsson and Halle⁵⁸ argued that the FSS response cannot sense these water motions because the exchange reactions would not be accompanied by a modulation of the local electric field; replacement of a bound water molecule with a free water molecule from the bulk would occur in a concerted fashion. Using the results from molecular dynamics (MD) simulations that featured calculations of the dielectric response of the protein and surrounding solvent at each step in the trajectory, they concluded instead that the motions of water molecules in the hydration layer are only somewhat slowed from those in the bulk solvent, with <1.5-ps correlation times being characteristic. Slower correlation times in the response function were assigned only to the motions of protein-derived groups as the timescales increase into the >10ps range and longer.⁵⁸ These conclusions are strongly supported by the recent MD simulations of Toptygin et al., but these authors add the interesting observation that their calculated response functions poorly reproduce the experimentally observed FSS timescales when protein motions are predominantly involved. ¹⁰⁵

There have been only a few observations of protein-derived motions using dynamic solvation methods in the >100-ps regime of time featured in the present work because the probe has usually been located in a binding site that is adjacent to or on the solvent-contact surface, where the electric-field fluctuations are dominantly those from the external water molecules. The very first picosecond time-resolved flu-

orescence investigations of dynamic solvation in small proteins, in the McLendon⁶⁵ and Boxer⁶⁶ laboratories, accessed ps-ns motions in apomyoglobin using extrinsic solvatochromic probes in the heme-binding site. Vincent *et al.*¹⁰⁷ used the single tryptophan residue in cytidine monophosphate kinase from *Escherichia coli* as a fluorescent probe in studies of the FSS response of the protein over the 100-ps-ns regime. Toptygin *et al.* subsequently characterized the solvation response over the 100-ps-10-ns regime in single-tryptophan-containing mutants of the IIA^{Glc} protein¹⁰⁶ and in the B1 domain fragment (GB1) of *Streptococcus* protein G.¹²⁶

Previously 76,77 in the Beck group we chose to characterize the FSS response of $\rm Zn^{II}$ -substituted cytochrome c (ZnCytc) because the intrinsic porphyrin could be exploited as a fluorescent probe that senses both internal and surface motions of the protein owing to its central position in the structure and its span to the solvent-contact surface via a cleft that mediates its physiological role in electron transfer (see Figure 1.3). The present study of fbCytc extends the work on ZnCytc by showing that the timescales assigned to the hydrophobic core and surface-contact layers are both lengthened in fbCytc and that no new timescales are detected. In contrast to the work on GB1 noted above, 126 the FSS response functions in both ZnCytc and fb-Cytc are well described by the sum of exponential components. This finding suggests that what is observed in fbCytc and ZnCytc are well isolated characteristic timescales for discrete protein motions. This point is significant especially because fbCytc is a partially unfolded structure under the equilibrium solution conditions used in the present experiments.

2.4.2 Activated Barrier-Crossing Model for Protein Fluctuations

While it would be obviously desirable eventually to compare the present FSS results with a full MD simulation of the time evolution of the dielectric response, as has been done for the protein G system mentioned above, ^{105,118,126-128} the long timescales

we observed experimentally for fbCytc would necessitate the calculation of especially long MD trajectories to obtain convergence of the calculated time-correlation functions for the structural fluctuations. An additional critical problem is that the fbCytc system does not have a well defined starting structure. In order to discuss further the structural implications of the lengthened FSS timescales detected in fbCytc, we apply in the following a model for the fluctuation timescales that would arise from diffusive motion on the protein-folding energy landscape. The goal of this analysis is to provide a reasonable framework for an interpretation of both the change in timescale that arises upon demetalation of ZnCytc to obtain fbCytc and also the effect of the change in solvent friction that occurs upon addition of glycerol.

Figure 2.7 describes qualitatively how the ground-to-excited-state energy gap for an electronic probe responds to a fluctuation of the structure of a protein. As the structure samples the energy landscape, it periodically passes over barriers in moving from one local free-energy minimum to the next. The presence of barriers can be inferred from the sensitivity of the correlation times to the external solvent friction or to internal (steric) friction^{129,130} and/or from their temperature dependence.¹³¹ If the displacement of the structure for a given motion results in a change of the local electric field at the position of the probe, the ground- and excited-state energy levels fluctuate synchronously; the energy gap between them is modulated because the dipole moment and polarizability of the probe are different in the two states. 132 The coupling strength $\langle (\Delta \omega)^2 \rangle$ term in the energy-gap time-correlation function, M(t)(Equation 2.10), relates how strongly the energy gap fluctuates in response to the motion of the protein and its surrounding solvent. In analogy to the rotational motions sensed in FSS experiments on the ps timescale in polar liquids, the motions that would primarily be sensed in the FSS response in proteins in the >100-ps regime are librational (hindered rotational or torsional) in character.

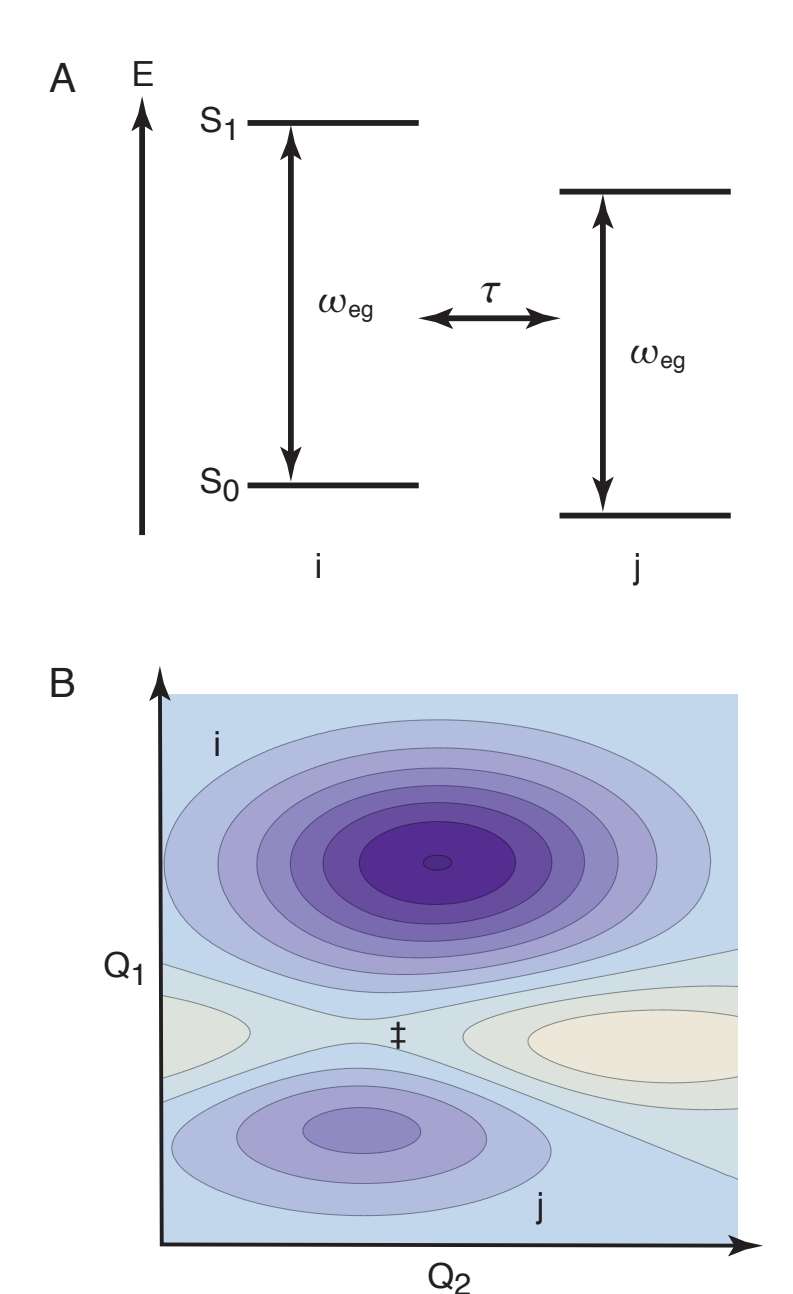


Figure 2.7. Model for equilibrium structural fluctuations in a protein involving barrier-crossing events: (a) Fluctuation with correlation time τ of the ground-to-excited-state energy gap $\omega_{\rm eg}$ for an electronic probe coupled to motion of the protein between two structures at minima in the energy landscape, i and j; (b) Contour representation of the energy landscape with respect to two structural coordinates Q_1 and Q_2 , showing minima for the structures i and j and a transition-state barrier, \dagger , between them.

In the theory discussed by García and Hummer⁹⁰ for a protein making diffusive motions with respect to its configurational coordinates, the resulting structural fluctuations are treated in terms of the stochastic displacements and velocities x(t) and $\zeta(t)$ for a Brownian particle,

$$x(t) = \int_0^t \zeta(t') dt' + x(0).$$
 (2.12)

If x(t) and $\zeta(t)$ are uncorrelated, the mean-square displacement for an ensemble of proteins is given by

$$\langle x^{2}(t) \rangle = \int_{0}^{t} dt' \int_{0}^{t'} dt'' \langle \zeta(t') \zeta(t'') \rangle. \tag{2.13}$$

For Brownian motion, the derivative of the mean-square displacement with respect to time returns a diffusion constant D expressed in terms of C(t), the time-correlation function for the velocity $\zeta(t)$,

$$\frac{\mathrm{d}}{\mathrm{d}t}\langle x^2(t)\rangle = 2\int_0^t \mathrm{d}t' \,\langle \zeta(t')\zeta(0)\rangle = 2\int_0^t \mathrm{d}t' \,C(t') = 2D. \tag{2.14}$$

This result has the important implication that Brownian motion is characterized by a linear relationship between the propagation time and the mean-square displacement, 133

$$\langle x^2(t) \rangle = 2Dt. \tag{2.15}$$

The sub-diffusion and super-diffusion regimes associated with motion impeded by traps or with longer range jumps over barriers, respectively, exhibit sublinear $(\langle x^2(t)\rangle \propto t^{n<1})$ or superlinear $(\langle x^2(t)\rangle \propto t^{n>1})$ dependences on time. 90

The correlation timescale τ for a fluctuation can then be expressed by an Arrhenius expression,

$$\tau = \tau_0 \exp(\Delta G^{\ddagger}/RT), \tag{2.16}$$

so that the correlation time increases as the barrier height ΔG^{\ddagger} increases. For Brownian diffusion, the transition-state structure at the peak of the barrier would be accessed at a characteristic timescale, τ_0 , defined by the diffusion constant D and the

mean-squared displacement, $\langle x^2(\tau_0) \rangle$,

$$\tau_0 = \langle x^2(\tau_0) \rangle / 2D. \tag{2.17}$$

This result shows that the correlation timescale τ is linearly proportional to the mean-square displacement for the fluctuation. The diffusion constant D would be expected to be inversely proportional to the friction f, ¹³⁴

$$D = k_B T / f \tag{2.18}$$

so an increase of friction would result in a lengthening of the correlation time. If the associated structural change for a fluctuation involves regions of the protein that are damped by the external solvent, as is observed for fbCytc and ZnCytc, τ_0 would be lengthened as the solvent friction increases. 85,129,130,135 If the solvent conditions are kept constant, however, a lengthening of the correlation time for a particular fluctuation would be consistent with an increase in the amplitude of the associated motion. Given that the barrier heights for motion on the energy landscape are likely to be strongly coupled to the conformational state, it should be clear that Equation 2.17 provides only a rule-of-thumb for qualitative use in the interpretation of correlation timescales. Nevertheless, it is fully consistent with the observations made by Webb and coworkers using fluorescence correlation spectroscopy of fluctuations associated with conformational changes in apomyoglobin on the μ s timescale. 136

2.4.3 Comparison of the Solvation Response in fbCytc and ZnCytc

The FSS response from fbCytc and ZnCytc with the excitation laser tuned to the 0–0 vibronic transition in the Q band consists of monotonic biexponential shifts of the time-resolved fluorescence to lower energy. Because the observed shifts are relatively small, a few hundred cm⁻¹ at most, the change in the porphyrin's dipole moment is relatively small, perhaps a few Debye, and because the porphyrin chromophore is

relatively large, it is reasonable to assume that the linear-response regime is applicable. Note that in addition to the polar solvation response to the optical transition, there is also a nonnegligible nonpolar solvation response in ZnCytc that arises from the biphasic photodissociation of the axial ligands to the Zn^{II} ion, the histidine (H18) and methionine (M80) side chains. We consider this a nonpolar response because the size of the probe effectively increases as it throws off the axial ligands. The timescales associated with the response of the protein and the external solvent to the ligand photochemistry are apparently uncorrelated with the timescales for the FSS response. ^{76,77} As discussed in the Introduction, however, with excitation of Zn-Cytc into the Soret-band region of the absorption spectrum, the protein is launched along an unfolding trajectory along a pathway that successively populates at least three partially unfolded states. A similar unfolding process is apparently triggered in fbCytc at much lower excess vibrational excitations. ^{78,79} The assumption of linear response in the interpretation of the FSS response is obviously not valid if the laser excitation is tuned above the unfolding activation thresholds. In the present work, the excitation laser was tuned close to the 0-0 transition precisely to avoid this issue and to avoid adding a vibrational relaxation component to the observed FSS response. The time constants returned by the FSS response functions can then be considered the correlation times for two analogous classes of structural fluctuations in fbCytc and ZnCytc.

The model outlined above for the fluctuation timescales detected in the FSS response suggests a simple structural picture for the change in protein dynamics caused by demetalation of ZnCytc to form fbCytc. The observed correlation times are almost an order of magnitude longer in fbCytc than in ZnCytc, and there is no evidence that the components observed in ZnCytc are present but strongly attenuated in fbCytc. These results are consistent either with a significant increase in the structural amplitudes of the fluctuations of the hydrophobic core and solvent-

contact regions or a significant increase in the height of the associated barriers. The former conclusion is obviously favored because the loss of the axial-ligand-metal interactions would, if anything, lower the barriers for motions of the folded protein orthogonal to the plane of the porphyrin (see Figure 1.3).

The molecular dynamics (MD) simulations obtained for horse-heart FeCytc by García and Hummer⁹⁰ include fluctuations that are associated with transitions between local minima on the 100-ps timescale. The most active (largest mean-squared displacements) region of the structure in the MD trajectories is the region spanning amino-acid residues 36–61, which bridges the loops on the left and right-hand sides of the protein (as shown in Figure 1.3) that project the axial ligands (the side chains of H18 and M80, respectively) towards the metal ion. The latter region is associated with especially rapid hydrogen-exchange rates in the work by Englander and coworkers.¹³⁷

The FSS responses observed in ZnCytc and fbCytc are well described by exponential components rather than by stretched exponentials or distributions of exponential components, which might be expected from a rough energy landscape characterized by a range of barrier heights. Thus, the response in ZnCytc and fbCytc might be considered *sparse*; only two classes of motion are coupled significantly to the $\pi \rightarrow \pi^*$ transition of the intrinsic porphyrin in ZnCytc or fbCytc on the fluorescence timescale. It is likely that the motions that are detected in the FSS response are *highly correlated* motions: only the motions that result in coherent electric field fluctuations at the probe will have nonzero coupling strengths. Of course, groups in motion near to the probe would be expected to be more strongly coupled, but the low dielectric constant of the protein medium permits the motion of even distant charges or dipoles to be sensed. Noisy, uncorrelated motions will project incoherent electric field fluctuations that are cancelled or attenuated when superimposed at the probe. The present results imply further that the fluorescence lifetime of the probe

limits the detected response to a fairly narrow range of timescales. The mean-square displacements for the ps-ns motions we have detected in ZnCytc and fbCytc are probably fairly short-range in character, so they are likely to be associated with hindered torsional motions of the side chains of amino acids or of the polypeptide backbone. Future studies of the barrier heights associated with these correlation times through variation of the temperature, as in the work by Bhattacharyya and coworkers, ¹³¹ may provide some additional guidance for assignments of the character of motion.

Lastly, the conclusion that the fluctuations detected on the fluorescence timescale in fbCytc exhibit much larger mean-squared displacements than those in ZnCytc should be considered in the context of the dynamics for unfolding reactions. Barrier-crossing processes associated with diffusive motion along a generalized onedimensional protein-folding reaction coordinate have been treated with transitionstate theory expressions that are similar in form to that of Equation 2.16.85,139-141 The two correlation times observed in our fluorescence experiments probably arise from fluctuations along distinct structural coordinates near the native minimum of the energy landscape, and an association of either motion with the unfolding/refolding reaction coordinate requires additional information. As mentioned above, we observed previously that the enthalpies of activation for the partial unfolding transitions in fbCytc are about one-third of those measured in ZnCytc under the same solution conditions. The products of these unfolding reactions probably correspond to intermediates that are populated late along the folding pathway of FeCytc, ⁷⁹ and the transition-state structures are likely to be found at small displacements from the native structure along coordinates that are perturbed by demetalation. It is accordingly reasonable to suggest that the short-range, metal-dependent fluctuations of the native structure observed in the FSS response function of fbCytc and ZnCytc are among those that promote the formation of the unfolding transition states under denaturing conditions and lead to longer-range unfolding/refolding motions on the $\mu s\text{-ms}$ timescale. 142

CHAPTER 3

Picosecond Fluorescence Anisotropy Decays from ZnCytc in the Presence of Gdm⁺

Summary

This chapter begins a discussion of how the addition of guanidinium ions (Gdm⁺) to the surrounding solution alters the fluctuation timescales and amplitudes in ZnCytc as the protein is denatured. The overall goal of this work is to determine the nature of the motions that are associated with the unfolding reaction coordinate and to learn how the thermodynamic stability of the protein correlates with the amplitude and character of the structural fluctuations. Using the fluorescence anisotropy (FA) response function, we probe directly the structural fluctuations of the protein that induce reorientational motions of the enclosed Zn^{II} porphryin. The unfolding transition in the presence of Gdm⁺ is reported in terms of an increased cone angle for the porphyrin's angular fluctuations. Additionally, an unfolding intermediate with both an increased cone angle and an lengthened correlation time is formed at 1 M, well

prior to the unfolding transition at 2 M. This intermediate has some of the structural aspects of an unfolding transition state.

3.1 Introduction

The thermodynamic stability of folded proteins is routinely determined by equilibrium titrations with denaturants, such as guanidinium ion or urea. 80,143 Many proteins exhibit a cooperative transition between the native and denatured states at a certain critical denaturant concentration. The unfolding transition is conveniently monitored using far-UV circular dichroism spectroscopy to probe the secondary structural composition of the protein. Alternatively, the transition can often be characterized using the fluorescence of an intrinsic or extrinsic probe chromophore. The latter approach permits one additionally to apply time-resolved fluorescence spectroscopy to characterize the protein dynamics that are associated with the unfolding reaction coordinate.

In some recent work,⁷⁷ we showed how the dynamic fluorescence Stokes shift (FSS) response^{51,54} of the intrinsic porphyrin chromophore can be used to characterize fluctuations of the structure of Zn^{II} -substituted cytochrome c in the native state. When the 0-0 vibronic transition in the Q absorption band is pumped, so that the S_1 electronic state is prepared with very little excess vibrational energy, the time-resolved fluorescence spectrum exhibits a conventional, unidirectional FSS response 51,54 to the red with two characteristic timescales, 250 ps and 1.45 ns. This response is assigned in analogy to that in polar liquids to a polar solvation response of the surrounding protein to the ground-to-excited-state change in the Zn^{II} -porphyrin's dipole moment. The two timescales were assigned to motions of the hydrophobic core and solvent-contact layers of the protein, respectively, because addition of glycerol to the external solvent medium slowed only the latter component. Subsequently

we showed that the correlation timescales obtained from the exponential time constants in the FSS response function in metal-free (or free-base) cytochrome c (fbCytc) were determined to be almost ten times longer than those of ZnCytc. He applying a model for the Brownian diffusive motion and thermally activated barrier crossing events hat are associated with structural fluctuations on the protein-folding energy landscape, we inferred that the increased polar solvation timescales observed in fbCytc correspond to significantly enhanced fluctuation amplitudes compared to those in ZnCytc under similar solvent conditions. This conclusion is consistent with the suggestion we made previously that fbCytc assumes a dynamic, partially unfolded structure with some of the characteristics of a molten globule owing to the loss of the stabilizing influence of the two axial metal-ligand interactions in the native ferricytochrome c structure.

In this contribution, we begin a discussion of how the addition of guanidinium ions (Gdm⁺) alters the fluctuation timescales and amplitudes in ZnCytc as the protein is denatured. The overall goal of this work is to determine the nature of the motions that are associated with the unfolding reaction coordinate and to learn how the thermodynamic stability of the protein correlates with the amplitude and character of the structural fluctuations. Our approach will be to compare the correlation timescales detected by the porphyrin chromophore for the fluctuations of ZnCytc in the presence and absence of Gdm⁺ using two methods: the FSS response, as discussed above, and the fluorescence anisotropy (FA) response. While the FSS response detects the motions of the protein structure indirectly using the fluctuating local electric field sensed by the chromophore, the FA response senses the motions of the porphyrin directly using the decay of the alignment of the photoselected ensemble that was initially prepared by a plane-polarized excitation laser pulse. Given that the protein structure prepares a tight-fitting cavity for the porphyrin (see Figure 1.3), the FA response primarily reports the structural fluctuations of the protein that induce

reorientational motions of the porphryin. Of course, on a longer timescale than those associated with internal motions of the protein, the FA response will also include a decay component associated with rotational diffusion of the entire solvated protein.

The present contribution focuses on the FA response in ZnCytc as a function of the Gdm⁺ concentration and compares directly the motions of the protein in the native and denatured states. The internal rotational diffusion timescale, 700–1150 ps, is comparable to that determined previously for the motions of the hydrophobic core using the FSS response. The results also show that a partially unfolded structure is populated in the presence of Gdm⁺ prior to the denaturation transition. The intermediate is distinctive in being characterized by equilibrium fluctuations with enhanced mean squared deviations relative to those in the native and denatured structures, so it possesses some of the properties of a transition-state structure.

3.2 Experimental

3.2.1 Sample Preparation

ZnCytc was prepared from horse-heart ferricytochrome c (FeCytc) from Sigma using the procedure developed by Vanderkooi and coworkers. 69,91 The metal free cytochrome c product of the demetalation reaction of FeCytc in liquid anhydrous HF was reconstituted with ZnII using a 10-fold molar excess of zinc acetate. The ZnCytc product was worked up using methods based on those employed by Winkler and coworkers 92 and Kostić and coworkers. 93 The final concentrated ZnCytc solution obtained after repeated ultrafiltration steps using a Millipore YM10 ultrafilter was divided into small aliquots and flash-frozen in liquid nitrogen for later use.

On the day of a fluorescence experiment, frozen samples were thawed and then diluted with a range of Gdm⁺ concentrations in a 25 mM phosphate buffer solution at pH 7.0. The resulting protein solution was then allowed to settle for an hour before

it was filtered through a 0.22 μ M microfilter to remove any large debris. The final concentration of the sample was then adjusted by adding additional diluent solution to obtain an absorption of 0.1–0.2 at the peak of the 0–0 absorption band for a path length of 1.0 cm. The sample was held in quartz cuvettes and the headspace was purged with dry nitrogen gas prior to an experiment.

3.2.2 Absorption and Fluorescence Spectroscopy

Absorption spectra were acquired with a Hitachi U-2000 spectrophotometer (2-nm band pass). Fluorescence spectra were obtained with a home-built spectrofluorimeter 79 consisting of a Jobin-Yvon AH10 100-W tungsten-halogen light source, a Jobin-Yvon H10 excitation monochromator (4-nm bandpass), an Acton Research SP-150 emission spectrograph (2-nm bandpass), and a Jobin-Yvon Symphony charge-coupled device (CCD) detector. The CCD detector employs a liquid nitrogen cooled, backilluminated, 2000×800 pixel silicon detector chip (EEV corporation). The sample cuvette was held in a Quantum Northwest TLC50F Peltier-effect temperature controller. As presented as a function of wavenumber, the fluorescence intensities are multiplied by the square of the wavelength in order to compensate for the fixed (in wavelength units) spectral bandpass of the emission spectrograph. The absorption and fluorescence instruments were controlled by LabVIEW (National Instruments) programs.

3.2.3 Time-Resolved Fluorescence Measurements

The time-resolved experiments described in chapter 2 were performed using a L-format photon counting system with only one detector. Single-wavelength fluorescence transients for the FA experiments discussed in this chapter and the FSS response in the following chapter were acquired using a T-format time-correlated single photon counting (TCSPC) instrument. Excitation pulses were obtained from a

synchronously pumped cavity-dumped dye laser (Coherent 702-2). The dye laser was pumped by a passively mode-locked, diode-pumped Nd^{III}:YVO₄ laser (Spectra-Physics Vanguard); it produced 13 ps pulses with an average power of 2.5 W at 355 nm and 532 nm and a repetition rate of 80 MHz. The dye laser produced 5 ps pulses over the 583–585 nm tuning range using either the Rhodamine-6G or Pyromethine 567 dyes. The repetition rate on the dye laser was adjusted to 4 MHz using the cavity dumping electronics (Gooch & Housego).

In the detection system, the vertically polarized excitation pulse from the dye laser was divided into two parts. One part of the pulse was fed to a reference photodiode (Becker & Hickl PHD-400-N), and the other part was directed to the sample. The fluorescence emission was collected using a Cassegranian reflective microscope objective (40× magnification). The collected emission was then split by a polarizing cube beam splitter into two orthogonal polarization components with planes of polarization parallel (0°) and perpendicular (90°) to that of the vertically polarized excitation pulse. The two components were detected simultaneously with microchannel plate photomultiplier tubes (MCP-PMT, Hamamatsu R3809U-50) after selection of the emission wavelength by subtractive double monochromators (Spectral products, CM-112). Emission transients were recorded with a two-channel TCSPC system (Becker & Hickl SPC-132). The instrument-response width was 65 ps. LabVIEW (National Instruments) programs were used to control the data-acquisition hardware and monochromators so that a set of single-wavelength fluorescence transients could be automatically acquired over a range of emission wavelengths. The sample was held in a water-cooled mount that was regulated at 22°C using a Neslab RTE-110 water circulating bath.

3.3 Results

3.3.1 Absorption and Fluorescence Emission Spectra

Figure 3.1 shows the *Q*-band region of the absorption and fluorescence emission spectra obtained from ZnCytc in water at 22°C and pH 7.0. The spectra are plotted as relative dipole strengths, $A(\nu)/\nu$ and $F(\nu)/\nu^3$, respectively, as a function of the wavenumber, ν . The 0-0 and 0-1 peaks of the fluorescence spectrum exhibit a near mirror-symmetry with respect to the 0-0 and 0-1 peaks of the absorption spectrum. An estimate for the lower limit for the solvation reorganization energy, $\lambda = 55 \pm 10 \text{ cm}^{-1}$, was then obtained using the shift of the wavenumber of the fluorescence spectrum's 0-0 peak, $\nu_{0-0,F}$, from that of the absorption spectrum, $\nu_{0-0,A}$: 100,144

$$\lambda = (\nu_{0-0,A} - \nu_{0-0,F})/2 \tag{3.1}$$

The peak maxima for the absorption and fluorescence 0–0 peaks were found using *Mathematica* peak-finding routines and the smoothed first-derivative spectra.

In some of the previous work on ZnCytc from this laboratory,^{77,78} the metal-free product (fbCytc) of the demetalation of FeCytc in liquid anhydrous HF and the ZnCytc product obtained after Zn^{II} reconstitution were worked up using Sephadex G-75 gel-filtration chromatography, as described by Vanderkooi and coworkers.⁹¹ The value for λ obtained with these preparations was typically 145 cm⁻¹. In subsequent work⁷⁹ and in the present work, we worked up the fbCytc and ZnCytc products using ion-exchange chromatography using the approach used by Winkler and coworkers and Kostić and coworkers.^{92,93} These preparations exhibit absorption and fluorescence spectra with narrower vibronic lineshapes; the reader should compare Figure 3.1 in this paper with the similar figure in reference 78. The smaller value for λ obtained with the ion-exchange procedure arises primarily from the narrower lineshapes, and we find that it is consistent from preparation to preparation.

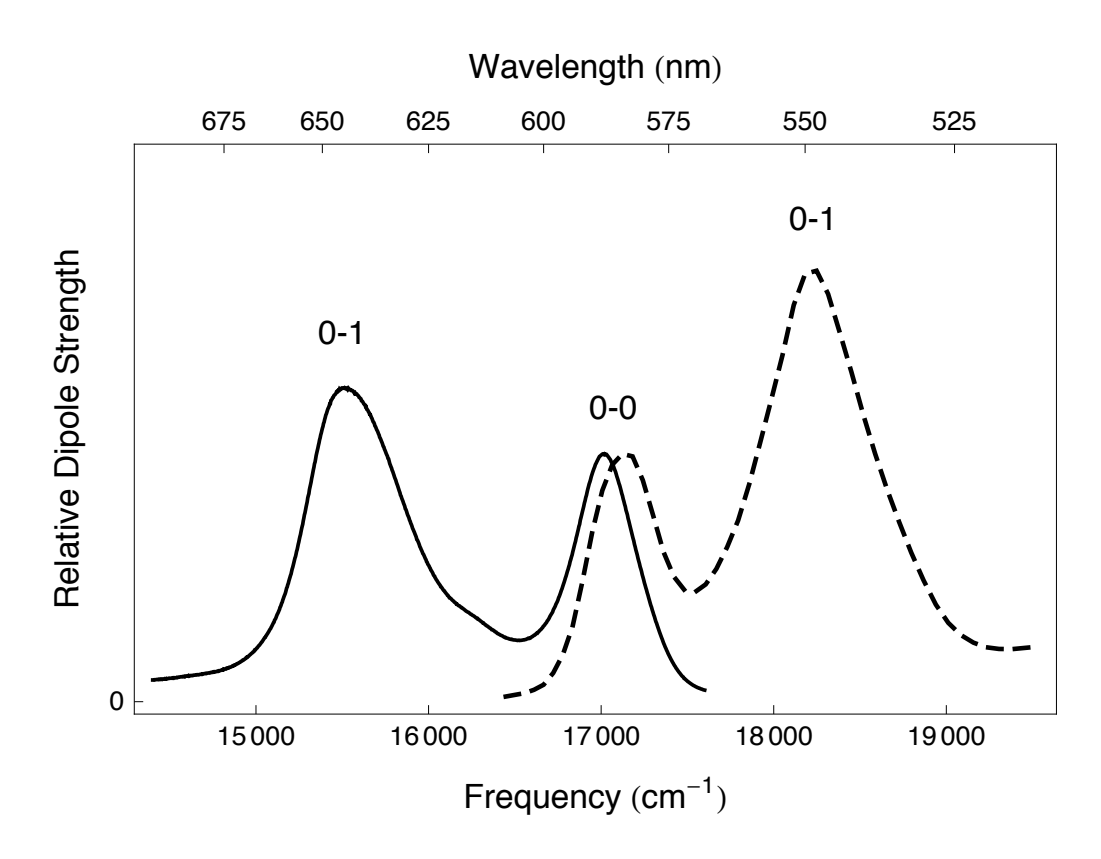


Figure 3.1. *Q*-band region of the absorption and fluorescence spectra from ZnCytc in water at 22°C and pH 7.0. The spectra are plotted as relative dipole strengths, A(v)/v (dashed line) and $F(v)/v^3$ (solid line), respectively. The spectra are scaled such that the 0-0 peaks have the same relative intensity.

As Gdm⁺ is added to ZnCytc solutions, the fluorescence spectrum exhibits two types of changes that report the denaturation of the protein structure (see Figure 3.2). The first is a shift to the blue according to a two-state cooperative transition with a midpoint Gdm⁺ concentration of ~2.0 M. Figures 3.3 and 3.4 show the Gdm⁺ titration curves from ZnCytc obtained by plotting separately the trends of the peak wavenumbers for the 0–0 and 0–1 fluorescence and absorption transitions, respectively, as a function of the Gdm⁺ concentration. The model curves used in Figures 3.3 and 3.4 assume an equilibrium between the unfolded (U) and native (N) states, here stated as a folding reaction:

$$\begin{array}{c}
K_{\text{eq}} \\
U \Longrightarrow N
\end{array} \tag{3.2}$$

The Gibbs free energy of folding can be then expressed as

$$\Delta G_{\text{Fold}} = -RT \ln \left(\frac{1 - f_u}{f_u} \right) = \Delta G_{\text{Fold}}^{\text{H}_2\text{O}} + m \left[\text{Gdm}^+ \right]$$
 (3.3)

where f_u represents the fraction of unfolded proteins in the ensemble, $\Delta G_{\rm Fold}^{\rm H_2O}$ relates the Gibbs free energy of folding in pure water, and m relates the change in Gibbs free energy that occurs with the addition of $\rm Gdm^+$ to the solution. Solving for f_u , we obtain

$$f_{\rm u} = \left[1 + \exp\left(-\frac{\Delta G_{\rm Fold}^{\rm H_2O} + m \left[\rm Gdm^+ \right]}{RT} \right) \right]^{-1}$$
 (3.4)

The titration curves, $f_{\rm u}$ as a function of Gdm⁺ concentration, were calculated from the observed 0-0 and 0-1 peak wavenumbers using a series of simulated spectra (see Figure 3.5) determined as the linear combination of the experimental spectra observed in the native ($f_{\rm u}=0$) and unfolded ($f_{\rm u}=1$) states, respectively. The lineshape parameters (center frequency, ω_0 , width, σ , and asymmetry, ρ , see Table 3.1) for the native and unfolded states were determined by fitting a lognormal lineshape 97 to the experimental spectra at 0.0 M and 5.0 M Gdm⁺. As shown in Figures 3.3 and 3.4, Equation 3.4 serves as a good fitting model for the experimental data and does a

good job of describing the blue shift of both vibronic peaks in absorption as well as emission spectra of ZnCytc as Gdm⁺ is added to the protein solution. At the midpoint ($f_u = 0.5$) of these transitions, the two states are at equilibrium ($\Delta G_{\rm Fold} = 0$); from Equation 3.3, we then obtain

$$\Delta G_{\text{Fold}}^{\text{H}_2\text{O}} = -m \left[\text{Gdm}^+ \right]_{1/2} = -m C_m \tag{3.5}$$

where C_m represents the denaturant concentration at the midpoint of the transition.

Table 3.2 lists the fit parameters obtained for the fluorescence and absorption Gdm⁺ titration curves for ZnCytc shown in Figures 3.3 and 3.4. The averaged thermodynamic parameters for the fluorescence and absorption transitions are statistically similar. While the transition midpoints for the 0-0 and 0-1 peaks of fluorescence are within 0.1 M on the Gdm⁺ axis, the midpoint for the 0-0 peak of the Q band absorption occurs about 0.16 M later on the Gdm⁺ axis than that for the 0-1 peak. This observation suggests that the Zn^{II}-porphyrin in ZnCytc is somewhat strained in the native state (vide infra); the response of the spectrum is somewhat inhomogeneous with respect to the effect of Gdm⁺ in both ground and excited state. Bhuyan et al. has shown that FeCytc in the presence of Gdm $^{+145}$ has a $\Delta G_{\mathrm{Fold}}^{\mathrm{H_2O}} = -30.96$ kJ/mol using fluorescence intensity from the intrinsic tryptophan residue as a measure of the folded state. On average, the fit parameters show that ZnCytc is significantly less stable than FeCytc but perhaps more stable than the metal free cytochrome c as evidenced from studies in urea induced unfolding;87,146 the Gibbs free energy of unfolding for ZnCytc is one-third that of FeCytc. The folded structure of ZnCytc is less sensitive than FeCytc to Gdm^+ , however, because the m value is significantly smaller.¹⁴⁵ This parameter largely controls the sharpness of the sigmoidal transition; the response is less abrupt in ZnCytc than FeCytc. These findings suggest that the axial coordination of the metal ion in cytochrome c plays an important role in controlling the stability of the native fold.

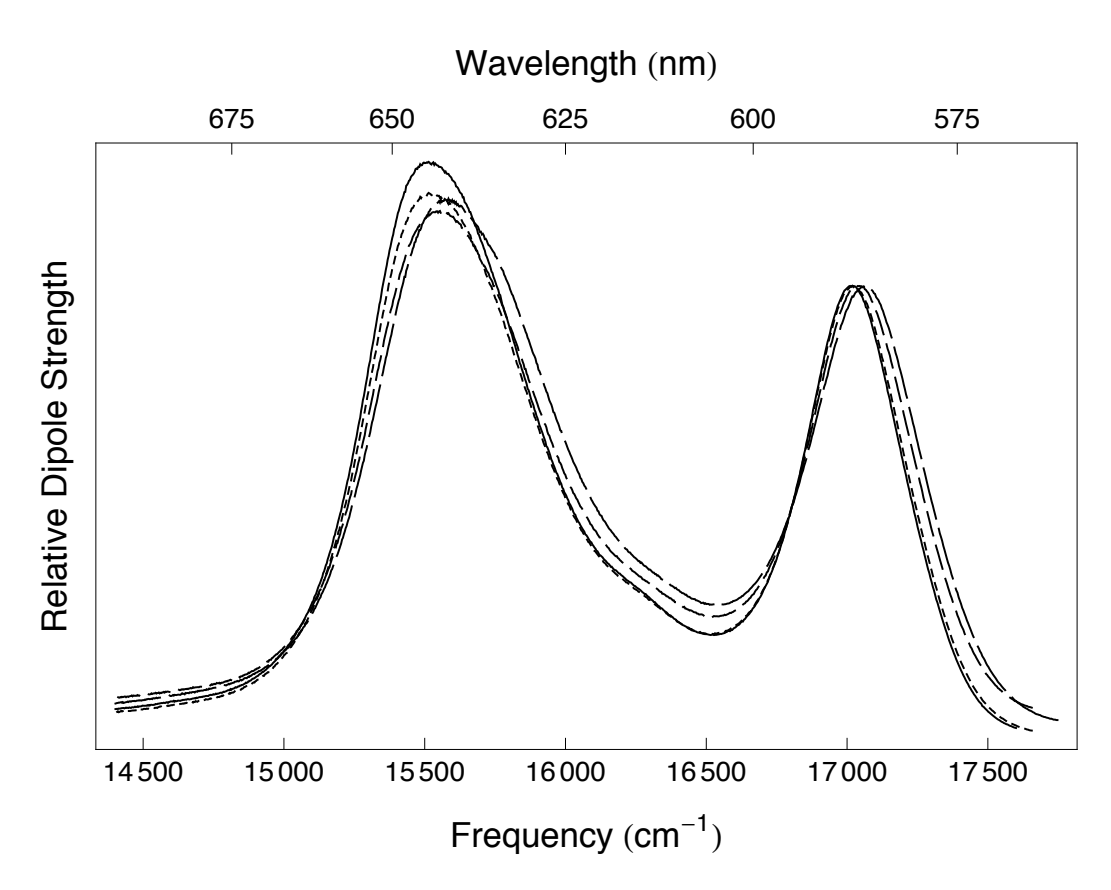


Figure 3.2. Fluorescence spectra from ZnCytc at 22°C and pH 7.0 in water (solid line) and in the presence of Gdm⁺ at 1 M (- - -), 2 M (- - -) and 3 M (— — —). The spectra are plotted as relative dipole strengths, $F(\nu)/\nu^3$, and are normalized by the intensity of the 0–0 peak.

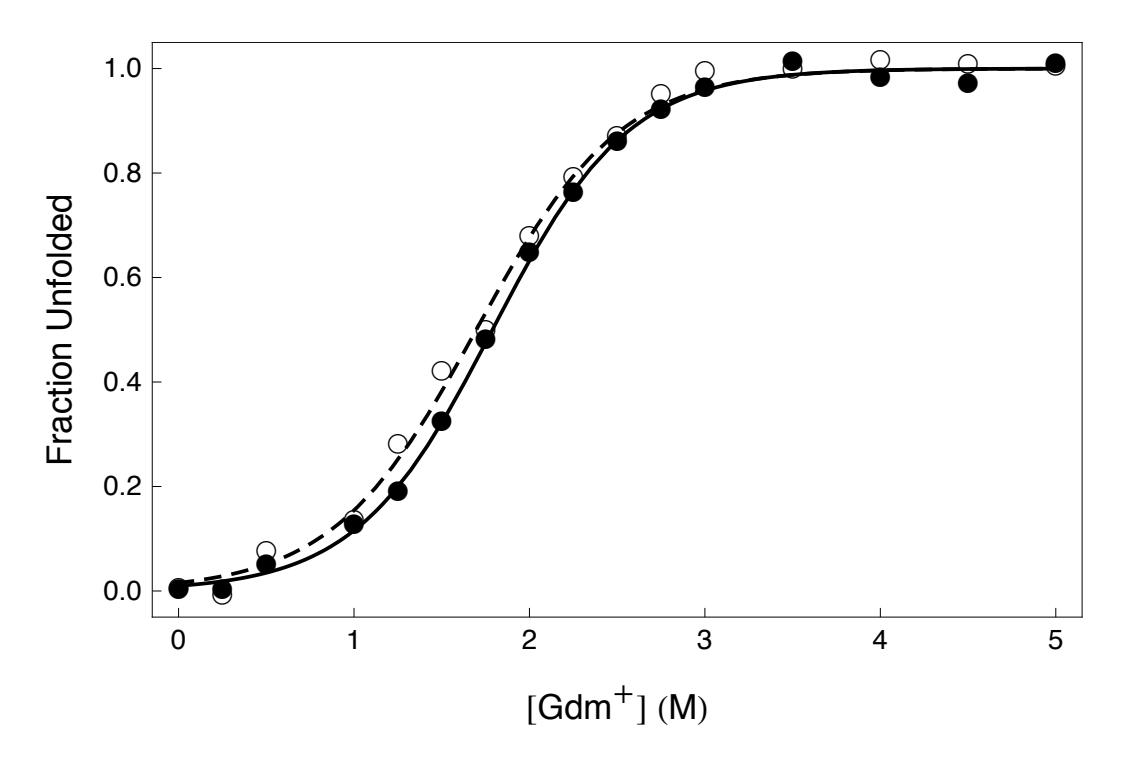


Figure 3.3. Gdm⁺ fluorescence titration curves for ZnCytc at 22°C and pH 7.0. The fraction of unfolded proteins in the ensemble determined from the wavenumber of the peak maximum of the 0–0 and 0–1 peaks in the fluorescence spectrum is plotted as a function of the Gdm⁺ concentration; the data points are superimposed upon separate models for a two-state unfolding transition (Equation 3.4). The thermodynamic parameters for the unfolding transition are listed in Table 3.2.

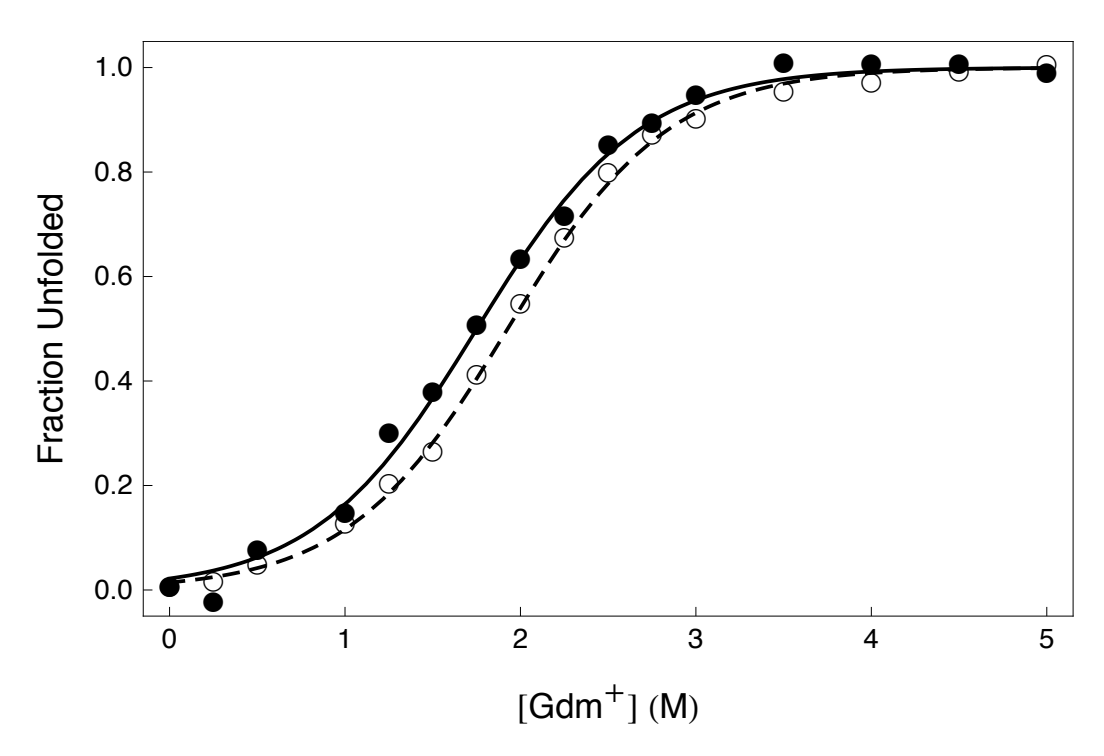


Figure 3.4. Gdm⁺ absorption titration curves for ZnCytc at 22°C and pH 7.0. The fraction of unfolded proteins in the ensemble determined from the wavenumber of the peak maximum of 0–0 and 0–1 peaks in the absorption spectrum is plotted as a function of the Gdm⁺ concentration; the data points are superimposed upon separate models for a two-state unfolding transition (Equation 3.4). The thermodynamic parameters for the unfolding transition are listed in Table 3.2.

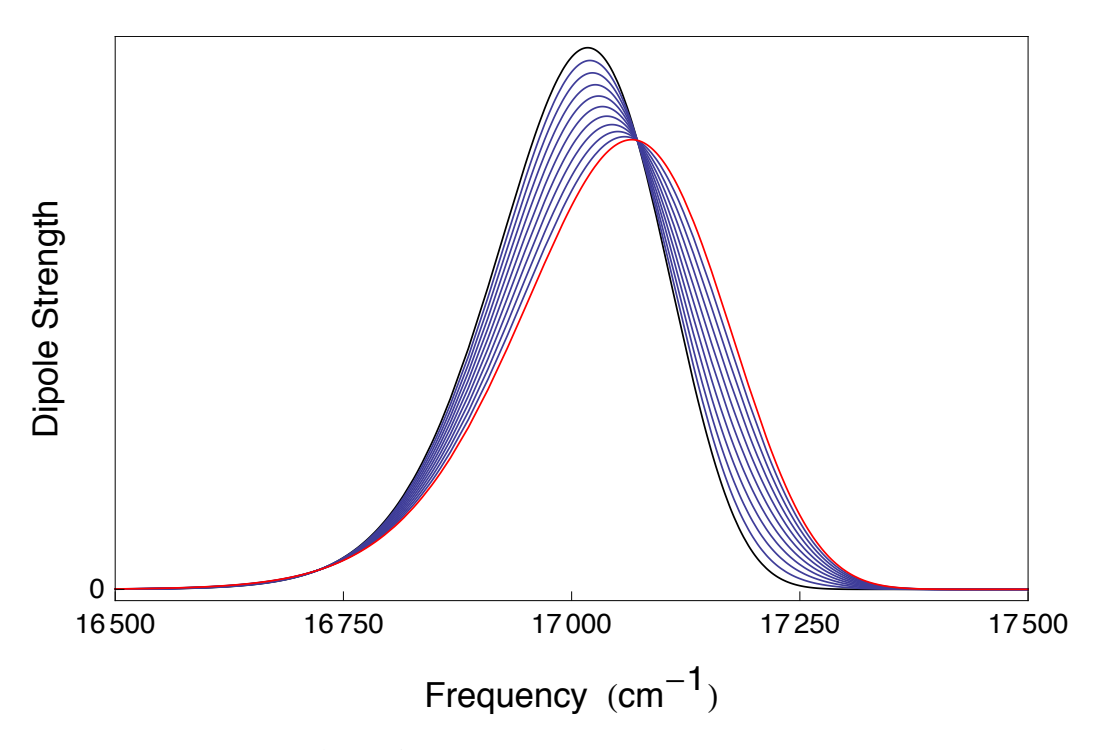


Figure 3.5. Simulation of the fluorescence spectral changes that accompany Gdm⁺ unfolding of ZnCytc. Fluorescence emission (dipole strength) spectra are shown for the native state (0 M Gdm⁺, black) and the unfolded state (5 M Gdm⁺, red) and at several states with fractional unfolding (0.1–0.9, blue curves). Table 3.1 lists the lognormal lineshape parameters that were used to calculate the fractionally unfolded spectra as linear combinations of native and unfolded spectra.

Table 3.1. Absorption (Q) and fluorescence (F) lognormal lineshape parameters^a for the unfolding transition of ZnCytc in the presence of Gdm^+ .

	$\omega_0 (\mathrm{cm}^{-1})$	σ (cm ⁻¹)	ρ
F_{0-0} , Native ^b	17017.6	220	1.2
F_{0-0} , Unfolded ^c	17065.9	265	1.2
F_{0-1} , Native	15513.1	437.8	1.2
F_{0-1} , Unfolded	15580.2	478.9	1.2
Q_{0-0} , Native Q_{0-0} , Unfolded Q_{0-1} , Native Q_{0-1} , Unfolded	17148.5	268.4	1.1
	17227.6	349.5	1.1
	18227.6	413.7	1.1
	18336.9	441.7	1.1

^a See the text.

b Native = 0 M Gdm⁺.

^c Unfolded = 5 M Gdm^+ .

Table 3.2. Thermodynamic parameters for the equilibrium unfolding transition^a for ZnCytc and the transition midpoints.

	$\Delta G_{\text{Fold}}^{\text{H}_2\text{O}}$ (kJ/mol)	m (kJ/mol/M)	C _m (M)
F_{0-0} F_{0-1} bAverage	-11.31 ± 0.30 -10.16 ± 0.45 -10.74 ± 0.54	6.32 ± 0.42 5.99 ± 0.25 6.16 ± 0.49	1.79 ± 0.13 1.70 ± 0.10 1.75 ± 0.16
Q_{0-0} Q_{0-1} ^c Average	-10.60 ± 0.63 -10.36 ± 0.35 -10.48 ± 0.52	5.99 ± 0.34 5.38 ± 0.18 5.69 ± 0.15	$\begin{array}{c} 1.77 \pm 0.15 \\ 1.93 \pm 0.09 \\ 1.85 \pm 0.10 \end{array}$

^a See Equation 3.4 and Figures 3.3 and 3.4.

^b Average of the two fluorescence transitions.

^c Average of the two absorption transitions.

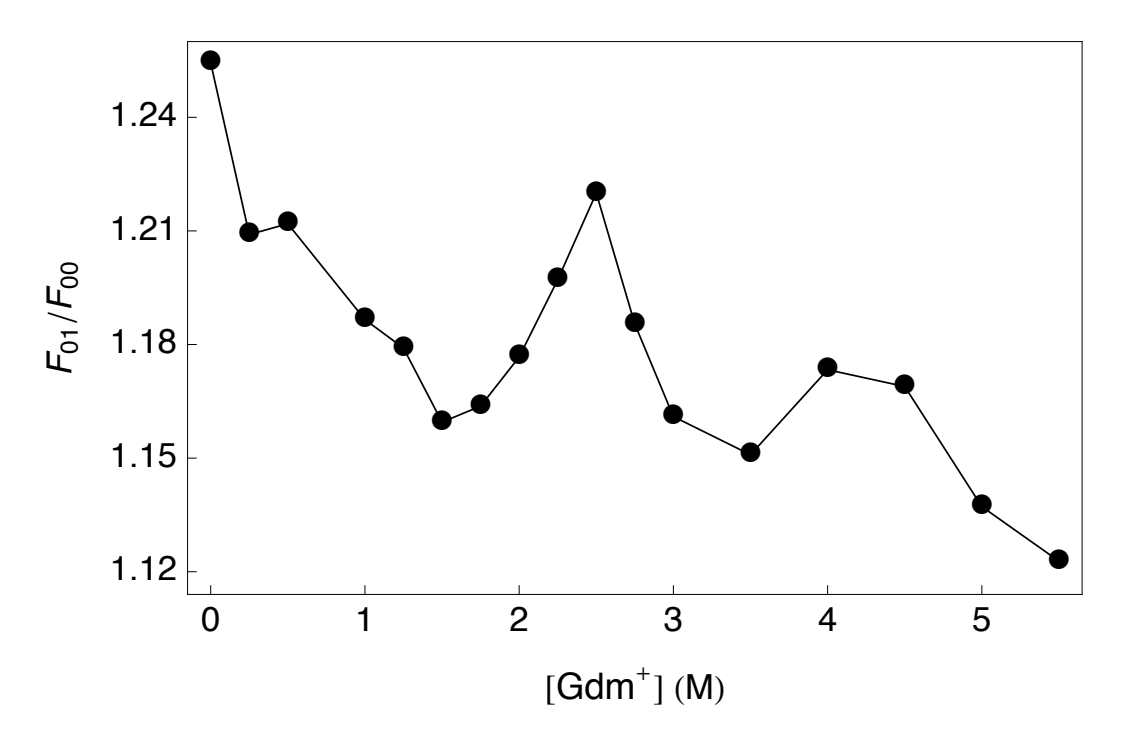


Figure 3.6. Dependence on the Gdm^+ concentration of the ratio of the intensity of the 0–1 and 0–0 vibronic peaks in the fluorescence spectrum from ZnCytc at $22^{\circ}C$ and pH 7.0.

The second change in the fluorescence spectrum that accompanies the denaturation reaction in the presence of Gdm^+ is a decrease in the ratio of the intensity of the 0–1 and 0–0 peaks, F_{01}/F_{00} (see Figure 3.6). The overall decreasing trend is broken by a positive peak at 2.5 M, and the ratio oscillates over the 3.5–5.0 M Gdm^+ range. As discussed previously, 76,79 the F_{01}/F_{00} ratio is sensitive to the dissociation and rebinding of axial ligands to the Zn^{II} ion; the ratio increases as the M80 and H18 ligands dissociate in the S_1 excited state. The trends in the F_{01}/F_{00} ratio suggest that the protein structure reorganizes as Gdm^+ is added so that alternate ligands are accessible to the Zn^{II} ion. 79

3.3.2 Picosecond Fluorescence Anisotropy Decays

FA transients from ZnCytc as a function of the Gdm⁺ concentration were acquired with the excitation laser tuned to the wavenumber of the 0–0 transition (see Figure 3.1) and with emission wavelengths scanned fully across the 0–1 peak. The parallel (I_{\parallel}) and perpendicularly (I_{\perp}) polarized fluorescence transients were acquired simultaneously, and the FA transient was computed directly as

$$r(t) = \frac{I_{\parallel}(t) - I_{\perp}(t)}{I_{\parallel}(t) + 2I_{\perp}(t)}$$
(3.6)

The FA transients were fit to a biexponential model

$$r(t) = A_1 e^{-t/\tau_1} + A_2 e^{-t/\tau_2}$$
(3.7)

As will be discussed in the following section, the shorter of the two anisotropy timescales corresponds essentially to motion of the Zn^{II}-porphyrin's transition dipole moment with respect to the protein, whereas the longer timescale is associated with rotational diffusion of the entire protein.

In order to assess whether the 0–1 peak is homogeneous with respect to the FA decays, we compared single-wavelength FA transients from ZnCytc in water detected

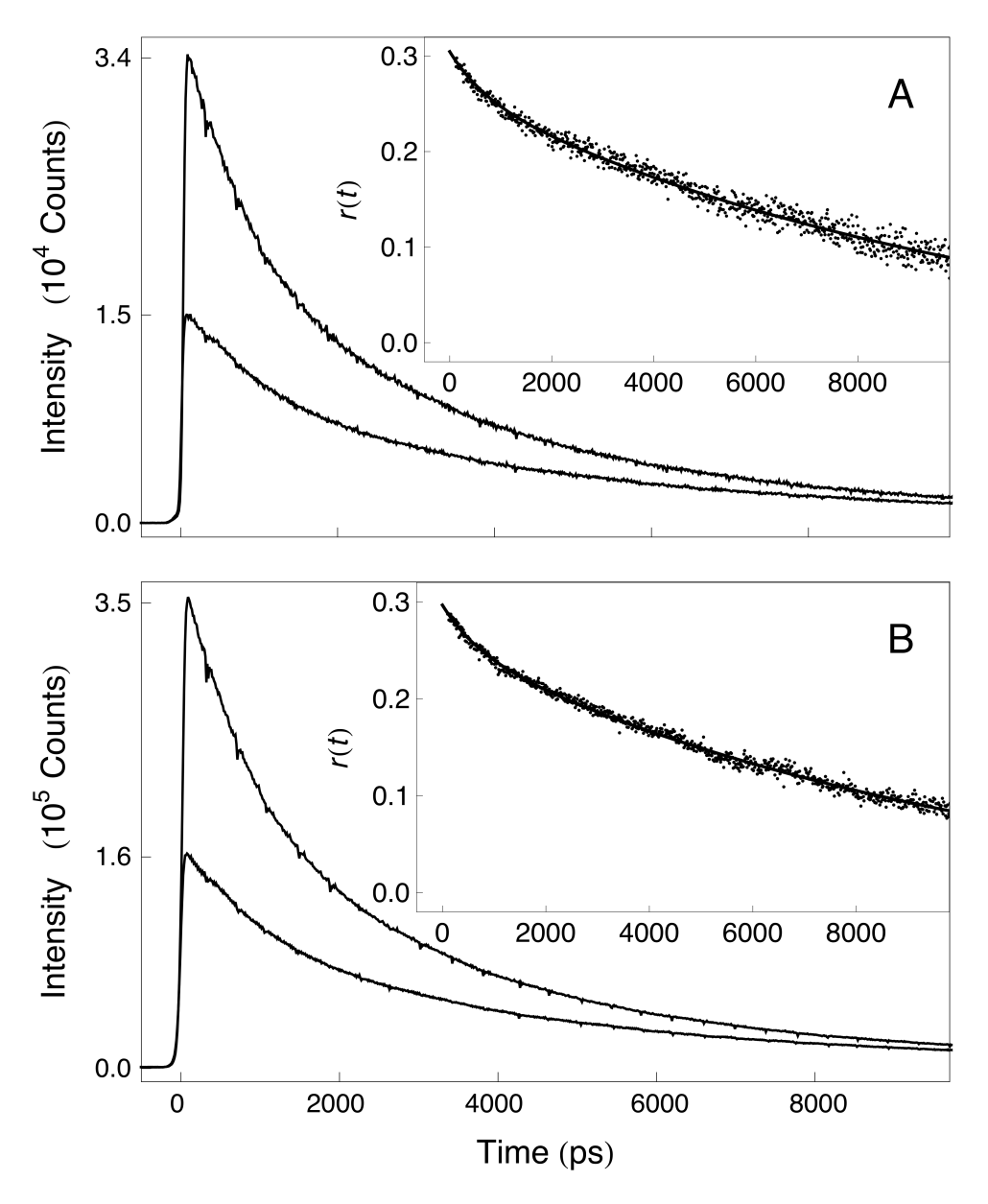


Figure 3.7. Polarized fluorescence emission transients from ZnCytc in water at 22°C. The parallel and perpendicular transients obtained from: (a) Single-wavelength transients recorded at 640 nm, at the peak of the 0–1 vibronic band. (b) Integral of single-wavelength transients across the 0–1 vibronic band (14750–16700 cm⁻¹). The spikes in the polarized emission transients arise from the timing electronics of the detection system. The insets for (a) and (b) show the anisotropy transients computed from the intensity transients using Equation 3.6 superimposed on a fitted biexponential decay defined by Equation 3.7. The model parameters for the fitted transients are: (a) $A_1 = 0.041$, $\tau_1 = 685.02$ ps, $A_2 = 0.306$, $\tau_2 = 10.63$ ns, and (b) $A_1 = 0.041$, $\tau_1 = 686.0$ ps, $A_2 = 0.285$, and $\tau_2 = 10.64$ ns.

at the peak maximum with those obtained by integrating over the entire width of the band. Figure 3.7 shows that the single-wavelength and integrated FA transients are described by indistinguishable biexponential models but that the integrated transients have significantly higher signal/noise ratios. In the following analysis, we employ the integrated FA transients exclusively.

The dichroism-free intensity of fluorescence emission was computed from the polarized transients as

$$I(t) = I_{\parallel}(t) + 2I_{\perp}(t) \tag{3.8}$$

Figure 3.8 compares the single-wavelength and integrated intensity transients. Both are well described by biexponential models with comparable intensities for the two components. The average fluorescence lifetime for the Zn^{II} -porphyrin in ZnCytc is 3.98 ns; Vanderkooi *et al.* has previously measured an average lifetime of \sim 3.2 ns. The biexponential decay of fluorescence intensity in ZnCytc was noted previously by Vanderkooi; the two lifetimes probably arise from distinct instantaneous conformations of the Zn^{II} -porphyrin. A similar biexponentiality is noted for Zn^{II} tetraphenylporphyrin (ZnTPP) and tetrakis (N-methyl-4-pyridyl) porphyrin Zn^{II} (ZnTMPyP). Thus, the results noted here for ZnCytc do not necessarily arise from a spectral or protein conformational heterogeneity.

Figure 3.9 shows a set of FA transients from ZnCytc over a range of Gdm⁺ concentrations. As was observed in the absence of Gdm⁺ (see Figure 3.7), a biexponential model (Equation 3.7) provides an excellent description of all the decays. Table 3.3 lists the model parameters for all the Gdm⁺ concentrations studied. Plots of the fit parameters (see Figures 3.10–3.12) show that significant changes in the anisotropy decays are observed at Gdm⁺ concentrations prior to the unfolding transition. Figure 3.10 shows that the amplitude A_1 that scales the component with the shorter time constant, τ_1 , increases as Gdm⁺ is added. In contrast, the amplitude A_2 for the slower component with the time constant τ_2 decreases as the concentration of

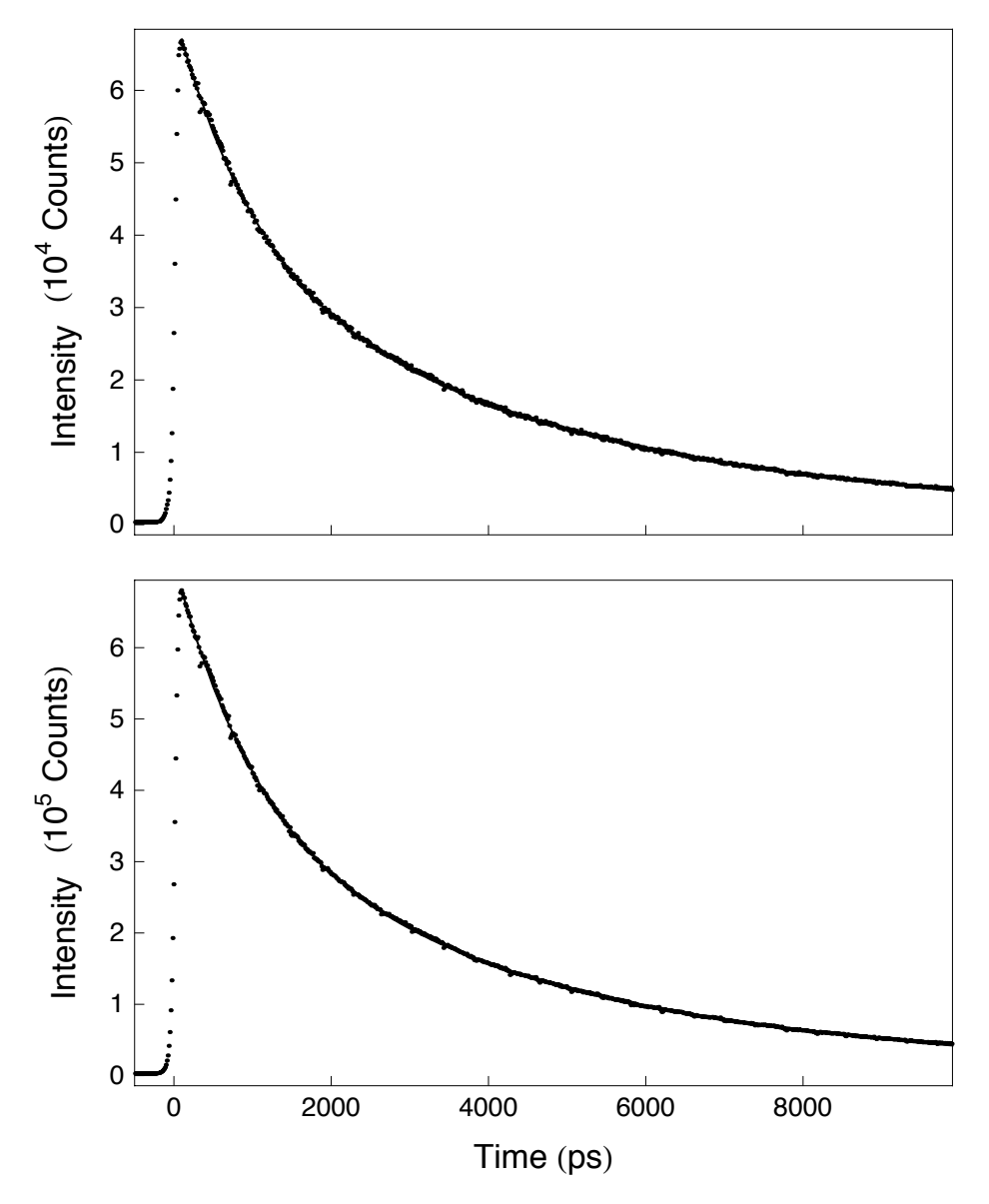


Figure 3.8. Comparison of single-wavelength (top) and integrated (bottom) dichroism-free fluorescence intensity transients from ZnCytc in water at 22°C calculated from the polarized fluorescence transients as $I_{\parallel} + 2I_{\perp}$. The single-wavelength transient was recorded at 640 nm, the peak of the 0–1 band. The integrated transient is the sum of the single-wavelength transients recorded at ten wavelengths across the 0–1 vibronic band. The data points in the two transients are each superimposed on a biexponential decay model. The model parameters for the single-wavelength transient are: I_1 =34563.5±175, τ_1 =1025.9±8.2 ps, I_2 =36429.8±203.7, τ_2 =4852.3±21 ps. The model parameters for the integrated transient are: I_1 =369290±1688, τ_1 =1041.2±7 ps, I_2 =352295±1960, τ_2 =4668±19 ps.

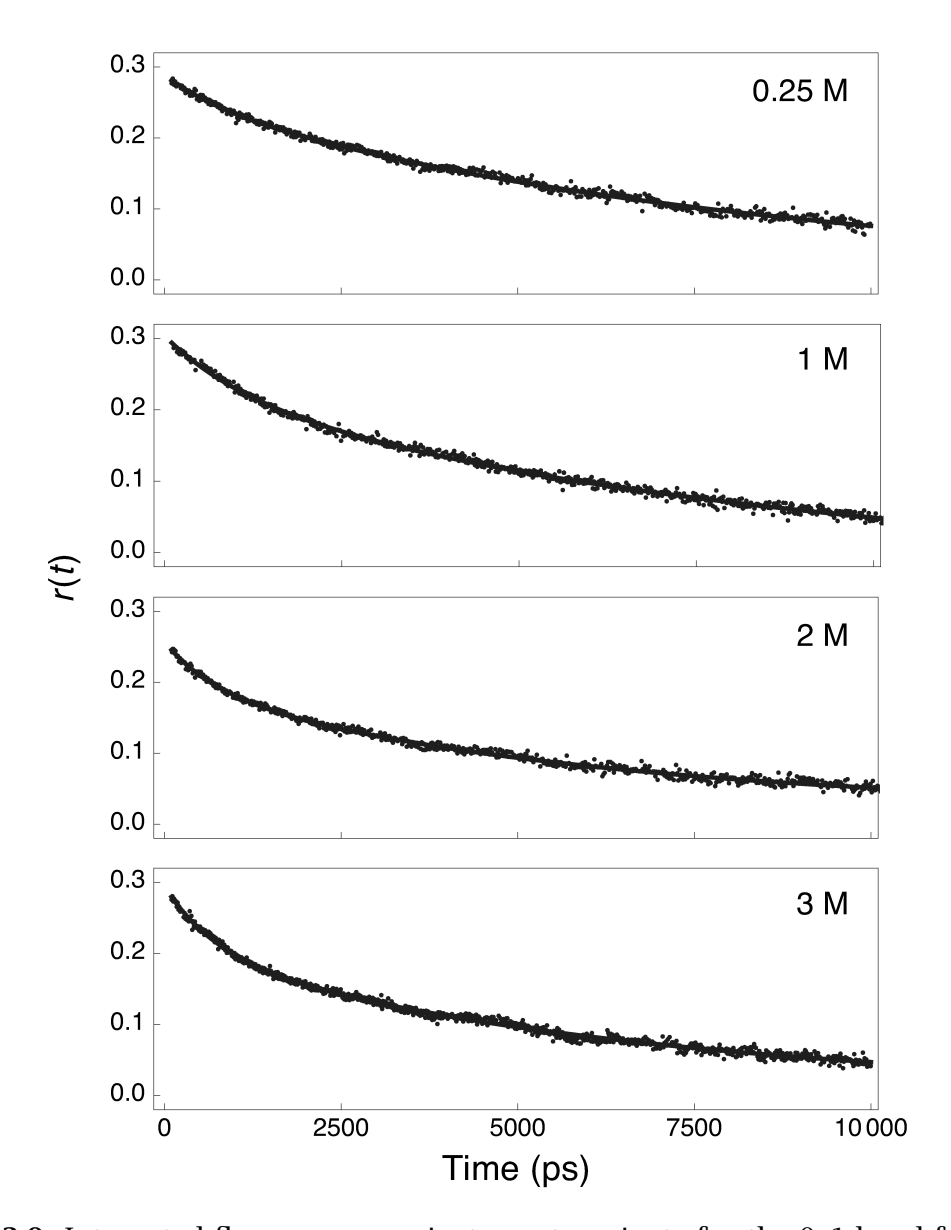


Figure 3.9. Integrated fluorescence anisotropy transients for the 0-1 band from Zn-Cytc at 22°C and pH 7.0 as a function of the Gdm⁺ concentration. The data points are superimposed on a biexponential model defined by Equation 3.7. The fit parameters are listed in Table 3.3.

Table 3.3. Fluorescence anisotropy decay parameters for ZnCytc in the presence of Gdm^+ at $22^{\circ}C$.

Gdm ⁺ (M)	A_1^{a}	τ_1 (ps)	A_2	τ_2 (ns)
0.00 0.25 0.50 1.00 1.50 2.00 3.00 4.00	0.048 ± 0.01 0.034 ± 0.005 0.04 ± 0.002 0.101 ± 0.019 0.10 ± 0.035 0.082 ± 0.029 0.095 ± 0.004 0.101 ± 0.033	780 ± 94 723 ± 141 860 ± 24 1157 ± 32 925 ± 157 776 ± 164 844 ± 114 $857 + 225$	0.278 ± 0.01 0.225 ± 0.029 0.229 ± 0.006 0.242 ± 0.022 0.220 ± 0.011 0.198 ± 0.021 0.195 ± 0.003 0.208 ± 0.021	10.47 ± 0.16 9.06 ± 0.53 8.21 ± 0.30 8.51 ± 0.62 7.14 ± 0.84 5.78 ± 0.21 7.33 ± 0.89 6.18 ± 0.46
5.00	0.105 ± 0.026	707 ± 158	0.209 ± 0.006	6.81 ± 0.56

^a See Equation 3.7.

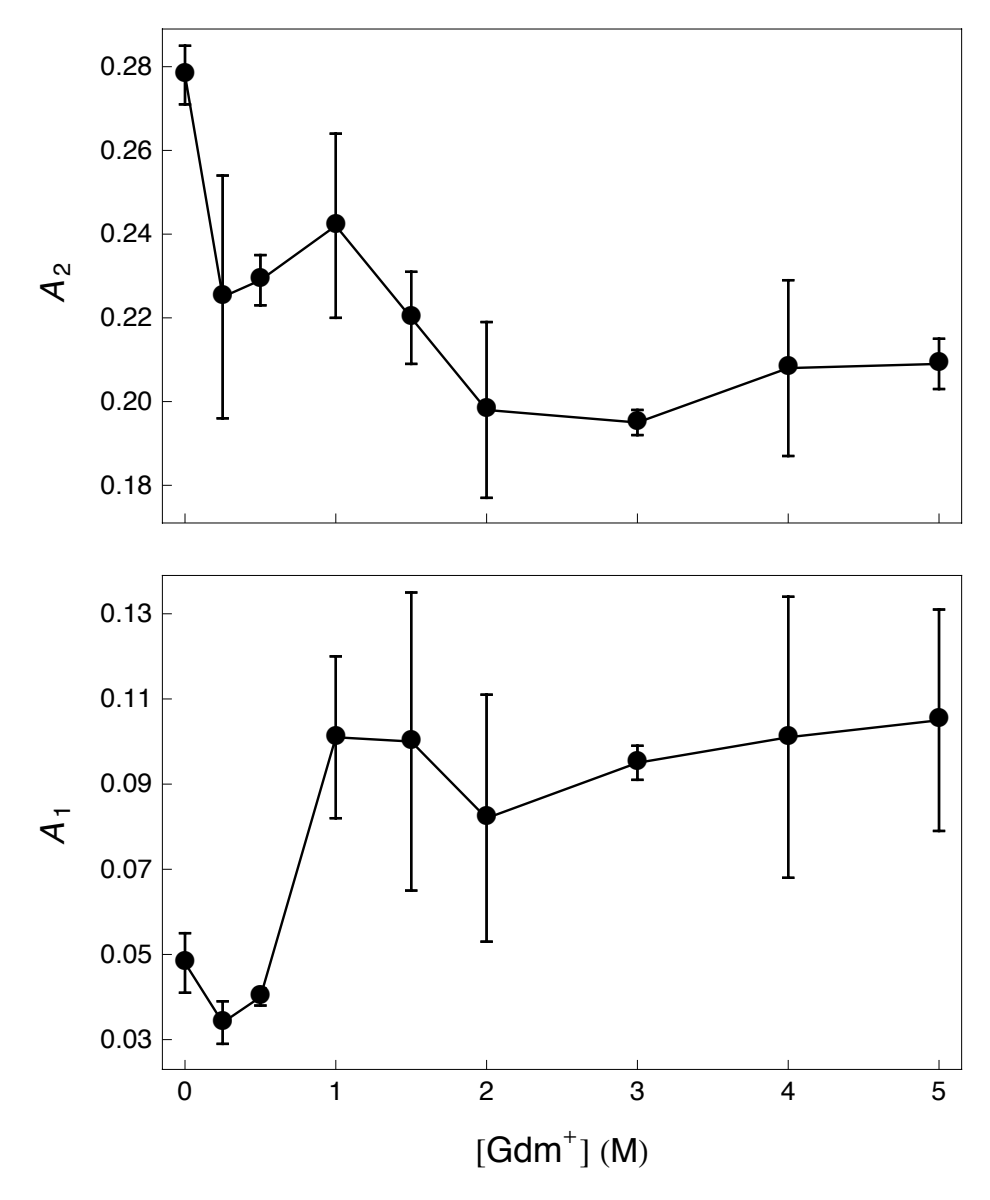


Figure 3.10. Anisotropy decay amplitudes (see Equation 3.7 and Table 3.3) for ZnCytc at 22°C and pH 7.0 as a function of the Gdm⁺ concentration.

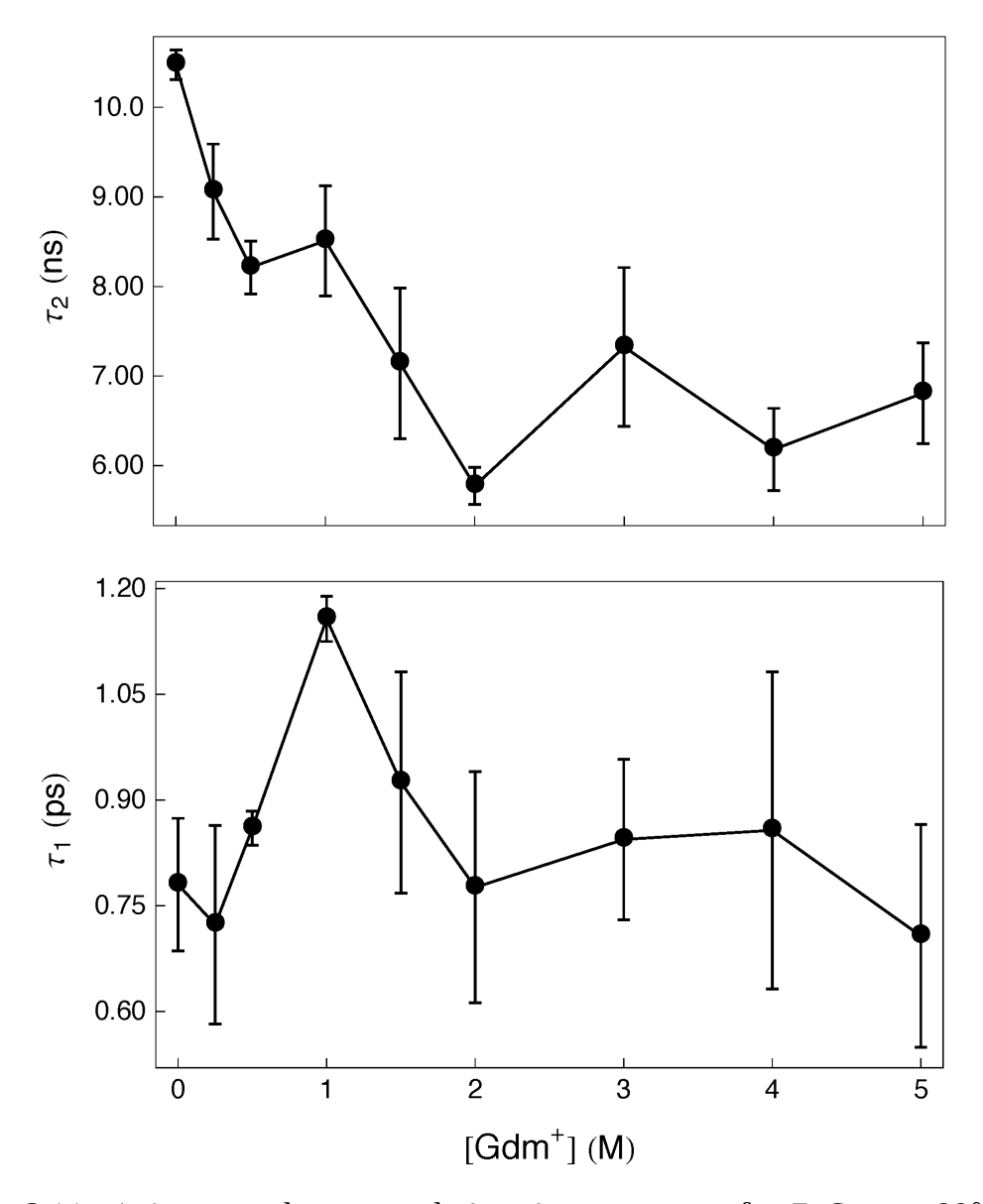


Figure 3.11. Anisotropy decay correlation time constants for ZnCytc at 22°C and pH 7.0 as a function of the Gdm⁺ concentration. The model parameters are listed in Table 3.3. These time constants are related to the time constants in the mechanical model via Equation 3.13 and 3.14.

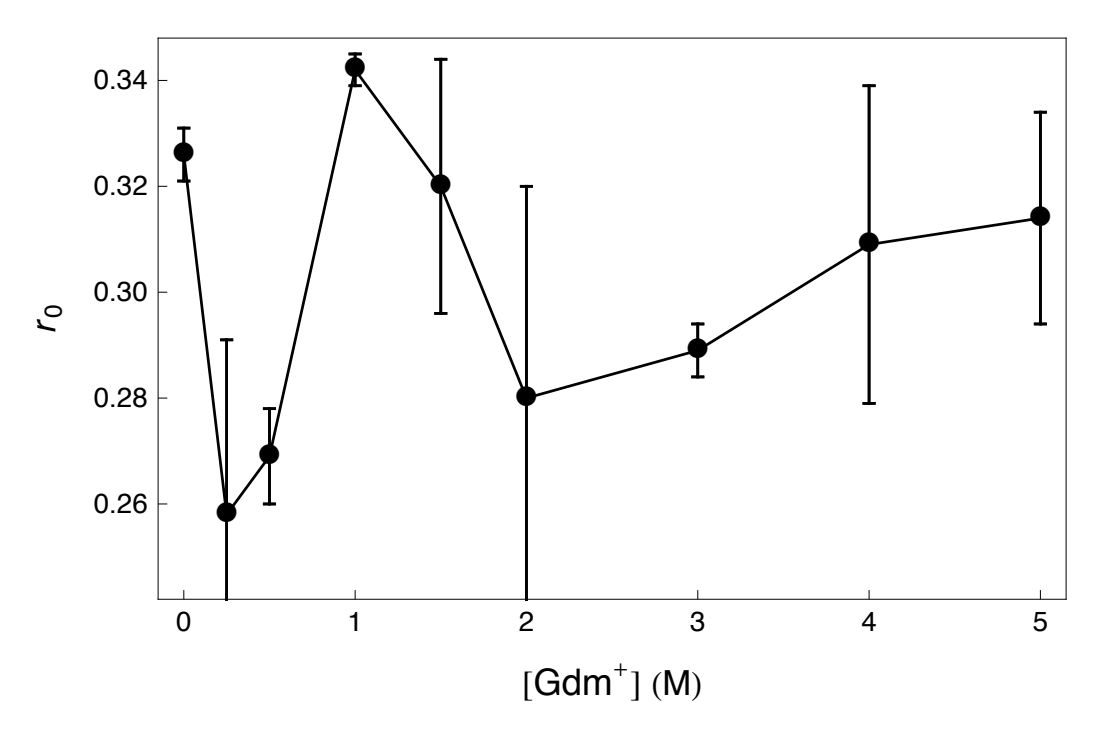


Figure 3.12. Gdm⁺ concentration dependence of r_0 , the total anisotropy amplitude (see Equation 3.7 and Table 3.3) at time t=0, for ZnCytc at 22°C and pH 7.

Gdm⁺ increases. Both curves show inflections in the 0.25 M and 1.0 M regions. Both amplitudes are more or less constant after the unfolding transition at 2.0 M Gdm⁺; A_1 is more or less constant after ~1.0 M if we consider the error bars. A similar trend is indicated by Figure 3.11, which shows that the time constants τ_1 and τ_2 are essentially constant at Gdm⁺ concentrations above 2.0 M. Well prior to the unfolding transition, however, τ_1 exhibits a broad peak, and τ_2 exhibits an inflection centered at 1 M Gdm⁺. Figure 3.12 shows that the initial (t = 0) anisotropy amplitude r_0 also exhibits a peak in the 1 M region that is superimposed on a generally increasing trend. Note that r_0 is significantly less than 0.4 in water and that an abrupt decrease in the 0-0.5 M Gdm⁺ region is observed; these observations imply that there is a fast depolarization on the <100-ps timescale that arises from electronic state degeneracy¹¹² and that the presence of Gdm⁺ even at very low concentrations has an effect on the electronic properties of the Zn^{II} porphyrin. Thus, even prior to the application of a mechanical model for the fluctuations that gives rise to the faster of the two anisotropy decay components, these results suggest that one or more partially unfolded structures are populated at Gdm⁺ concentrations below the unfolding transition.

3.3.3 Wobbling-in-Cone Mechanical Model

A mechanical model that describes the internal motion of the transition dipole moment of the Zn^{II}-porphryin in ZnCytc with respect to the overall protein structure is the wobbling-in-cone (WIC) model (see Figure 3.13) introduced by Kinosita *et al.* to describe the anisotropy decay of a fluorescent probe in lipid membranes. ^{149,150} This model has been used extensively to treat internal motion of a probe in proteins. ^{151–153} The WIC model describes how the diffusive tilting motion of the transition dipole moment of a probe around its center exhibits a limiting cone angle with respect to the frame of a tumbling protein to which the probe is bound. This

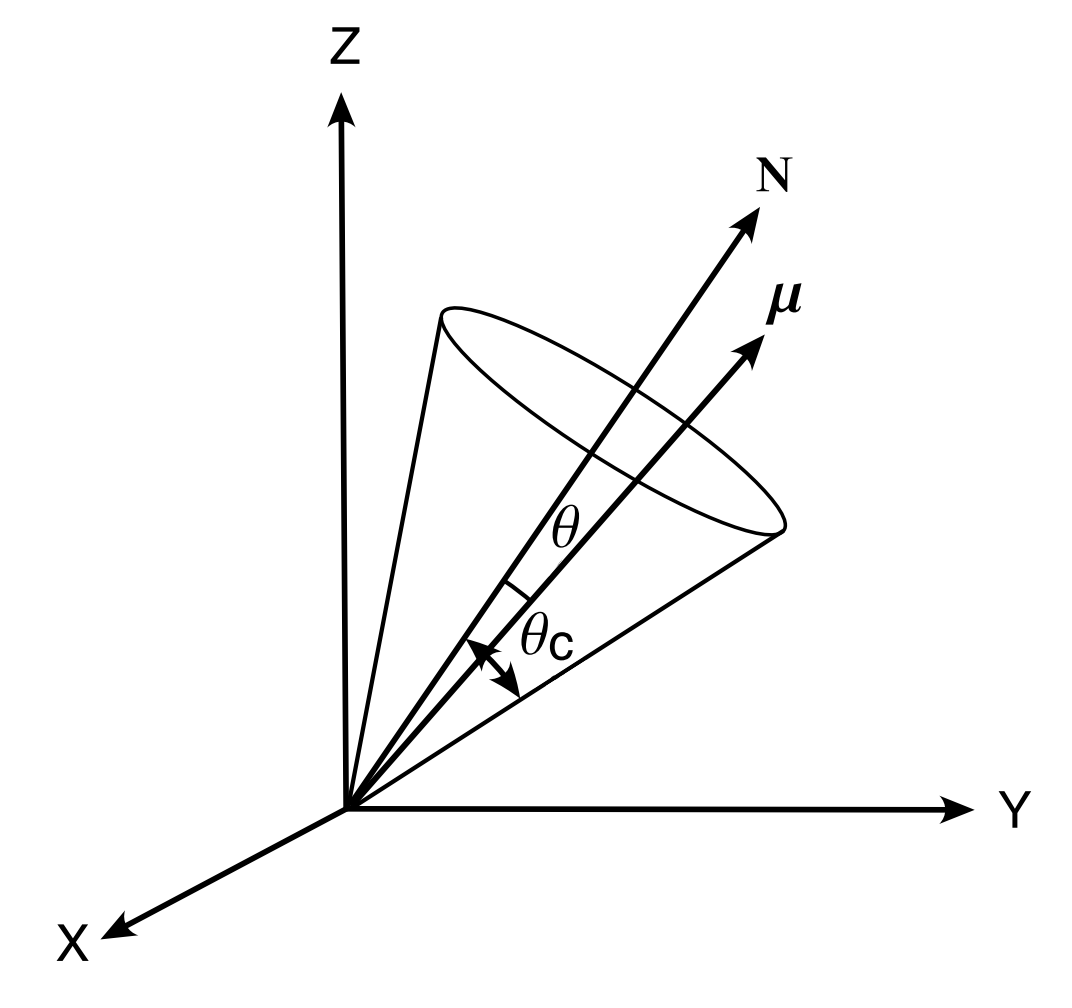


Figure 3.13. Wobbling-in-cone model for fluorescence depolarization arising from protein dynamics. The probe's transition dipole moment μ diffuses within a cone of half angle θ_c with respect to the normal vector, N, which is carried by the protein's frame. Adapted from reference 149.

model can be reasonably applied to ZnCytc because the porphyrin is linked to the polypeptide backbone by the two cysteine residues C14 and C17 at one corner of the macrocycle, and the axial ligands to the Zn^{II} ion from the histidine and methionine residues H18 and M80 and the cleft in the native structure constrain the porphyrin orthogonally to its plane (see Figure 1.3).

Using the notation of reference 149, the total anisotropy, r(t), of the system can be expressed as the product of the anisotropy due to the motion of the probe, $r_p(t)$, and that due to the overall rotation of the protein, $r_r(t)$, as

$$r(t) = r_p(t) \times r_r(t) \tag{3.9}$$

The WIC model assumes that the internal and tumbling motions are mechanically independent. If the internal motions are constrained by a structural limitation, the resulting anisotropy decay is described by, 94,154

$$r(t) = r_0[(1 - S^2) e^{-t/\tau_{\text{int}}} + S^2] e^{-t/\tau_{\text{rot}}}$$
(3.10)

where τ_{int} and τ_{rot} are the correlation time scales for the internal and tumbling motions and S is a generalized order parameter that can be expressed in terms of the ensemble average of the second Legendre polynomial,

$$S = \langle P_2(\cos \theta) \rangle \tag{3.11}$$

where θ is the angle between the instantaneous transition dipole-moment vector, μ , and the normal vector, N, along the symmetry axis of the protein molecule (see Figure 3.13). In terms of the cone angle, θ_c , that describes the structural constraint, S is determined as

$$S = \frac{1}{2}\cos\theta_C(\cos\theta_C + 1) \tag{3.12}$$

The fit parameters obtained from the phenomenological biexponential models for the experimental anisotropy decays (see Equation 3.7) can be used to calculate the parameters in Equation 3.10 as follows. The internal and tumbling correlation times are determined by

$$\tau_{\text{int}} = (1/\tau_1 - 1/\tau_2)^{-1} \tag{3.13}$$

$$\tau_{\text{rot}} = \tau_2 \tag{3.14}$$

Thus, the slower of the two anisotropy decay time constants corresponds directly to the tumbling timescale, and the internal timescale is obtained as the harmonic mean of the two experimental time constants. The relation for the square of the order parameter is obtained from the amplitudes of the anisotropy decay components as

$$S^2 = A_2/r_0 = A_2/(A_1 + A_2) \tag{3.15}$$

Table 3.4 lists the model parameters we obtained from the fitted ZnCytc anisotropy decays in the presence of Gdm⁺.

Figure 3.14 shows the dependence of the correlation times for internal motion and overall tumbling on the Gdm⁺ concentration. The correlation time constants $\tau_{\rm int}$ and $\tau_{\rm rot}$ are almost an order of magnitude different in time scale (see Table 3.4). Except for a peak centered at 1.0 M Gdm⁺, the $\tau_{\rm int}$ plot is essentially constant at ~900 ps. In contrast, the $\tau_{\rm rot}$ plot shows a generally decreasing trend from 10 ns to 6 ns over the 0–5 M Gdm⁺ range.

The peak in the $\tau_{\rm int}$ plot (see Figure 3.14) suggests that an intermediate structure is formed in the presence of 1.0 M Gdm⁺, well prior to the global unfolding transition at ~2.0 M. Figure 3.15 shows that the trends exhibited by the cone angle, θ_c , or the order parameter, S, has two inflection points over the 0.25–2.0 M Gdm⁺ range. The main transition correlates with the 1.0 M feature in the $\tau_{\rm int}$ plot; θ_c abruptly increases from 17° to 27°, and S decreases from 0.92 to 0.83. At Gdm⁺ concentrations above 1.0 M, both parameters are more or less constant, if the 95 % confidence intervals are considered; only a small decrease in S and a small increase in θ_c accompany the unfolding transition at 2 M. These results suggest that the protein assumes

Table 3.4. Wobbling-in-cone model parameters^a and the apparent hydrodynamic radius, $R_{\rm h}$, for ZnCytc in the presence of Gdm⁺ at 22°C.

Gdm ⁺ (M)	τ _{int} (ps)	$ au_{ m rot}$ (ns)	S	$\theta_{\mathcal{C}}$	R _h (nm)
0.00	844 ± 111	10.47 ± 0.16	0.924 ± 0.01	18.42 ± 1.37	2.17 ± 0.02
0.25	790 ± 171	9.06 ± 0.53	0.933 ± 0.003	17.34 ± 0.28	2.06 ± 0.04
0.50	960 ± 17.4	8.21 ± 0.30	0.923 ± 0.003	18.54 ± 0.28	1.98 ± 0.02
1.00	1341 ± 58	8.51 ± 0.62	0.839 ± 0.034	27.15 ± 3.05	1.99 ± 0.05
1.50	1071 ± 219	7.14 ± 0.84	0.831 ± 0.054	27.79 ± 4.96	1.86 ± 0.07
2.00	900 ± 218	5.78 ± 0.21	0.843 ± 0.036	26.83 ± 3.21	1.72 ± 0.02
3.00	954 ± 131	7.33 ± 0.89	0.821 ± 0.003	28.86 ± 0.28	1.82 ± 0.07
4.00	1002 ± 293	6.18 ± 0.46	0.821 ± 0.05	28.70 ± 4.41	1.67 ± 0.04
5.00	798 ± 205	6.81 ± 0.56	0.818 ± 0.037	29.10 ± 3.22	1.67 ± 0.05

^a See Equation 3.12.

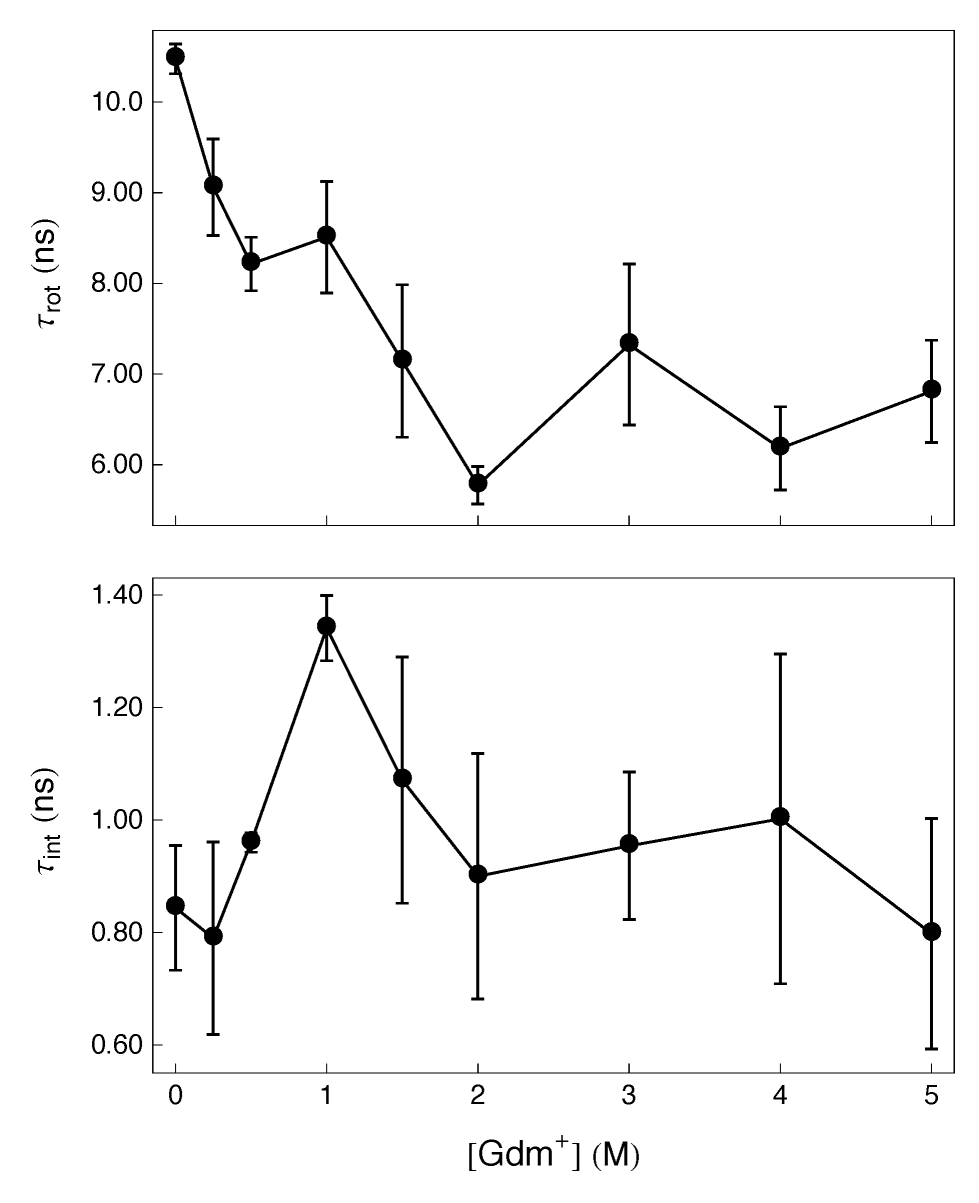


Figure 3.14. Anisotropy decay correlation times (Equation 3.13 and 3.14) for ZnCytc at 22°C and pH 7.0 as a function of the Gdm⁺ concentration. The model parameters are listed in Table 3.4.

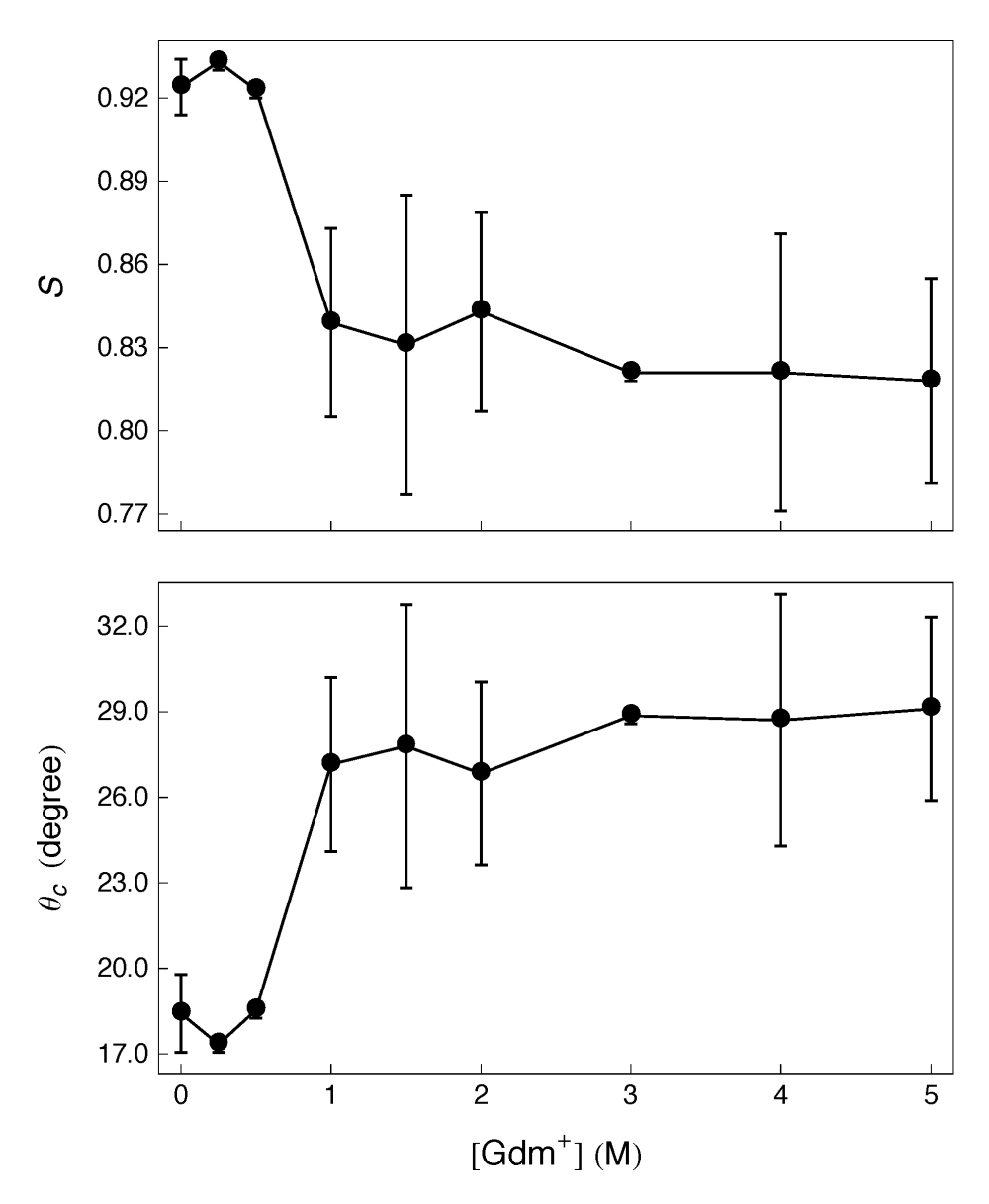


Figure 3.15. Gdm⁺ concentration dependence for S, the anisotropic order parameter, and θ_C , the cone angle (see Equation 3.12), for ZnCytc at 22°C and pH 7. The parameters are listed in Table 3.4.

a partially unfolded state at ~ 1.0 M Gdm⁺ that allows the Zn^{II} porphyrin to exhibit a significantly larger range of motion with respect to the protein than is observed in the native state. It is interesting to note that the range of motion for the Zn^{II} porphyrin does not increase as dramatically at the 2.0 M global unfolding transition even though the change in the environment of the Zn^{II} porphyrin makes a significant shift during the unfolding transition.

The tumbling correlation time, $\tau_{\rm rot}$, obtained from the ZnCytc anisotropy decays as the longer of the two exponential time constants, can be used to determine an estimate for the effective hydrodynamic radius, $R_{\rm h}$, using a relation obtained from the Stokes-Einstein-Debye Equation¹⁵⁵

$$R_{\rm h}^3 = \frac{3RT}{4\pi\eta} \tau_{\rm rot} \tag{3.16}$$

Figure 3.16 shows that the calculated $R_{\rm h}$ decreases as the Gdm⁺ concentration increases. This finding is at odds with the expectation that $R_{\rm h}$ should increase owing to the unfolding transition because a less compact structure should result and because the cone angle θ_c increases. Further, an increased $R_{\rm h}$ is observed for the unfolded forms of several similar proteins. ^{145,156-158} Pielak and coworkers ¹⁵⁹ used pulsed-field gradient NMR spectroscopy to determine that the effective $R_{\rm h}$ for FeCytc expands from 18 Å in the native state to 31 Å in the acid (pH 2) denatured state. Thus, it is probable that the reduced $\tau_{\rm rot}$ we observe in the unfolded state in the presence of Gdm⁺ arises from the protein's assumption of an elongated, non-spheroidal structure from which more than one rotational correlation time would be expected. ¹⁶⁰ If one of the rotational moments in the unfolded state exhibits a correlation time that is significantly longer than the fluorescence timescale, its contribution to the anisotropy decay would be attenuated relative to that of a shorter moment.

The trend of the effective $R_{\rm h}$ as a function of Gdm⁺ shown in Figure 3.16 includes distinct inflections centered at 1.0 M and between 2.0–3.0 M that are statistically significant if the confidence intervals are considered. The 1 M inflection correlates with

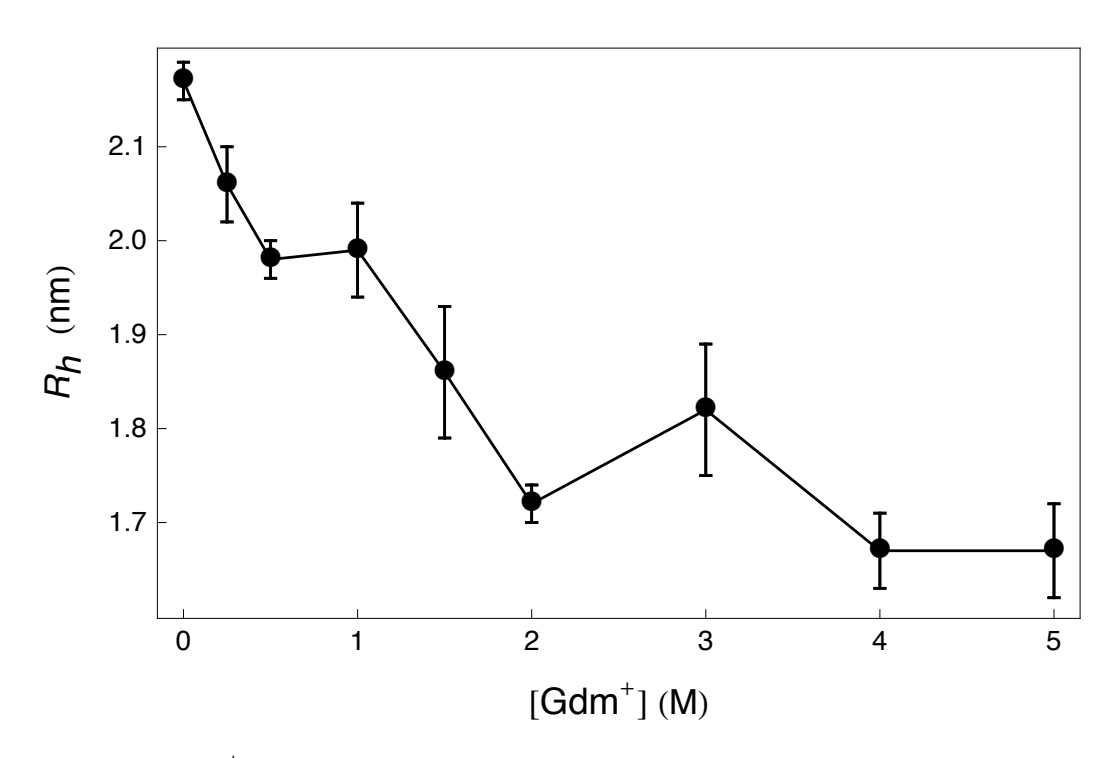


Figure 3.16. Gdm⁺ concentration dependence for the effective hydrodynamic radius, $R_{\rm h}$, as calculated from the anisotropy decay time constant $\tau_{\rm rot}$ and Equation 3.16 for ZnCytc at 22°C and pH 7. (See Table 3.4.)

the intermediate suggested by the increased θ_c and the increased internal correlation time $\tau_{\rm int}$, so there is some global structural evidence for a change in overall size for this intermediate. The 2.0–3.0 M inflection occurs as the ensemble finishes the unfolding transition and accompanies the peak in the F_{01}/F_{00} vibronic structure ratio that is associated with a change in the axial coordination of the Zn^{II} ion (see Figure 3.6).

3.4 Discussion

The finding that the global unfolding transition of ZnCytc is preceded during the titration with Gdm⁺ by formation of an intermediate raises some important questions about how it relates dynamically and structurally to the native and unfolded states. In the following, we discuss how the internal correlation time and the order parameter or cone angle returned from the picosecond fluorescence anisotropy decays suggest that the intermediate has some of the properties of an unfolding transition state.

The anisotropy results show that an intermediate structure characterized by an enhanced cone angle for the Zn^{II} porphyrin is populated at 1 M Gdm⁺, well below the overall unfolding transition at 2 M Gdm⁺ (see Figure 3.15). The intermediate structure exhibits a significantly longer internal correlation time than observed either in the native state or in the unfolded state (see Figure 3.14). Despite the significant change in correlation timescale, the intermediate is formed in the absence of a large change in overall structure. The Gdm⁺ titrations do not evidence significant inflections of either the absorption spectrum or fluorescence spectrum in the 1 M Gdm⁺ range (see Figures 3.4 and 3.3), so the local environment of the Zn^{II} porphyrin does not change much on average as the intermediate is formed. Figure 3.16 shows that the apparent hydrodynamic radius has an inflection in the Gdm⁺ range that accompanies formation of the intermediate, but the rearrangement of the protein that produces

an asymmetric tumbling structure is smoothly associated with the overall unfolding transition that is more or less complete at 3 M Gdm^+ . Thus, the formation of the intermediate at 1 M Gdm^+ is primarily marked by changes in the fluctuations of the protein structure that are reported by the correlation timescale and by the change in the Zn^{II} porphyrin's range of motion.

The relationship between the correlation timescale for internal motion obtained from the anisotropy decay, $\tau_{\rm int}$, and the amplitude of the corresponding structural fluctuation can be obtained in analogy to that discussed previously ¹⁴⁴ for fluctuations detected in the dynamic fluorescence Stokes shift (FSS) response. The internal motions can be considered Brownian diffusive motions over the protein-folding energy landscape along an effective one-dimensional coordinate. ^{90,144} As averaged over the ensemble of proteins in solution, the structural fluctuations that contribute to the diffusive motion are characterized by the mean-square displacement, $\langle x^2(t) \rangle$, and the propagation time, t, as

$$\langle x^2(t) \rangle = 2Dt \tag{3.17}$$

The diffusion constant, D, would be expected to be inversely proportional to the internal or external solvent friction f

$$D = k_B T / f \tag{3.18}$$

The correlation timescale, τ , for a fluctuation can then be expressed by an Arrhenius equation as that for a thermally driven crossing of a local barrier of height ΔG^{\ddagger} ,

$$\tau = \tau_0 \exp(\Delta G^{\ddagger}/RT) \tag{3.19}$$

where τ_0 is the characteristic timescale at which the transition-state structure at the barrier is accessed:

$$\tau_0 = \langle x^2(\tau_0) \rangle / 2D \tag{3.20}$$

Thus, the correlation time τ increases as as the barrier height, ΔG^{\ddagger} , increases. Equation 3.20 indicates that the correlation timescale τ is linearly proportional to the mean-square displacement for the associated structural motion, the width of the overall probability distribution.

In contrast, the cone angle is a measure of the range of motion for the Zn^{II} porphyrin; it marks the probability distribution's upper half-maximum point. 149 The intermediate structure's longer correlation timescale and enhanced cone angle is consistent, then, with a looser structure that makes longer range motions across the energy landscape owing to the lowering of activation barriers, so it has some of the properties of a transition state for unfolding. Such a structure can be populated thermally during a denaturant titration only if relatively low activation barriers along the folding/unfolding coordinate divide it on both sides from the native and unfolded states. Owing to the addition of Gdm⁺ during a titration, the Gibbs free energy of the equilibrium ensemble decreases (see Equation 3.3) until the ensemble unfolds, at Gdm^+ concentrations above ~ 2 M. The usual assumption made in the interpretation of a denaturant titration is that only two states, the native and unfolded states, contribute significantly to the ensemble at any Gdm⁺ concentration because either the folding reaction or the unfolding reaction is spontaneous and goes to completion. The results obtained in this paper show that this assumption is not valid for ZnCytc and Gdm⁺. At 1 M Gdm⁺, the ensemble is poised so that the intermediate structure is predominantly populated.

As the Gdm⁺ concencentration is increased further so that the ensemble increasingly populates the unfolded structure, the cone angle for the internal motions remains at the same level accessed by the intermediate at 1 M. That the mean-squared amplitude for the fluctuations in the unfolded state decays from that of the intermediate back to the level of the native state (see Figure 3.14) is distinctive. These observations suggest that the unfolded state is less condensed than the native state,

so the Zn^{II} porphyrin's motions are constrained less tightly than in the native state, but that the activation barriers along the unfolding coordinate that limit the mean-squared amplitudes of the fluctuation are nearly as large as they were in the native state.

In closing, this study provides to our knowledge the first evidence from picosecond anisotropy decays using an intrinsic fluorescent probe for the formation of a transition-state-like, partially unfolded structure during titration of a protein by a denaturant. That one or more intermediates are populated along the folding/unfolding reaction coordinate of FeCytc has been discussed extensively in the work by Englan $der,^{161,162}$ Roder,¹⁶³ Rousseau,^{164–166} and their coworkers; a non-two state folding behavior was observed previously in the refolding of ferricytochrome c evidenced by the circular dichroism (CD222) signal at around 1.3 M Gdm⁺.¹⁶⁷ Rate-limiting steps along the folding pathway involve exchange of non-native histidine and water axial ligands from the Fe^{II} porphryin complex in FeCytc to obtain finally the native state's methionine (M80) ligation. 165 The change in the vibronic structure of the fluorescence spectrum that occurs during the Gdm⁺ unfolding of ZnCytc (see Figure 3.6) evidences an release of axial ligands from those present in the native state. A suggestion for the intermediate populated at 1 M Gdm⁺ would be one in which both of the native axial ligands have been released from the Zn^{II} porphyrin, at least in its $\pi \rightarrow \pi^*$ excited state. Such a structure would be expected to exhibit both an enhanced cone angle and a larger mean-squared deviation for the angular fluctuations; the internal correlation time is comparable to that obtained from the FSS response of fbCytc. 144 In the native state of ZnCytc, the folded protein's packing forces impose a six-coordinate structure, whereas the unfolded structure would be very likely to assume a five-coordinate structure with a non-native axial ligand. ^{76,79} Either of these two limiting structures might be expected to exhibit smaller fluctuation amplitudes for the Zn^{II} porphyrin than a deligated intermediate structure.

CHAPTER 4

Fluorescence Stokes Shift Response Functions from ZnCytc in the Presence of Gdm⁺

Summary

We report the changes in shift amplitude and correlation timescales from the dynamic fluorescence Stokes shift (FSS) response that occur during the unfolding titration of Zn^{II}-substituted cytochrome *c* with guanidinium ion (Gdm⁺). The FSS response functions are compared with the picosecond fluorescence anisotropy (FA) response functions, which report how the fluctuations of the protein structure cause angular motions of the intrinsic Zn^{II} porphyrin macrocycle with respect to its equilibrium orientation. The presence of Gdm⁺, even at the lowest concentrations and well below the global denaturation limit, destabilizes the native fold and causes the optical transition of the Zn^{II} porphyrin to depart from the linear-response regime at Gdm⁺ concentrations well below those that prepare the transition-state-like partially unfolded intermediate that was detected using the FA response. These results strongly

implicate structural changes in the hydration layer as the origin of the dynamical changes reported in the FSS response as the protein approaches the unfolded state.

4.1 Introduction

The structural fluctuations detected in small proteins using the dynamic fluorescence Stokes shift (FSS) response function on the >100-ps timescale arise from diffusive, barrier-crossing motions on the folding energy landscape. 47,81,82 In recent work from this laboratory, we have examined how the fluctuation correlation timescales of Zn^{II}-substituted cytochrome c (ZnCytc) change as the structure moves away from the native fold towards perturbed, partially unfolded structures. Three different methods have been used to prepare the nonnative structures: intramolecular vibrational excitation (IVE) via the radiationless decay and vibrational relaxation of the intrinsic Zn^{II} porphyrin chromophore, 78,79 structural modification via demetalation of the porphyrin, 144 and, most recently, by the addition of guanidinium ion, as was discussed in the previous chapter. These investigations are intended to apply the long-standing question from chemical dynamics of how the thermodynamic stability of a folded protein relates to the motions and energetics along the reaction coordinate for folding and unfolding.

Our finding that the correlation timescales obtained from the exponential time constants in the FSS response function in metal-free (or free-base) cytochrome c (fb-Cytc) are almost ten times longer than those of ZnCytc shows directly that the FSS response function is sensitive to protein motions that are pertinent to the stability of a folded protein. Using a model for Brownian diffusive motion on the energy land-scape associated with thermally activated barrier-crossing events, 83,84 we concluded that the increased polar solvation timescales observed in fbCytc correspond to significantly enhanced fluctuation amplitudes compared to those in ZnCytc under similar

solvent conditions. 144 Because fbCytc lacks the stabilizing influence of the two axial metal-ligand interactions that are present in the native ferricytochrome c (FeCytc) structure, it assumes a dynamic, partially unfolded structure with the characteristics of a molten globule. 79,146

The addition of guanidinium ions (Gdm⁺) destabilizes the native fold of ZnCytc externally by acting on the structure and dynamics of the hydration layer.⁸⁰ In order to learn how the dynamics of ZnCytc in the presence of Gdm⁺ compare with those of the native state, we performed studies of the fluorescence anisotropy (FA) response using the intrinsic Zn^{II}-porphyrin as a probe. These studies were discussed in the previous chapter. The FA response directly reports the structural fluctuations of the protein that induce reorientational motions of the probe from the initial alignment of the photoselected ensemble of probe molecules that was prepared by a planepolarized excitation laser pulse. The results show that a partially unfolded ZnCytc structure is populated in the presence of 1.0 M Gdm⁺, well prior to the denaturation transition at 2.0 M Gdm⁺. This intermediate is characterized by wobbling motions of the porphyrin macrocycle that are significantly enhanced in mean-squared deviation compared to the native and denatured structures. The correlation timescale obtained from the FA response of the intermediate is comparable to that observed for fbCytc, so it is possible that the intermediate is a structure in which both of the axial-ligand interactions to the Zn^{II} porphyrin have been lost. Such a structure would have some of the characteristics of the transition state along the folding/unfolding reaction coordinate for FeCytc, where the axial-ligand exchange reactions are key rate-limiting steps. 161-166 The general picture that emerges from this work and the fbCytc study is that the structural fluctuations increase in amplitude as the protein approaches the equilibrium conditions that favor unfolding.

Using the same picosecond fluorescence data set used in the FA work, we now report the FSS response that occurs during the titration of ZnCytc with Gdm⁺. For

the first time to our knowledge, this work permits us to assess experimentally several aspects of the structural character of the protein fluctuation timescales that are associated with the electric-field fluctuations measured by the FSS response. The results show that the presence of Gdm⁺, even at the lowest concentrations and well below the global denaturation limit, destabilizes the native fold enough that the optical transition of the Zn^{II}-porphyrin chromophore departs from the linear-response regime. This action of Gdm⁺ saturates well prior to the formation of the unfolding intermediate that was detected using the FA response. These results strongly implicate structural changes in the hydration layer as the origin of the dynamical changes reported in the FSS response as the protein approaches the unfolded state.

4.2 Experimental

4.2.1 Sample Preparation

ZnCytc was prepared using using horse-heart ferricytochrome c (FeCytc, Sigma) as the starting material following the procedure established by Vanderkooi and coworkers. 69,91 The metal free product from the demetalation reaction of FeCytc was reconstituted with the metal ion in presence of 10-fold molar excess of zinc acetate. The ZnCytc product was worked up following the methods adapted from the ones employed by Winkler and coworkers 92 and Kostić and coworkers. 93 The final ZnCytc solution was concentrated using repeated ultrafiltration steps through an Amicon YM10 ultrafilter (Millipore). The concentrated ZnCytc solution was divided into small aliquots and flash frozen in liquid nitrogen prior to storage at $^{-85}$ °C.

When required, a ZnCytc sample was prepared for use in a picosecond fluorescence experiment by diluting a thawed aliquot with a 25 mM phosphate buffer solution at pH 7.0 that also contained Gdm⁺ at concentrations ranging over the 0–5-M range. After thorough mixing, the solution was allowed to settle for an hour before

it was passed through a 0.22 μ M microfilter. The ZnCytc concentration was then adjusted by adding additional buffer solution with the same Gdm⁺ concentration to obtain an absorption between 0.1–0.2 at the peak of the absorption band for a path length of 1.0 cm. The sample was held in a 1-cm quartz cuvette; the headspace was purged with dry nitrogen gas prior to exposure to laser light.

4.2.2 Absorption and Fluorescence Spectroscopy

Absorption spectra were acquired with a Hitachi U-2000 spectrophotometer (2-nm band pass). Fluorescence spectra were obtained with a home-built spectrofluorimeter 79 consisting of an Jobin-Yvon AH10 100-W tungsten-halogen light source, a Jobin-Yvon H10 excitation monochromator (4-nm bandpass), an Acton Research SP-150 emission spectrograph (2-nm bandpass), and a Jobin-Yvon Symphony charge-coupled device (CCD) detector. The CCD detector employs a liquid nitrogen cooled, back-illuminated, 2000×800 pixel silicon detector chip (EEV corporation). The sample cuvette was held in a Quantum Northwest TLC50F Peltier-effect temperature controller. As presented as a function of wavenumber, the fluorescence intensities are multiplied by the square of the wavelength in order to compensate for the fixed (in wavelength units) spectral bandpass of the emission spectrograph. The absorption and fluorescence instruments were controlled by LabVIEW (National Instruments) programs.

4.2.3 Time-Resolved Fluorescence Measurements

Single-wavelength polarized fluorescence transients were recorded using a T-format time-correlated single photon counting (TCSPC) instrument as described in chapter 2. The picosecond excitation pulses were obtained from a synchronously pumped cavity-dumped dye laser (Coherent 702-2). The dye laser was pumped by a passively mode-locked, diode-pumped Nd^{III}-YVO₄ laser (Spectra-Physics Vanguard), which pro-

duced 13-ps pulses with an average power of 2.5 W at a repetition rate of 80 MHz. The dye laser produced 5-ps pulses over the 583–585 nm tuning range using either the Rhodamine-6G or Pyromethine 567 dyes. The repetition rate on the dye laser was adjusted to 4 MHz using Gooch & Housego cavity dumping electronics.

In the detection system, the vertically polarized excitation pulse from the dye laser output was divided into two parts. One part of the pulse was fed to a reference photodiode (Becker & Hickl PHD-400-N), and the other part was directed to the sample. The fluorescence emission was collected using a Cassegranian reflective microscope objective ($40 \times$ magnification). The collected emission was then split by a polarizing cube beam splitter into two orthogonal polarization components with planes of polarization parallel (0°) and perpendicular (90°) to that of the vertically polarized excitation pulse. The two components were detected simultaneously with microchannel plate photomultiplier tubes (MCP-PMT, Hamamatsu R3809U-50) after selection of the emission wavelength by subtractive double monochromators (Spectral products, CM-112). Emission transients were simultaneously recorded with a two-channel TCSPC system (Becker & Hickl SPC-132). The instrument-response width was 65 ps (fwhm). LabVIEW (National Instruments) programs were used to control the data-acquisition hardware and monochromators in order to acquire a set of single-wavelength fluorescence transients automatically over a range of emission wavelengths. The sample was held in a temperature-controlled mount that was regulated at 22°C using a Neslab RTE-110 water circulating bath.

4.3 Results

4.3.1 Absorption and Fluorescence Emission Spectra

Figure 4.1 shows the *Q*-band region of the absorption (A) and fluorescence (F) spectra from ZnCytc in water at 22°C and pH 7.0. The spectra are plotted as relative

dipole strengths, A(v)/v and $F(v)/v^3$, respectively, as a function of wavenumber v. The 0-0 and 0-1 vibronic peaks in the fluorescence spectrum exhibit a near mirror-symmetry with respect to the corresponding vibronic peaks in the absorption spectrum. The 0-0 transition is approximately at the wavenumber where the two spectra cross each other; with the excitation laser tuned to this wavenumber in the picosecond dynamic solvation experiments, the S_1 state is prepared without any excess vibrational energy, so the FSS response should not exhibit a significant component arising from vibrational relaxation.

The solvation reorganization energy, λ , was estimated using the shift of the wavenumber of the fluorescence spectrum's 0-0 peak, $\nu_{0-0,F}$, from that of the absorption spectrum, $\nu_{0-0,A}$: 100,144

$$\lambda = (\nu_{0-0,A} - \nu_{0-0,F})/2 \tag{4.1}$$

The value of λ obtained for ZnCytc in water in the present work is $55 \pm 10 \, \mathrm{cm}^{-1}$. This value is significantly smaller than reported in some of the previous work on ZnCytc from this laboratory.^{77,78} The observed value for λ evidently depends on how the samples are processed. When the metal-free product (fbCytc) of the demetalation of FeCytc in liquid anhydrous HF and the ZnCytc product obtained after Zn^{II} reconstitution are worked up using Sephadex G-75 gel-filtration chromatography, as described by Vanderkooi and coworkers,⁹¹ the value for λ obtained is larger, $145 \, \mathrm{cm}^{-1}$. In our subsequent work,⁷⁹ the fbCytc and ZnCytc products were worked up using ion-exchange chromatography using the approach described by Winkler and coworkers and by Kostić and coworkers.^{92,93} These preparations exhibit absorption and fluorescence spectra with narrower vibronic lineshapes; the reader should compare Figure 4.1 in this paper with the similar figure in reference 78. Note that the FSS response from both types of ZnCytc samples exhibit nearly the same correlation timescales and relative component amplitudes as first reported,⁷⁶ so the larger value of λ from the older ZnCytc preparations probably arises from heterogeneity.

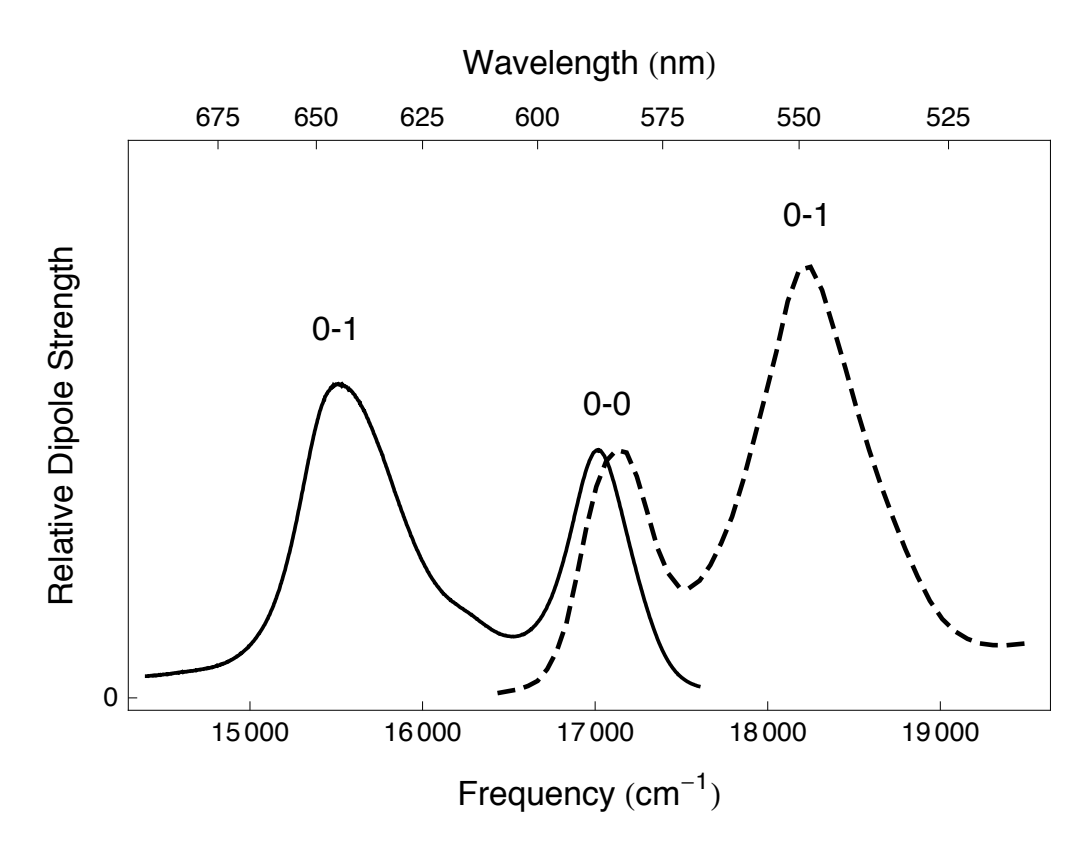


Figure 4.1. *Q*-band region of the absorption and fluorescence spectra from ZnCytc in water at 22°C and pH 7.0. The spectra are plotted as relative dipole strengths, A(v)/v (dashed curve) and $F(v)/v^3$ (solid curve), respectively.

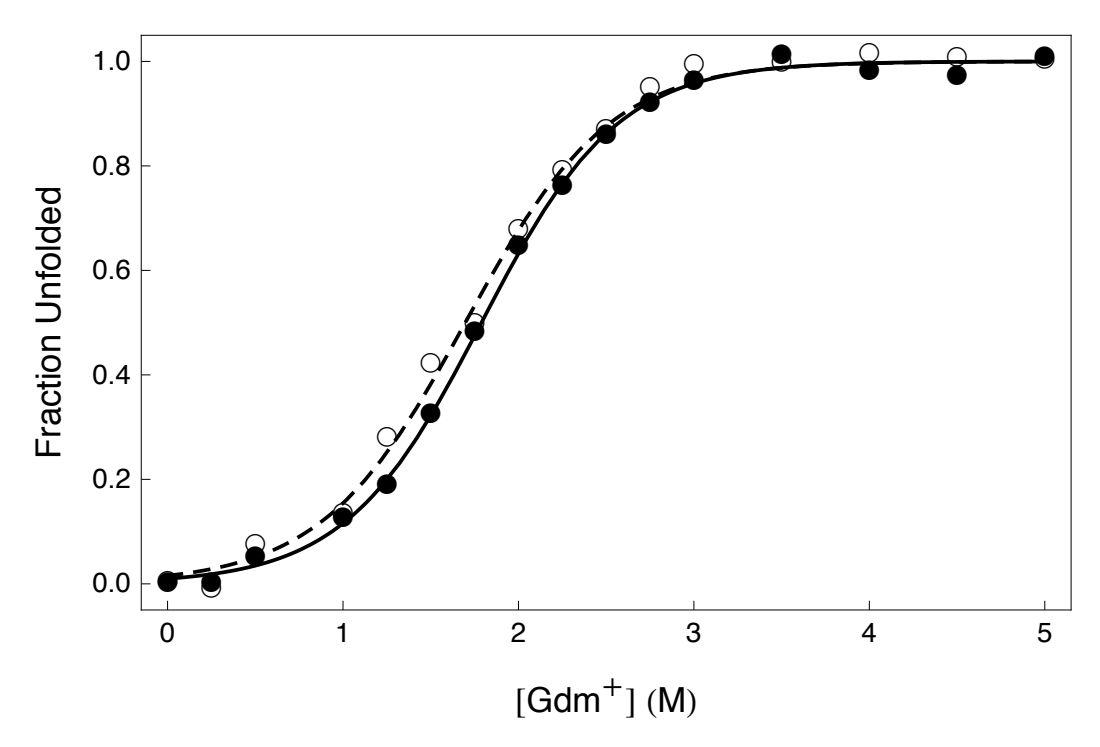


Figure 4.2. Gdm⁺ fluorescence titration curves for ZnCytc at 22°C and pH 7.0. The fraction of unfolded proteins in the ensemble was determined from the wavenumber of the peak maximum of the 0–0 (dashed curve) and 0–1 peaks (solid curve) in the fluorescence spectrum; the data points are superimposed upon separate models for a two-state unfolding transition (Equation 4.2). The average thermodynamic parameters for the unfolding transition are: $\Delta G_{\rm Fold}^{\rm H_2O} = -10.74 \pm 0.54$ kJ/mol, $m = 6.16 \pm 0.49$ kJ/mol, and $C_{\rm m} = 1.75 \pm 0.16$ M.

Addition of Gdm⁺ to ZnCytc solutions results in an apparent two-state denaturation response that results in a shift of the fluorescence and absorption maxima to the blue. Figure 4.2 shows the unfolding transition in terms of the fraction of unfolded proteins in the ensemble, $f_{\rm u}$, as determined from the experimentally observed 0–0 and 0–1 peak wavenumbers using the precedure discussed in the previous chapter. The transition is modeled using an equation derived from a two-state native-to-unfolded equilibrium,

$$f_{\rm u} = \left[1 + \exp\left(-\frac{\Delta G_{\rm Fold}^{\rm H_2O} + m\left[\rm Gdm^+\right]}{RT}\right)\right]^{-1}$$
(4.2)

where $\Delta G_{\rm Fold}^{\rm H_2O}$ relates the Gibbs free energy of folding in water, and m determines the Gdm⁺ concentration dependence of the change in Gibbs free energy. The average thermodynamic parameters obtained from the 0-0 and 0-1 fluorescence titration curves of ZnCytc are: $\Delta G_{\rm Fold}^{\rm H_2O} = -10.74 \pm 0.54$ kJ/mol, $m = 6.16 \pm 0.49$ kJ/mol, and the midpoint of transition, $C_{\rm m} = 1.75 \pm 0.16$ M. The absorption spectra exhibit similar titration parameters, but note that the unfolding transition occurs at a slightly higher Gdm⁺ concentration: $\Delta G_{\rm Fold}^{\rm H_2O} = -10.48 \pm 0.52$ kJ/mol, $m = 5.69 \pm 0.15$ kJ/mol and $C_{\rm m} = 1.85 \pm 0.10$ M. These results were interpreted previously as showing that the folded structure in the ground electronic state, S_0 , is more stable than the resonant first-excited singlet state, S_1 , owing to photodissociation of the axial ligands to the metal ion in the excited state.⁷⁶

4.3.2 Picosecond Time-Resolved Fluorescence Spectroscopy

Time-resolved fluorescence spectra from ZnCytc in water and a range of Gdm⁺ concentrations were acquired as slices from a time-wavelength-intensity dipole-strength surface, $F_D(v,t)$. The excitation laser was tuned in these experiments to the wavenumber of the 0-0 transition (see Figure 4.1). The dipole-strength surface was acquired as a set of dichroism-free, single-wavelength transients spaced by 5.0 nm,

the bandpass of the emission monochromators, over the entire 0–1 band and nearly to the peak of the 0–0 band. The intensity transients were computed from the simultaneously acquired parallel (I_{\parallel}) and perpendicular (I_{\perp}) polarized fluorescence transients as

$$I(t) = I_{\parallel}(t) + 2I_{\perp}(t) \tag{4.3}$$

The polarized transients in these data sets were used to calculate the anisotropy decays that were discussed in the previous chapter. The dipole-strength surface was constructed by normalizing the integral of each intensity transient to the dipole strength observed in the continuous-wave fluorescence spectrum at the emission wavenumber of the transient. The transients were used without deconvolution of the instrument-response function, and they were truncated so that the first data point used in further analysis was that of the 100-ps delay, almost a full instrument response width from the center of the excitation pulse.

Figure 4.3 shows a set of time-resolved fluorescence dipole-strength spectra at five time delays from ZnCytc in water at 22 °C. The data points are shown superimposed with fitted lognormal lineshapes.⁹⁷ As the delay time increases, the spectra exhibit a decay in area (integrated dipole strength) as the excited-state population decays, and the peak wavenumber shifts to lower frequency (see Table 4.1 for the lineshape parameters).

The time evolution of the mean fluorescence dipole strength, $\langle v(t) \rangle$, was obtained by integrating over the time-resolved spectrum at a given time t to obtain the first moment,

$$\langle v(t) \rangle = \frac{\int_{v_1}^{v_2} dv \, v \, F_D(v, t)}{\int_{v_1}^{v_2} dv \, F_D(v, t)} \tag{4.4}$$

The $\langle v(t) \rangle$ response is used here as a direct measure of the FSS response function

$$S_{\mathcal{V}}(t) = \frac{\langle v(t) \rangle - \langle v(\infty) \rangle}{\langle v(0) \rangle - \langle v(\infty) \rangle}.$$
(4.5)

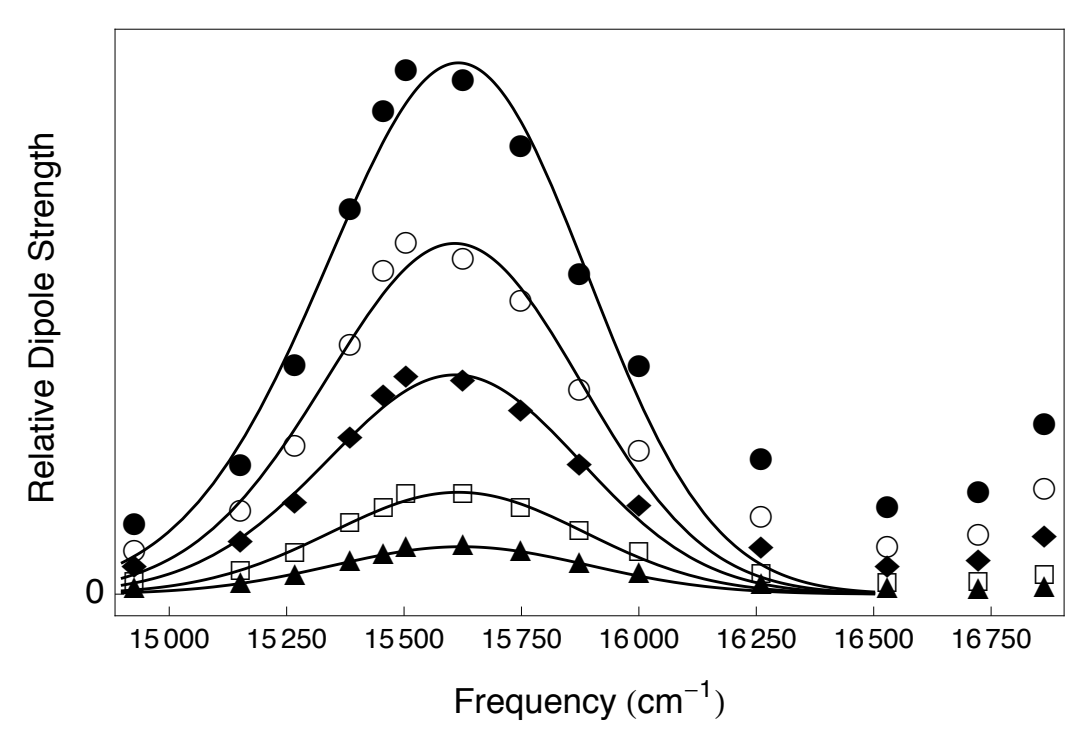


Figure 4.3. Time-resolved fluorescence dipole strength spectra from ZnCytc in water at delay times of 100 ps (\bullet), 1 ns (\circ), 2 ns (\bullet), 5 ns (\square), and 9 ns (\blacktriangle). The displayed spectral region spans the 0–1 vibronic band and the onset of 0–0 band. The spectra are superimposed with lognormal lineshapes fitted over the 14900–16500 cm⁻¹ region.

Table 4.1. Lognormal lineshape parameters^a for the 0–1 vibronic feature of the time-resolved fluorescence spectra from ZnCytc in water at 22°C.

delay (ps)	A	v_0 (cm ⁻¹)	σ (cm ⁻¹)	ρ
100	1139.11	15660.6	629.99	1.31
1000	729.52	15644.1	629.99	1.24
2000	452.16	15642.2	629.53	1.22
5000	209.72	15639.6	644.47	1.15
9000	98.34	15632.4	648.66	1.06

^a Area (integrated dipole strength), A; center frequency, v_0 ; width, σ ; asymmetry (skew), ρ .

over the ps-ns regime without normalization 105,144 in order to avoid the need to estimate the mean fluorescence emission frequencies at t=0 and at $t=\infty$. The limits of the integration for the mean frequency determination with Equation 4.4, v_1 and v_2 , were chosen to enclose the 0-1 peak but to avoid the congested region at the onset of the 0-0 peak. In some of the earlier work on the FSS response function from ZnCytc from this laboratory, 77 the FSS response was determined from the time evolution of the 0-0 peak wavenumber, which was obtained from a fitted vibronic progression for the 0-0 and 0-1 peaks. The first-moment approach was used in our recent paper on the FSS response function of fbCytc 144 where it was shown to be robust even when the signal/noise ratio was not especially high.

The top panel of Figure 4.4 shows that the FSS response function from ZnCytc in water is a monotonic decay to the red that is well described by a biexponential function

$$\langle \nu_{0-1}(t) \rangle = A_1 e^{-t/\tau_1} + A_2 e^{-t/\tau_2} + \nu_{\infty}$$
 (4.6)

The time constants, $\tau_1 = 135$ ps and $\tau_2 = 1.6$ ns, and the relative magnitudes of the corresponding amplitudes, A_1 and A_2 , are similar to those reported previously.⁷⁷ The monotonic character of the FSS response function is consistent with its interpretation (*vide infra*) as a solvation time-correlation function arising from the dielectric response of the protein and solvent medium around the Zn^{II} porphyrin chromophore.

In contrast, the addition of even a small amount of Gdm⁺ to the ZnCytc solution results in an unusual *bidirectional* response; the first and faster part is a shift to the blue in all the Gdm⁺ concentrations studied. The bottom panel of Figure 4.4 shows the FSS response from ZnCytc in the presence of 0.25 M Gdm⁺, the lowest concentration we characterized. The blue shift has a time constant of $\tau_1 = 819$ ps, which is more than four times longer than that of the fast phase of the red shift in water. The red shifting component that completes the FSS response in 0.25 M Gdm⁺

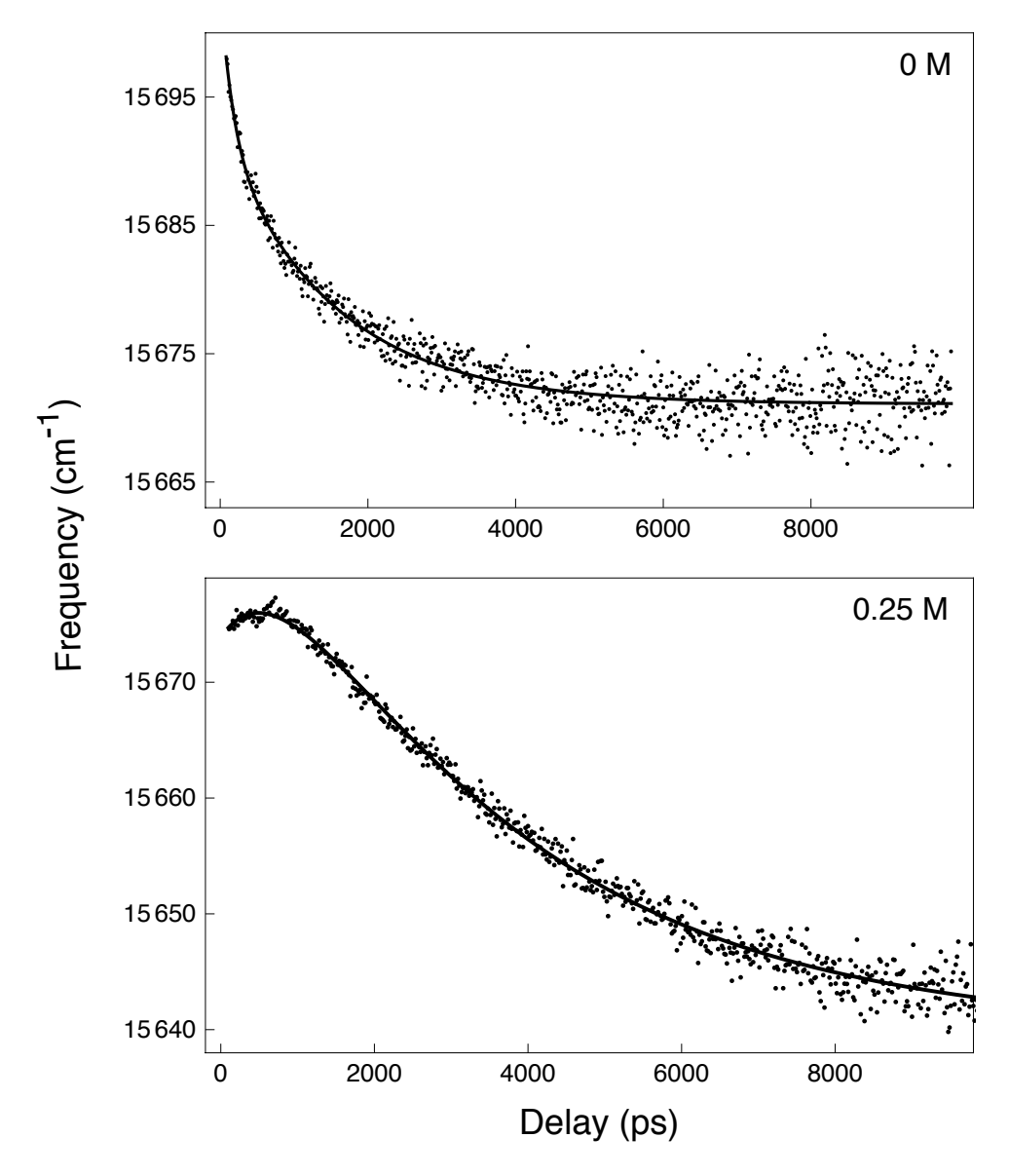


Figure 4.4. Time evolution of the mean frequency of the 0-1 fluorescence emission, $\langle v_{01} \rangle$, from ZnCytc in water (*top*) and in the presence of 0.25M Gdm⁺ (*bottom*) at 22 °C. The data points are superimposed with fitted biexponential models. The fit parameters are listed in Table 4.3.

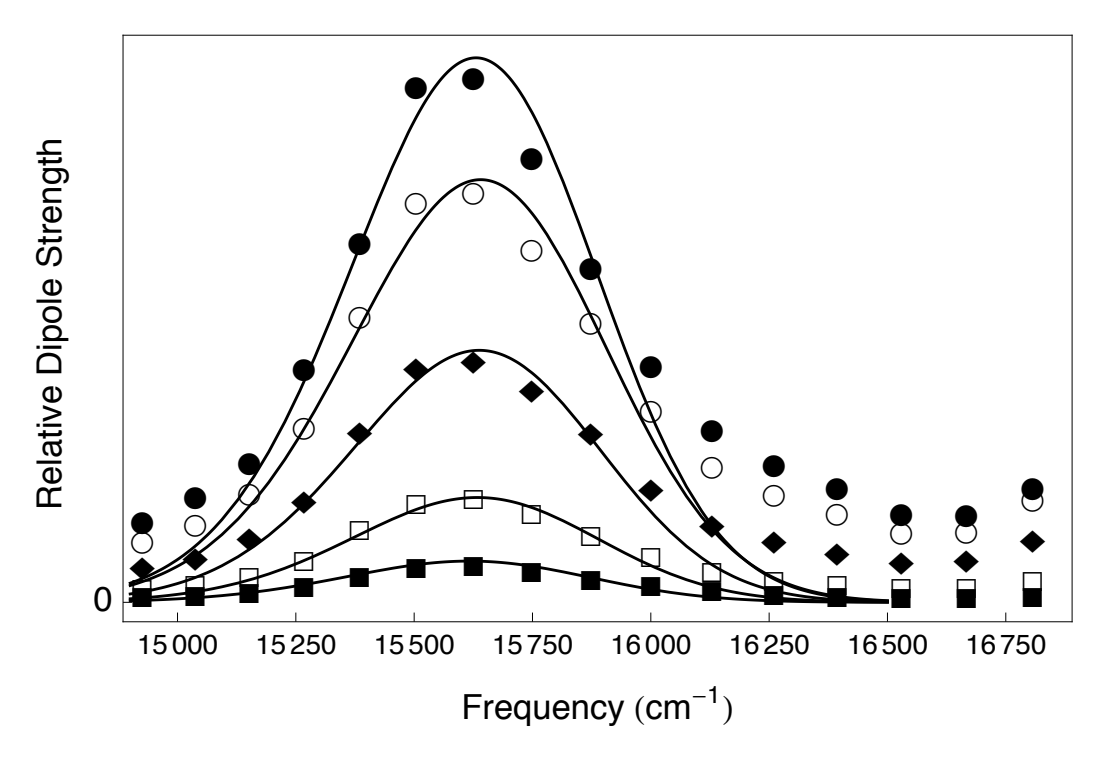


Figure 4.5. Time-resolved fluorescence dipole strength spectra from ZnCytc in 2.0 M Gdm⁺ concentration at delay times 200 ps (\bullet), 500 ps (\circ), 1.2 ns (\bullet), 4 ns (\square), and 8 ns (\square). The displayed spectral region spans the 0–1 vibronic band till the onset of the 0–0 band. The spectra are superimposed with lognormal lineshapes fitted over the 14900–16500 cm⁻¹ region.

Table 4.2. Lognormal lineshape parameters^a for the 0–1 vibronic feature of the time-resolved fluorescence spectra from ZnCytc in $2.0~M~Gdm^+$ at $22^{\circ}C$.

delay (ps)	A	v_0 (cm ⁻¹)	σ (cm ⁻¹)	ρ
200	931.10	15672.1	589.99	1.31
500	747.28	15683.4	609.99	1.31
1200	430.90	15678.9	589.94	1.31
4000	178.90	15674.7	589.42	1.31
8000	70.15	15657.1	588.55	1.30

^a Area (integrated dipole strength), A; center frequency, v_0 ; width, σ ; asymmetry (skew), ρ .

has a time constant of $\tau_2 = 3.53$ ns, which is about twice that of the $\tau_2 = 1.6$ -ns time constant in water.

The appearance of the initial blue shift in the presence of Gdm⁺ indicates that rather than arising purely from solvation dynamics, the observed FSS response arises from a prompt structural change in the Zn^{II} porphyrin itself or its protein surroundings that is followed by a reorganizational relaxation of the surrounding protein medium. The latter's red-shifting direction of response would be formally a solvation response, but its starting configuration would be significantly displaced from that of the ground state porphyrin and the protein and solvent that was initially in equilibrium with it. We examined the time-resolved fluorescence spectra observed in the presence of Gdm⁺ during the FSS response to see if the lineshapes evidence a structural change in the porphyrin. For example, Figure 4.5 shows a set of time-resolved fluorescence dipole-strength spectra at five delays from ZnCytc in 2.0 M Gdm⁺. As shown in Table 4.2, the blue and red shifts of the FSS response are reported by the trends in the peak wavenumber, v_0 , but the linewidths and asymmetry parameters, σ and ρ , respectively, are essentially constant with time. These results are consistent with the interpretation that the FSS response arises from a structural response of the surrounding protein medium rather than from a large change in structure of the Zn^{II} porphryin itself.

The trends of the amplitudes and time constants for the biphasic FSS response from ZnCytc were characterized as a function of the Gdm⁺ concentration to probe the changes in protein dynamics that accompany the unfolding transition. Figure 4.6 shows the FSS response functions for a range of Gdm⁺ concentrations. Each was well fit by a biexponential model that includes a fast blue shift and a slower red shift. The fit parameters for the entire series of Gdm⁺ concentrations we studied are listed in Table 4.3; the indicated 95% confidence intervals were obtained from a set of at least three repeated measurements. The trends in the fit parameters

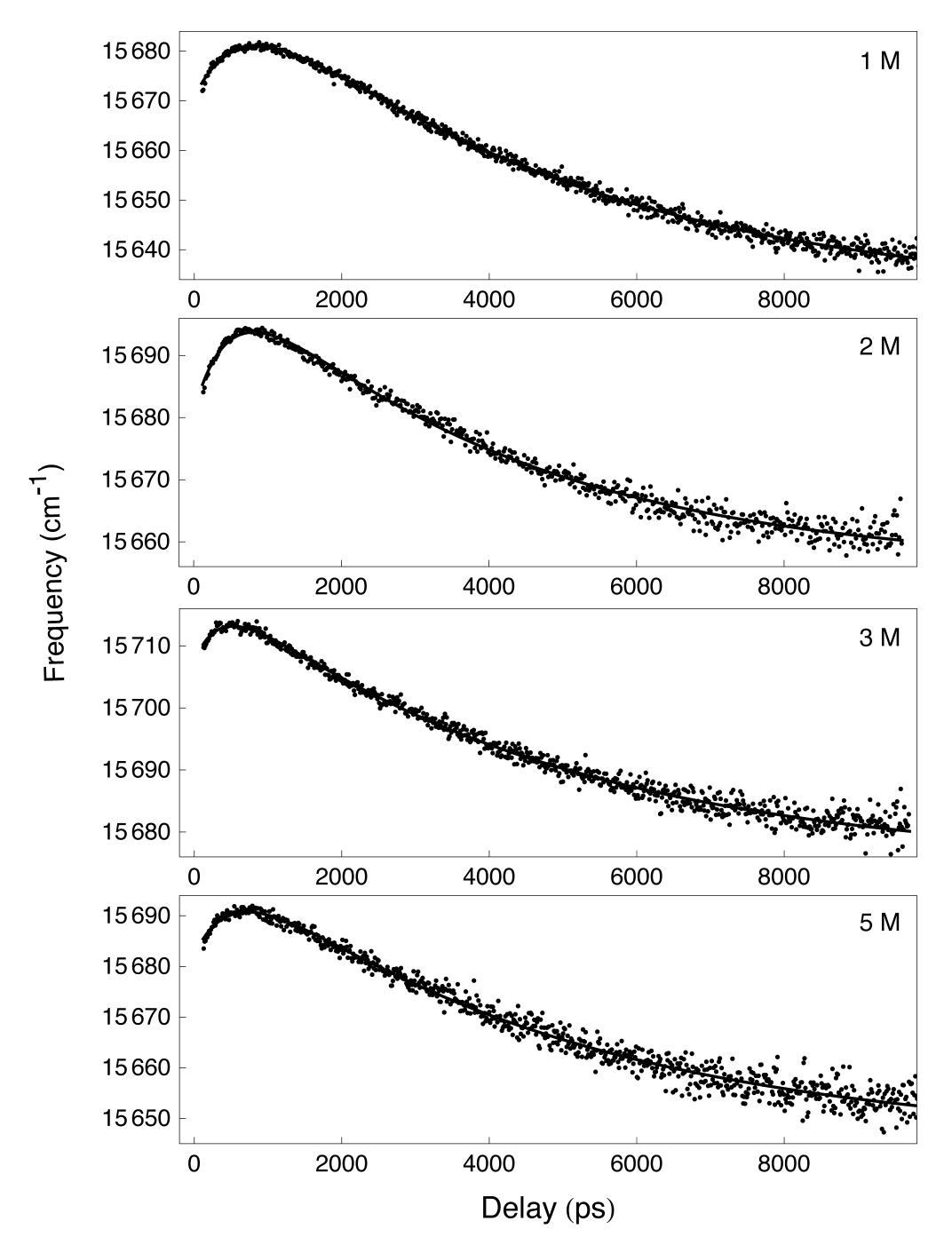


Figure 4.6. Time evolution of the mean frequency of the 0–1 fluorescence emission, $\langle v_{01} \rangle$, from ZnCytc at Gdm⁺ concentrations of 1.0, 2.0, 3.0 and 5.0 M, at 22°C and pH 7.0. The data points are superimposed on a biexponential model defined by Equation 4.6. The fit parameters are listed in Table 4.3.

Table 4.3. Model parameters for the time evolution of the Fluorescence Stokes shift^a for ZnCytc in the presence of Gdm^+ at $22^{\circ}C$.

Gdm ⁺ (M	A_1	τ ₁ (ps)	A_2	τ_2 (ns)	$ u_{\infty}$
0.00 0.25 0.50 1.00 1.50 2.00	9.84 ± 1.69 -21.05 ± 1.15 -27.69 ± 3.94 -26.46 ± 4.21 -26.34 ± 1.47 -27.51 ± 4.87	$ \begin{array}{c} 135 \pm 36 \\ 819 \pm 30 \\ 577 \pm 144 \\ 695 \pm 28 \\ 658 \pm 49 \\ 575 \pm 120 \end{array} $	20.69 ± 1.38 58.81 ± 4.30 61.76 ± 9.3 58.12 ± 11.88 55.92 ± 1.28 62.74 ± 8.5	$ \begin{array}{c} 1.60 \pm 0.22 \\ 3.53 \pm 0.13 \\ 3.69 \pm 0.08 \\ 4.35 \pm 0.1 \\ 4.49 \pm 0.29 \\ 4.34 + 0.22 \end{array} $	15666.8 ± 4.5 15638.9 ± 0.9 15635.8 ± 9.4 15642.4 ± 6.1 15634.1 ± 10.8 15637.1 ± 18.8
3.00 4.00 5.00	-11.21 ± 1.15 -29.64 ± 5.68 -22.67 ± 4.68	282 ± 49 440 ± 142 562 ± 44	52.37 ± 1.28 67.88 ± 2.58 63.57 ± 1.90	4.40 ± 0.28 4.41 ± 0.33 4.95 ± 0.15	15657.1 ± 21.3 15653.0 ± 17.6 15664.2 ± 3.2

a $\langle v_{0-1}(t) \rangle = A_1 e^{-t/\tau_1} + A_2 e^{-t/\tau_2} + v_{\infty}.$

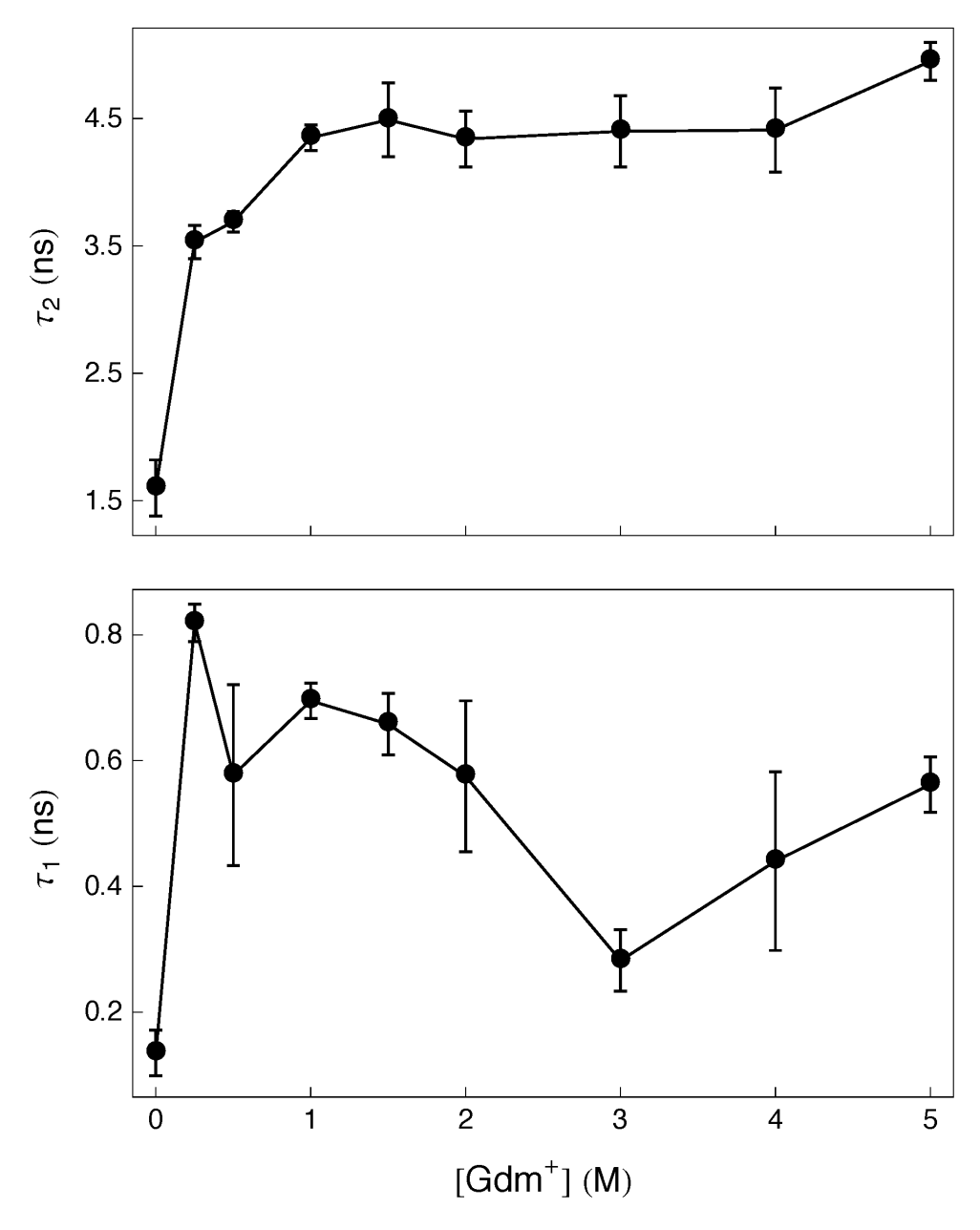


Figure 4.7. Fluorescence Stokes shift time constants for ZnCytc at 22°C and pH 7.0 as a function of the Gdm⁺ concentration, as obtained from fits to Equation 4.6. *Top:* Time constant τ_2 , of the slower component, for the final shift to the red. *Bottom:* Time constant τ_1 , of the faster component, for the initial shift to the blue when Gdm⁺ is present. The plotted values are listed in Table 4.3.

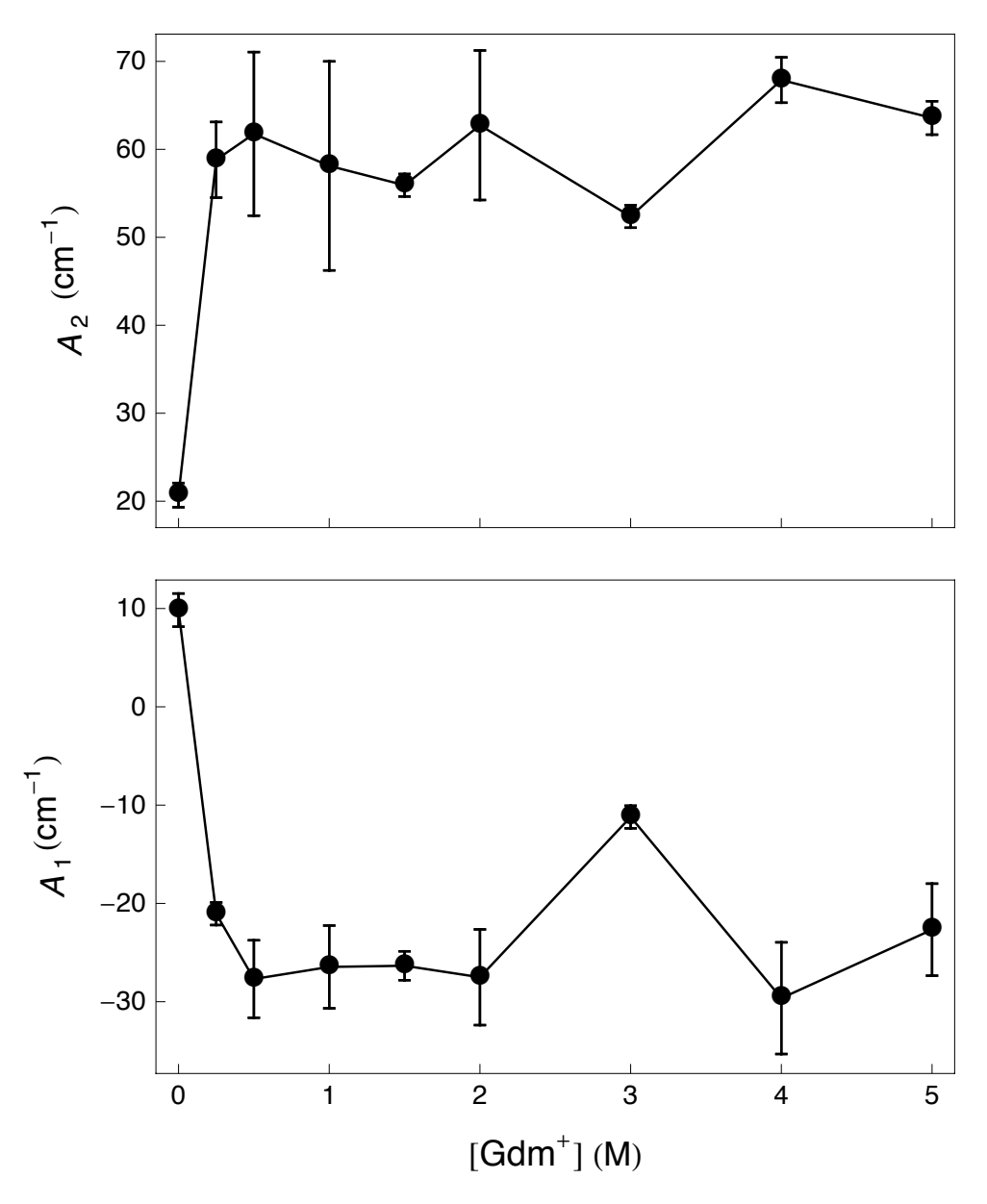


Figure 4.8. Fluorescence Stokes shift amplitudes for ZnCytc at 22°C and pH 7.0 as a function of the Gdm⁺ concentration, as obtained from fits to Equation 4.6. *Top:* Amplitude A_2 , of the slower component, for the final shift to the red. *Bottom:* Amplitude A_1 , of the faster component, for the initial shift to the blue when Gdm⁺ is present. The plotted values are listed in Table 4.3.

are shown in Figures 4.7 and 4.8 for the time constants and the shift amplitudes, respectively. These plots suggest that Gdm⁺ affects the stability and dynamics of the folded protein by saturating sites on the protein surface at low concentration and that at least one folding intermediate is formed well below the overall unfolding transition.

The bottom panel of Figure 4.7 shows that the time constant τ_1 for the fast component of the FSS response from ZnCytc exhibits two main changes as Gdm⁺ is added. As noted above, the red shift observed in water is converted to a blue shift somewhere in the region above 80 mM Gdm⁺, assuming a linear connectivity, and the time constant is abruptly lengthened to 800 ps at 0.25 M. Subsequently, the blue shift speeds up as Gdm⁺ is added except for an inflection in the 1.0 M region. The unfolding transition at 2.0 M Gdm⁺ is accompanied by a decrease in the fast time constant from 700 ps at 1.0 M to 300 ps at 3.0 M. Above the unfolding transition, however, the time constant gradually lengthens. Although the fast component observed in the FSS response from ZnCytc in water is associated with motions of the hydrophobic core⁷⁷ and are accordingly short ranged in mean-squared deviation, ¹⁴⁴ it is evidently rather sensitive to global changes in structure or conformation.

The trend for the amplitude A_1 for the fast component in the FSS response from ZnCytc is shown in the bottom panel of Figure 4.8. The amplitude abruptly increases in magnitude and changes sign as the fast part of the FSS response abruptly shifts from the red to the blue as Gdm^+ is initially added, but above 0.5 M Gdm^+ it remains essentially constant. The unfolding transition at 2 M is followed, however, by a significant jump in A_1 ; the value at 3 M is statistically well resolved from those at 2 M and 4 M, which are indistinguishable. Thus, the trends in A_1 and τ_1 together indicate that the internal structural dynamics in ZnCytc are markedly affected by the presence of Gdm^+ at concentrations that are well below the unfolding transition.

The top panel of Figure 4.7 shows that the time constant for the slow component of the FSS response, τ_2 , exhibits two main changes as Gdm⁺ is added to ZnCytc solutions. At low Gdm^+ concentrations, τ_2 exhibits a biphasic increase that resembles a binding equilibrium that is saturated at 1 M, well before the unfolding transition. The most rapid part of this increase accompanies the initial addition of Gdm⁺ to the solution, and then a second phase of increase occurs over the 0.5-1-M range. The trend in the amplitude for this component is shown in the top panel of Figure 4.8. It also exhibits a response like that of a binding equilibrium, but only a single phase is observed that saturates immediately, at 0.25 M Gdm⁺, and then remains essentially constant as Gdm⁺ is added over the range of the unfolding transition. The saturation of A2 at very low concentration suggests, but does not prove, that Gdm⁺ acts initially either by binding to sites on the solvent-contact layer of the folded protein structure and/or by altering the hydrogen-bonding structure of the hydration layer that surrounds it.⁸⁰ That the amplitudes A_1 and A_2 mirror each other as Gdm^+ is initially added (see Figure 4.7) is a strong indication that the transition to the biphasic character and the dramatic lengthening of the slow part of the FSS response mark a global change in structure and dynamics. This transition occurs more rapidly than the change in bulk viscosity (see Figure 4.9) that accompanies the addition of Gdm⁺ to the solution.

Figure 4.10 shows the dependence of the total amplitude of the FSS response from ZnCytc, $A_1 + A_2$, on the Gdm⁺ concentration. The trend in this plot should be compared to that in Figure 4.2 of fluorescence peak maxima. The latter plot is of the time-integrated fluorescence Stokes shift, whereas the former is obtained from the time-resolved spectral response. The trend for $A_1 + A_2$ clearly projects out three distinct phases of structure and dynamics as Gdm⁺ is added to a ZnCytc solution. The peak in $A_1 + A_2$ at 0.25 M Gdm⁺ apparently marks the initial saturation by Gdm⁺ of the binding sites that induce the transition to a biphasic, blue/red FSS response. The

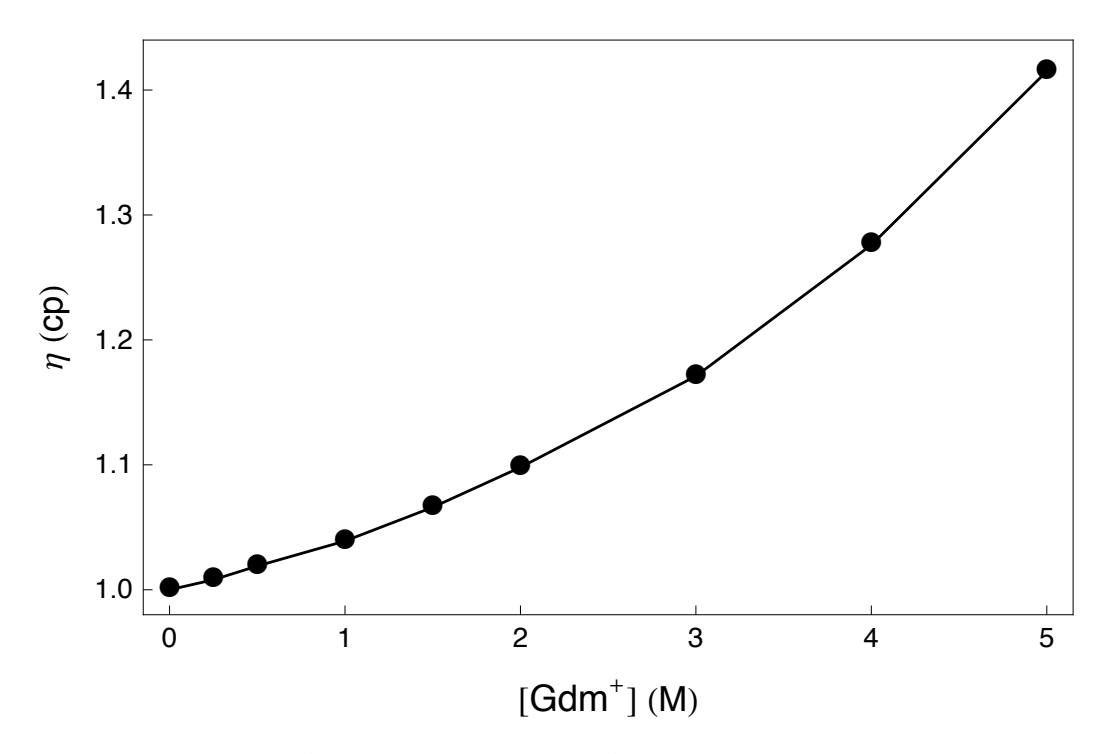


Figure 4.9. Viscosity of aqueous solutions of guanidinium hydrochloride at room temperature as a function of the Gdm⁺ concentration. From ref. 168.

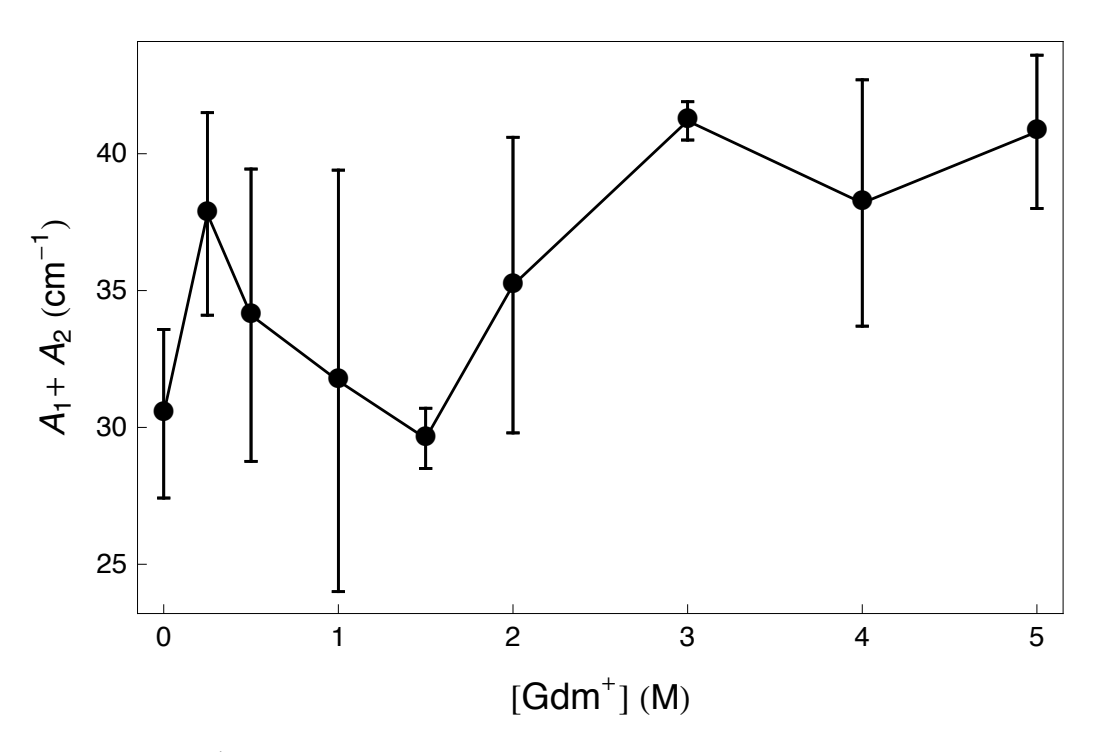


Figure 4.10. Gdm⁺ concentration dependence of total fluorescence Stokes shift amplitude, A_1+A_2 , in ZnCytc at 22°C and pH 7.

decreasing transition in $A_1 + A_2$ that follows over the 0.5-1.5-M Gdm⁺ range marks the formation of an intermediate structure that precedes the overall unfolding transition. Finally, the unfolding transition at 2 M Gdm⁺ is accompanied by an increase in $A_1 + A_2$; this increase matches the shift to the blue observed in Figure 4.2. It is interesting to note that the magnitude of the 95% confidence intervals for $A_1 + A_2$, the total range between the error bars, suggests the presence of an inhomogeneous ensemble especially at the 1-M and 2-M Gdm⁺ concentrations that mark the midpoints of transitions. In contrast, the endpoints of these transitions, at 1.5 M and 3 M, respectively, suggest the presence of relatively homogeneous ensembles because they have especially small 95% confidence intervals. Note that the precision of the measurements at all of the Gdm⁺ concentrations was comparable, given that the total experimental time for counting of fluorescence photons was fixed for each transient, and further that an effort was made to narrow the confidence intervals especially at 1 M Gdm⁺ by performing a large number of replicate experiments. In our hands, then, it appears that the partially unfolded ensembles indicated by the intermediate points in Figure 4.10 are inherently inhomogeneous or that some of the dynamic properties of these ensembles are controlled by external variables that we did not control, despite considerable effort.

4.4 Discussion

The results show that the FSS response function from ZnCytc is especially sensitive to the presence of Gdm⁺ in two concentration regimes: at the lowest concentrations, below 0.5 M, where the overall stability of the folded protein is altered so that the $\pi \rightarrow \pi^*$ transition of the intrinsic Zn^{II} porphyrin becomes a significant local perturbation of the motions of the surrounding protein and solvent, and at an intermediate concentration, 1 M, where a transition-state-like intermediate structure

on the unfolding reaction coordinate is populated. The FA response, obtained using the polarization information in the same data set, is surprisingly insensitive to the low-concentration part of the Gdm⁺ response, but it is especially sensitive to the formation of the intermediate at 1 M Gdm⁺. In the following, we compare the correlation timescales obtained from the FSS response functions with those obtained from the FA response. This comparison makes it clear that the FSS response is more sensitive than the FA response to the overall stability of the folded protein.

In our previous work on the FSS response of fbCytc, 144 we discussed how the correlation timescale returned from the FSS response from an intrinsic fluorescent probe can be taken as a measure of the amplitude of the equilibrium structural fluctuations made by the host protein. The FSS response function arises from the dielectric response of the probe's surroundings, so it is sensitive to motions of charges or dipoles, even at a considerable distance, that modulate the electric field sensed at the probe's location. Assuming that the optical transition of the probe does not impart a significant perturbation on its surroundings so that the linear-response regime is maintained, $^{54-56}$ the fluctuation-dissipation relation allows one to equate the experimentally measured solvent-response function, $S_V(t)$ (Equation 4.5), with the time-correlation function for the fluctuations of the medium,

$$M(t) = \frac{\langle \Delta \omega(0) \Delta \omega(t) \rangle}{\langle (\Delta \omega)^2 \rangle},\tag{4.7}$$

where

$$\Delta\omega(t) = \langle \omega \rangle - \omega(t) \tag{4.8}$$

relates the instantaneous ground-to-excited-state energy gap for the probe from that averaged over time or averaged instantaneously over the ensemble. 54-56

As a protein propagates on the protein-folding energy landscape, its structure fluctuates owing to thermally driven passages over the activation barriers that divide adjacent potential minima. We modeled this process as Brownian diffusion over a one-dimensional effective coordinate.¹⁴⁴ The main result is that there is a linear relationship between the correlation timescale for a fluctuation, τ , as obtained from the FSS response function, and the mean squared displacement, $\langle x^2(\tau_0) \rangle$,

$$\tau = (\langle x^2(\tau_0) \rangle / 2D) \exp(\Delta G^{\ddagger} / RT) \tag{4.9}$$

The correlation time τ is related by an Arrhenius equation to the characteristic timescale, τ_0 , at which the transition-state structure at the top of a barrier of height ΔG^{\ddagger} is accessed owing to diffusion on the structural coordinate x at a given temperature T. The diffusion constant D is inversely proportional to the friction from internal protein motion or from the surrounding solvent, so an increase in friction causes a lengthening of the correlation time. The relation between the correlation time for a particular fluctuation and the amplitude (mean-squared deviation) of the associated motion assumes that the conditions are kept constant. Considering that the barrier heights for motion on the energy landscape are likely to be strongly coupled to the conformational or folding state, it should be clear that Equation 4.9 can be used only qualitatively in interpreting the correlation timescales.

As discussed previously, the FA response from ZnCytc directly detects the subset of fluctuations that impart angular deviations onto the Zn^{II} porphryin from the mean structure. We modeled the FA decays using the wobbling-in-cone (WIC) mechanical model introduced by Kinosita *et al.* to describe the dynamics of a fluorescent probe in lipid membranes. Figure 4.11 shows how the correlation times for internal angular motion, $\tau_{\rm int}$ and the limiting cone angle, θ_c , vary with the Gdm⁺ concentration in ZnCytc solutions. The cone angle plot reports the formation of the intermediate structure at 1 M Gdm⁺ in terms of a transition to a significantly larger range of angular motion for the Zn^{II} porphyrin, such as that permitted by a less condensed fold. The $\tau_{\rm int}$ plot marks the intermediate as having a significantly longer correlation time, 1.35 ns, than either the native state in water or the unfolded state at Gdm⁺ concentrations above 2 M. Applying the relation above (Equation 4.9), the

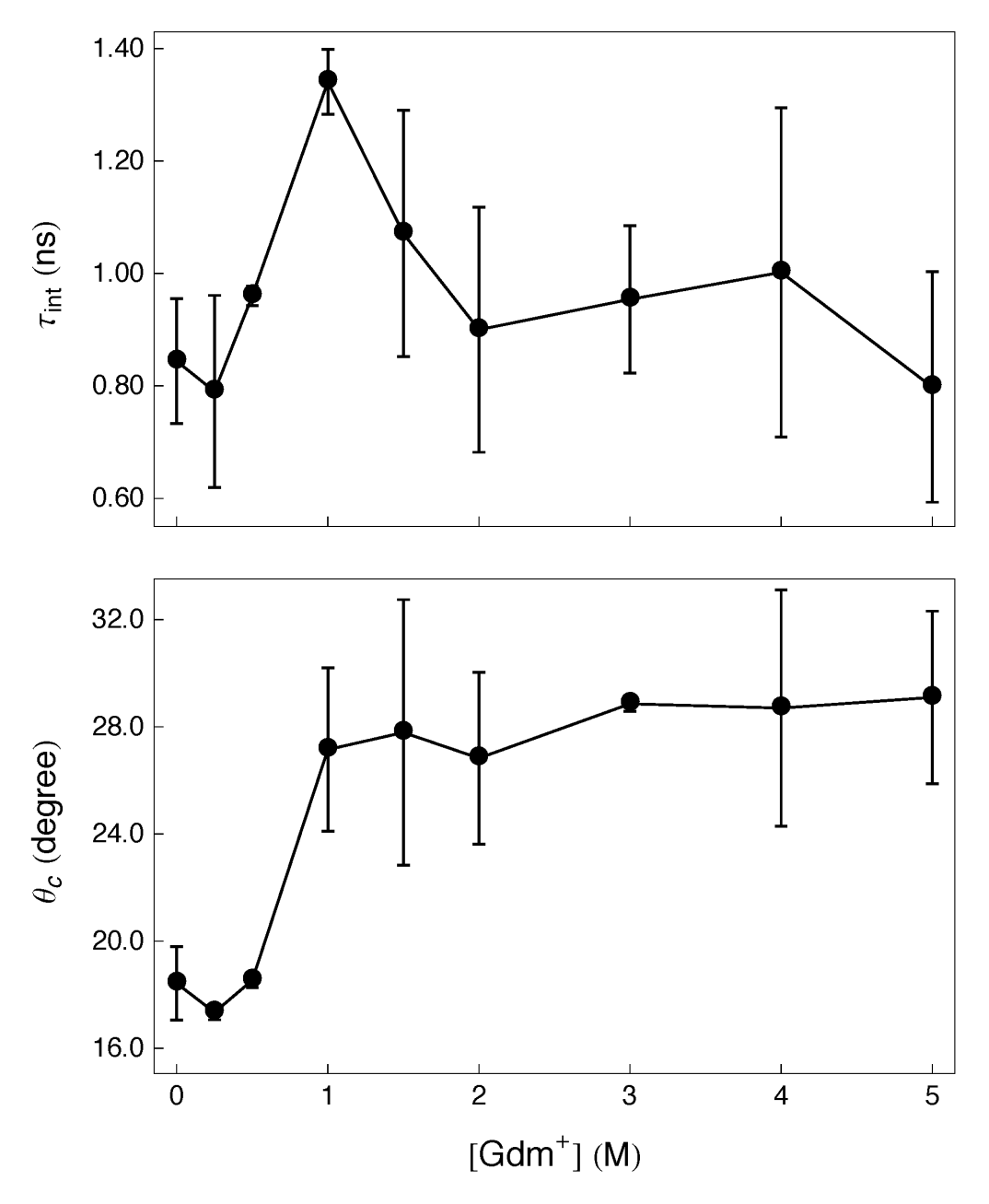


Figure 4.11. Gdm⁺ concentration dependence of $\tau_{\rm int}$, the correlation time for internal motion, and θ_c , the wobbling cone angle, from the picosecond anisotropy decays observed with ZnCytc at 22°C and pH 7.0.

mean-squared deviations of the intermediate are almost twice as large as those in the native state. It is notable that at 1 M Gdm⁺, the τ_{int} correlation time is quite comparable to the shorter of the two correlation time detected in the FSS from fbCytc, where the fluctuations are especially enhanced in amplitude by the protein's assumption of a molten-globule-like, partially unfolded state.¹⁴⁴

In comparison, the faster of the two timescales obtained for ZnCytc in water from the FSS response function, au_1 , is significantly shorter than that obtained from the FA response (see Figure 4.7). As Gdm^+ is introduced, however, the τ_1 timescale rises abruptly and reaches a maximum at 0.25 M at approximately the same timescale, \sim 800 ps, as that in the FA plot. The intermediate at 1 M is not marked by a dominant peak in the correlation time trend like the one observed in the FA response. Further, the unfolding transition at 2 M is associated with a decrease in τ_1 ; at the same time, the $au_{ ext{int}}$ trend from the FA response remains essentially constant. These comparisons show that the FA and FSS responses detect different types of characteristic fluctuations. The FSS response is apparently much more sensitive to the overall fold of the protein than is the FA response. As mentioned in the previous chapter, the angular motion of the Zn^{II} porphryin would be expected to be particularly sensitive to the presence or absence of the axial ligands. The 1-M intermediate may exhibit large angular fluctuations because it is likely to be a four-coordinate structure without native or non-native axial ligands from the surrounding protein. Such an intermediate would be transition-state-like in that an exchange of one axial ligand with another would require a four-coordinate transition state if the Zn^{II} porphryin binds only a single axial ligand along the unfolding pathway.

A comparison of the faster of the two timescales obtained from the FSS response in ZnCytc to the internal timescale from the FA response treats the former as if it is really a correlation timescale rather than a relaxation or reaction timescale. That the shift of the time-resolved fluorescence spectrum for this component is to the blue, rather than the red, is a strong indication that the optical excitation of the Zn^{II} porphryin is a larger perturbation on its protein and solvent surroundings than expected by the assumption of linear response. Still, it is reasonable to consider the timescales of the two components in the FSS response as indicating the range of motion required to relax to the initial structure prior to the excitation. The shorter timescale, τ_1 , would be taken then as a shorter-range motion than that arising from the longer timescale, τ_2 . In water, the τ_1 timescale is insensitive to the presence of glycerol in the external solvent, so it was assigned previously to the hydrophobic core of the folded protein. The glycerol dependence of τ_2 recommended an assignment to the motions of the solvent-contact layer of the protein, which would be expected to exhibit longer-range motions than the core of the protein.⁷⁷ These assignments seem to be applicable even in the presence of Gdm⁺. In particular, the blue shift associated with τ_1 is best explained by the reduced polarizability of the protein/solvent surroundings that would accompany an expansion of the Zn^{II} porphyrin's hydrophobic binding pocket in response to the optical excitation. The photodissociation of the axial ligands from the methionine (M80) and histidine (H18) ligands⁷⁶ probably contributes to this response, but note that the lineshape of the time-resolved fluorescence spectrum in the presence of Gdm⁺ did not suggest that a large change in the porphyrin's structure occurs during the blue shift or during the subsequent red shift.

That the transition from a normal, monotonic FSS response in water to a bidirectional FSS response occurs in ZnCytc at such low Gdm⁺ concentrations, below 0.25 M, suggests that Gdm⁺ alters the dynamics of the protein by acting directly on the hydrogen-bonding structure of the hydration layer.⁸⁰ The exposure of the Zn^{II} porphryin directly to the hydration layer is small¹⁶⁹ and the π -electron density is essentially orthogonal to the exposure, so a direct action of Gdm⁺ on the porphyrin is less likely than a general effect on the protein stability. It would be especially in-

teresting, then, to probe how the structure and dynamics of the hydration layer are altered in the presence of Gdm⁺ by placing a fluorescent probe on the surface of ZnCytc or tethered at a distance away from the surface. Femtosecond spectroscopy studies of this type are already underway in the Beck laboratory to explore how the inertial and diffusive motions of water molecules in the hydration layer are correlated with motions in the folded protein structure.

CHAPTER 5

Conclusion

5.1 Overview

This dissertation represents an attempt to obtain a better structural picture for the motions that contribute to the FSS response detected by an intrinsic fluorescent probe in the interior of a small globular protein. The first part of this project was a comparison of the FSS response in fbCytc with ZnCytc, which had been previously characterized in the Beck laboratory by Sanela Lampa-Pastirk. One of the main findings is that the FSS response function for fbCytc in water is much slower than that obtained for ZnCytc in water. The FSS response for fbCytc in water is biexponential, and the two time constants, 1.4 ns and 9.1 ns, are about 10 times longer than those obtained for ZnCytc in water, where the slower time constant is 1.5 ns. The two correlation times describe the motions of the hydrophobic core and the solvent-contact layer sensed by the intrinsic porphyrin probe. The correlation times were further lengthened in the presence of 50% (v/v) glycerol. These results were best interpreted using a Brownian diffusion model with thermally activated barrier crossings on the folding energy landscape. The longer of the two correlation times in fbCytc arise from increased mean-squared displacements of the core and surface fluctuations than in

ZnCytc. This finding supports the conclusion that fbCytc has some characteristics of a molten globule with a dynamic, partially unfolded structure.

The fbCytc studies provide information about the nature of the fluctuations but lack a detailed structural picture. The next phase of the project, a study of the motions associated with the unfolding of ZnCytc, was aimed at probing the dynamical and structural origin of the equilibrium fluctuations. The motions associated with the unfolding reaction coordinate were probed using the FA response in the presence of the denaturant Gdm⁺. The results show that the unfolding transition is preceded by the formation of a structural intermediate. The intermediate exhibits longer correlation times and an enhanced angular fluctuation of the porphyrin probe compared to the native and unfolded states. The intermediate exhibits some of the properties that would be expected for a transition-state structure along the folding/unfolding reaction coordinate. The correlation time for internal angular motions for the intermediate obtained from the FA response is similar to that observed for the FSS response of fbCytc. This comparison suggests that the intermediate has lost both of its axial ligands for the Zn^{II} porphyrin.

Even at the lowest concentrations studied, the presence of Gdm⁺ strongly impacts the dynamics of ZnCytc by affecting the interaction of the protein with the hydration layer. The FSS response obtained as ZnCytc is titrated with Gdm⁺ shows that the presence of Gdm⁺ destabilizes the native fold of the protein; the optical excitation of the Zn^{II} porphyrin chromophore perturbs the motions of the surrounding protein and solvent molecules such that they depart from the linear-response regime. The deviation from the linear response regime is evident from the unusual bidirectional FSS response observed in presence of Gdm⁺. The action of Gdm⁺ appears to saturate well prior to the formation of the intermediate at 1.0 M. These results imply that the origin of the dynamical changes reported in the FSS response lies in the structural changes in the hydration layer surrounding the folded protein.

5.2 Comparison to Other Studies

The established theory that proteins exhibit a hierarchy of conformational substates was originally suggested by Frauenfelder et al.⁴⁷ based on their studies on reaction rate of photochemical dissociation of carbon monoxide from myoglobin. These studies suggested that the protein motions involve sampling a rough energy land-scape with a hierarchy of barrier heights. Our results add the importance concept that the fluctuations observed in proteins are the result of barrier-crossing events on the folding energy landscape. As discussed in Chapter 2, the characteristic time scales of fluctuations observed in the fluorescence experiments probably arise from distinct structural motions near the native minimum of the energy landscape. Association of either of these motions along generalized structural coordinates with unfolding/refolding reaction requires additional information.

Englander and coworkers, ^{161,162,170–172} and Rousseau and coworkers ^{164,166} have extensively studied the intermediates populated along the folding/unfolding reaction coordinate of FeCytc. Englander and coworkers ¹⁷⁰ and Myer ¹⁶⁷ showed that the unfolding/refolding of FeCytc involves formation of rate-limiting intermediates. Myer's work suggests that the nature of the unfolding process that is induced by Gdm⁺ and urea arise from different kinds of interactions between the denaturant and the protein. Maity et al. ¹⁷² used equilibrium and kinetic hydrogen exchange experiments to show that sequential assembly of small folding units called foldons leads to progress along the folding reaction coordinate of FeCytc. These studies also suggest that a discrete folding intermediate accumulates prior to the global unfolding.

The results discussed in this dissertation strongly support the conclusion that discrete intermediates are populated prior to the unfolding of ZnCytc. The observed correlation time scales and cone angles suggest the formation of at least one intermediate at 1.0 M Gdm⁺ well prior to the global unfolding transition. The ligand-exchange

studies by Yeh and coworkers 173 suggest that the folding and refolding reactions in cytochrome c involve more than one pathway and populate discrete intermediates that have molten globule-like properties. The FSS response obtained for ZnCytc as a function of Gdm^+ in our experiments are consistent with this conclusion. The measured correlation times in the FA and FSS response functions suggest a change in the compactness of the protein that is accompanied by axial ligand exchanges prior to the global unfolding transition. The 1.0~M intermediate is more likely to be four-coordinate transition state while the folded protein in the ground state is believed to be six-coordinate structure.

5.3 Conclusions and Next Steps

This work shows that the FSS and FA response functions can be used to detect the formation of intermediates during unfolding/refolding reactions in small proteins. The FSS response function from ZnCytc shows it is more sensitive to the dynamical effects of Gdm⁺ at the low concentration of 0.5 M and 1.0 M region. In the 0.5 M Gdm⁺ regime the overall stability of the folded protein is altered so that the local perturbation from the $\pi \rightarrow \pi^*$ transition of the intrinsic Zn^{II} porphyrin leads transiently to the formation of nonequilibrium structures. At 1.0 M Gdm⁺, a transition-state-like intermediate structure is formed which exhibits longer range motions. The FSS response is sensitive to motions of the protein over long distances owing to the low dielectric constant of the protein's interior, whereas the FA response is more sensitive to local motions of the protein around the Zn^{II} porphyrin. The transition of the FSS response function from a normal monotonic response to the unusual biphasic response observed even at very low Gdm⁺ concentrations suggests that Gdm⁺ may act on the hydrogen-bonding structure of the hydration layer, which in turn alters the dynamics of the protein.

An obvious next step to take in this line of research would be to consider how the structure and dynamics of the hydration layer is altered by the addition of Gdm⁺. We suggest that one might consider this question using ultrafast spectroscopy using a fluorescent probe tethered to the surface of the protein, which would be able to sense changes in the inertial and diffusive motions of the water molecules in the hydration layer. Work of this type is currently ongoing in the Beck laboratory.

BIBLIOGRAPHY

BIBLIOGRAPHY

- (1) van Grondelle, R.; Dekker, J. P.; Gillbro, T.; Sundström, V. Energy transfer and trapping in photosynthesis. *Biochim. Biophys. Acta* **1994**, *1187*, 1-65. DOI: 10.1016/0005-2728(94)90166-X.
- (2) Deisenhofer, J.; Michel, H. The photosynthetic reaction center from the purple bacterium *Rhodopseudomonas viridis*. *Science* **1989**, *245*, 1463–1473. DOI: 10.1126/science.245.4925.1463.
- (3) Deisenhofer, J.; Epp, O.; Miki, K.; Huber, R.; Michel, H. X-ray structure analysis of a membrane protein complex: electron density map at 3 Å resolution and a model of the chromophores of the photosynthetic reaction center from *Rhodopseudomonas viridis*. *J. Mol. Biol.* **1984**, *180*, 385–398. DOI: 10.1016/S0022-2836(84)80011-X.
- (4) Deisenhofer, J.; Epp, O.; Miki, K.; Huber, R.; Michel, H. Structure of the protein subunits in the photosynthetic reaction center of *Rhodopseudomonas viridis* at 3.1 Å resolution. *Nature* **1985**, *318*, 618–624. DOI: 10.1038/318618a0.
- (5) Krauss, N.; Hinrichs, W.; Witt, I.; Fromme, P.; Pritzkow, W.; Dauter, Z.; Betzel, C.; Wilson, K. S.; Witt, H. T.; Saenger, W. Three-dimensional structure of system I of photosynthesis at 6 A resolution. *Nature* **1993**, *361*, 326–331.
- (6) Schiffer, M.; Norris, J. R. Structure and Function of the Photosynthetic Reaction Center of extitRhodobacter sphaeroides. In *The Photosynthetic Reaction Center*; Deisenhofer, J., Norris, J. R., Eds.; Academic Press, Inc.: San Diego, 1993; Vol. I, pp 1-12.
- (7) Kleinfled, D.; Okamura, M. Y.; Feher, G. Electron-transfer kinetics in photosynthetic reaction centers cooled to cryogenic temperatures on the charge-separated state: Evidence for light-induced structural changes. *Biochemistry* **1984**, *23*, .
- (8) Feher, G.; Allen, J. P.; Okamura, M. Y.; Rees, D. C. Structure and function of bacterial photosynthetic reaction centers. *Nature* **1989**, *339*, 111–116.
- (9) Parson, W. W. The bacterial reaction center. In *Photosynthesis (New Comprehensive Biochemistry, Volume 15)*; Amesz, J., Ed.; Elsevier: New York, 1987; pp 43–61.

- (10) Allen, J. P.; Feher, G.; Yeates, T. O.; Rees, D. C.; Deisenhofer, J.; Michel, H.; Huber, R. Structural homology of reaction centers from Rhodopseudomonas sphaeroides and Rhodopseudomonas viridis as determined by x-ray diffraction. *Proc. Natl. Acad. Sci. U.S.A.* **1986**, *83*, 8589–8593.
- (11) Allen, J. P.; Feher, G.; Yeates, T. O.; Komiya, H.; Rees, D. C. Structure of the reaction center from Rhodobacter sphaeroides R-26: the cofactors. *Proc. Natl. Acad. Sci. U.S.A.* **1987**, *84*, 5730–5734.
- (12) Rhee, K. -; Morris, E. P.; Barber, J.; Kuhlbrandt, W. Three-dimensional structure of the plant photosystem II reaction centre at 8 A resolution. *Nature* **1998**, *396*, 283–286.
- (13) Zouni, A.; Witt, H. -Y.; Kern, J.; Fromme, P.; Kraus, N.; Saenger, W.; Orth, P. Crystal structure of photosystem II from Synechococcus elongatus at 3.8 A resolution. *Nature* **2001**, *409*, 739–742.
- (14) Jordan, P.; Fromme, P.; Witt, H. T.; Klukas, O.; Saenger, W.; Kraus, N. Three-dimensional structure of cyanobacterial photosystem I at 2.5 A resolution. *Nature* **2001**, *411*, 909–917.
- (15) Wasielewski, M. R. Photoinduced electron transfer in supramolecular systems for artificial photosynthesis. *Chem. Rev.* **1992**, *92*, 436–461.
- (16) Wasielewski, M. R.; Wiederrecht, G. P.; Svec, W. A.; Niemczyk, M. P. Chlorin-based supramolecular assemblies for artificial photosynthesis. *Solar Energy Mat. Solar Cells* **1995**, *38*, 127–134.
- (17) Redmore, N. P.; Rubtsov, I. V.; Therien, M. J. Synthesis, electronic structure, and electron transfer dynamics of (aryl)ethynyl-bridged donor-acceptor systems. *J. Am. Chem. Soc.* **2003**, *125*, 8769–8778.
- (18) Splan, K. E.; Stern, C. L.; Hupp, J. T. Two coordinatively linked supramolecular assemblies constructed from highly electron deficient porphyrins. *Inorg. Chim. Acta* **2004**, *357*, 4005–4014.
- (19) Gust, D.; Moore, T. A.; Makings, L. R.; Liddell, P. A.; Nemeth, G. A.; Moore, A. L. Photodriven electron transfer in triad molecules: a two-step charge recombination reaction. *J. Am. Chem. Soc.* **1986**, *108*, 8028–8031.
- (20) Gust, D.; Moore, T. A.; Moore, A. L.; Lee, S. -; Bittersmann, E.; Luttrull, D. K.; Rehms, A. A.; DeGaraziano, J. M.; Ma, X. C.; Gao, F.; Belford, R. E.; Trier, T. T. Efficient multistep photoinitiated electron transfer in a molecular pentad. *Science* **1990**, *248*, 199–201.

- (21) Gust, D.; Moore, T. A. Mimicking photosynthesis. Science 1989, 244, 35-41.
- (22) Prathapan, S.; Johnson, T. E.; Lindsey, J. S. Building-block synthesis of porphyrin light-harvesting arrays. *J. Am. Chem. Soc.* **1993**, *115*, 7519–7520.
- (23) Hsiao, J. -; Krueger, B. P.; Wagner, R. W.; Johnson, T. E.; Delayen, J. K.; Mauzerall, D. C.; Fleming, G. R.; Lindsey, J. S.; Bocian, D. F.; Donohoe, R. J. Soluble Synthetic Multiporphyrin Arrays. 2. Photodynamics of energy-transfer processes. *J. Am. Chem. Soc.* **1996**, *118*, 11181–11193.
- (24) Loewe, R. S.; Lammi, R. K.; Diers, J. R.; Kirmaier, C.; Bocian, D. F.; Holten, D.; Lindsey, J. S. Design and synthesis of light-harvesting rods for intrinsic rectification of the migration of excited-state energy and ground-state holes. *J. Mater. Chem.* **2002**, *12*, 1530–1552.
- (25) Stenberg-Yfrach, G.; Rigaud, J.-L.; Durantini, E. N.; Moore, A. L.; Gust, D.; Moore, T. A. Light-driven production of ATP catalysed by F0F1-ATP synthase in an artificial photosynthetic membrane. *Nature* **1998**, *392*, 479–482.
- (26) Gust, D.; Moore, T. A.; Moore, A. L. Mimicking photosynthetic solar energy transduction. *Acc. Chem. Res.* **2001**, *34*, 40–48.
- (27) Rischel, C.; Spiedel, D.; Ridge, J. P.; Jones, M. R.; Breton, J.; Lambry, J. C.; Martin, J. -L.; Vos, M. H. Low frequency vibrational modes in proteins: changes induced by point-mutations in the protein-cofactor matrix of bacterial reaction centers. *Proc. Natl. Acad. Sci. U.S.A.* **1998**, *95*, 12306–12311. DOI: 10.1073/pnas.95.21.12306.
- (28) Bixon, M.; Jortner, J. Activationless and pseudoactivationless primary electron transfer in photosynthetic bacterial reaction centers. *Chem. Phys. Lett.* **1989**, *159*, 17–20. DOI: 10.1016/S0009-2614(89)87445-7.
- (29) Jortner, J. Dynamics of the primary events in bacterial photosynthesis. *J. Am. Chem. Soc.* **1980**, *102*, 6676–6686.
- (30) Zuber, H. Structure and function of light-harvesting complexes and their polypeptides. *Photochemistry and Photobiology* **1985**, *42*, 821–844.
- (31) Pearlstein, R. M. Exciton migration and trapping in photosynthesis. *Photochemistry and Photobiology* **1982**, *35*, 835–844.
- (32) Zuber, H.; Brunisholz, R.; Sidler, W. Structure and function of light-harvesting pigment-protein complexes. In *Photosynthesis*; Amesz, J., Neuberger, A., Deenen, L. L. M. V., Eds.; Elsevier: New York, 1987; Vol. 15, pp 233–272.

- (33) Knox, R. S. Photosynthetic efficiency and exciton transfer and trapping. In *Primary Processes of Photosynthesis*; Barber, J., Ed.; Elsevier: Amsterdam, 1977; pp 55–97.
- (34) Zuber, H. Structural features of photsynthetic light-harvesting systems. In *The Photosynthetic Reaction Center*; Deisenhofer, J., Ed.; Academic Press, Inc.: San Diego, 1993; Vol. I, pp 43-100.
- (35) McDermott, G.; Prince, S. M.; Freer, A. A.; Hawthornthwaite-Lawless, A. M.; Papiz, M. Z.; Cogdell, R. J.; Isaccs, N. W. Crystal structure of an integral membrane light-harvesting complex from photosynthetic bacteria. *Nature* **1995**, *374*, 517–521.
- (36) van Grondelle, R. Excitation energy transfer, trapping and annihilation in photosynthetic systems. *Biochim. Biophys. Acta* **1985**, *811*, 147–195.
- (37) Sundstrom, V.; van Grondelle, R. Energy transfer in photosynthetic light-harvesting antennas. *J. Opt. Soc. Am. B* **1990**, *7*, 1595–1603.
- (38) Du, M.; Xie, X.; Jia, Y.; Mets, L.; Fleming, G. F. Direct observation of ultrafast energy transfer in PSI core antenna. *Chemical Physics Letters* **1993**, *201*, 535–542.
- (39) Du, M.; Xie, X.; Mets, L.; Fleming, G. R. Direct observation of ultrafast energy-transfer processes in light harvesting complex II. *J. Phys. Chem.* **1994**, *98*, 4736–4741.
- (40) Bittner, T.; Irrgang, K.; Renger, G.; Wasielewski, M. R. Ultrafast excitation energy transfer and exciton-exciton annihilation processes in isolated light harvesting complexes of photosystem II (LHC II) from spinach. *J. Phys. Chem.* **1994**, *98*, 11821–11826.
- (41) Bradforth, S. E.; Jimenez, R.; van Mourik, F.; van Grondelle, R.; Fleming, G. R. Excitation transfer in the core light-harvesting complex (LH-1) of Rhodobacter sphaeroides: an ultrafast fluorescence depolarization and annihilation study. *J. Phys. Chem.* **1995**, *99*, 16179–16191.
- (42) Jimenez, R.; Dikshit, S. N.; Bradforth, S. E.; Fleming, G. R. Electronic excitation transfer in the LH2 complex of Rhodobacter sphaeroides. *J. Phys. Chem.* **1996**, *100*, 6825–6834.
- (43) Scholes, G. D.; Harcourt, R. D.; Fleming, G. R. Electronic interactions in photosynthetic light-harvesting complexes: The role of carotenoids. *J. Phys. Chem. B* **1997**, *101*, 7302–7312.

- (44) Kreuger, B. P.; Scholes, G. D.; Jimenez, R.; Fleming, G. R. Electronic excitation transfer from carotenoid to bacteriochlorophyll in the purple bacterium Rhodopseudomonas acidophila. *J. Phys. Chem. B* **1998**, *102*, 2284–2292.
- (45) Edington, M. D.; Riter, R. E.; Beck, W. F. Interexciton-state relaxation and exciton localization in allophycocyanin trimers. *J. Phys. Chem.* **1996**, *100*, 14206–14217. DOI: 10.1021/jp960454b.
- (46) Homoelle, B. J.; Edington, M. D.; Diffey, W. M.; Beck, W. F. Stimulated photon-echo and transient-grating studies of protein-matrix solvation dynamics and interexciton-state radiationless decay in α phycocyanin and allophycocyanin. *J. Phys. Chem. B* **1998**, *102*, 3044–3052. DOI: 10.1021/jp972782x.
- (47) Frauenfelder, H.; Sligar, S. G.; Wolynes, P. G. The energy landscapes and motions of proteins. *Science* **1991**, *254*, 1598–1603. DOI: 10.1126/science.1749933.
- (48) Frauenfelder, H.; Wolynes, P. G. Biomolecules: Where the physics of complexity and simplicity meet. *Physics Today* **1994**, *47*, 58–64.
- (49) Khajehpour, M.; Troxler, T.; Vanderkooi, J. M. Effect of protein dynamics upon reactions that occur in the heme pocket of horseradish peroxidase. *Biochemistry* **2003**, *42*, 2672–2679.
- (50) Genberg, L.; Richard, L.; McLendon, G.; Miller, R. J. D. Direct observation of global protein motion in hemoglobin and myoglobin on picosecond time scales. *Science* **1991**, *251*, 1051–1056.
- (51) Stratt, R. M.; Maroncelli, M. Nonreactive dynamics in solution: the emerging molecular view of solvation dynamics and vibrational relaxation. *J. Phys. Chem.* **1996**, *100*, 12981-12996. DOI: 10.1021/jp9608483.
- (52) Fleming, G. R. *Chemical Applications of Ultrafast Spectroscopy*; Oxford University Press: New York, 1986.
- (53) Barbara, P. F.; Jarzeba, W. Ultrafast photochemical intramolecular charge transfer and excited state solvation. *Adv. Photochem.* **1990**, *15*, 1-68.
- (54) Maroncelli, M. The dynamics of solvation in polar solvents. *J. Mol. Liq.* **1993**, *57*, 1–37. DOI: 10.1016/0167-7322(93)80045-W.
- (55) Joo, T.; Jia, Y.; Yu, J. -Y.; Lang, M. J.; Fleming, G. R. Third-order nonlinear time domain probes of solvation dynamics. *J. Chem. Phys.* **1996**, *104*, 6089–6108. DOI: 10.1063/1.471276.

- (56) Cho, M.; Yu, J.-Y.; Joo, T.; Nagasawa, Y.; Passino, S. A.; Fleming, G. R. The integrated photon echo and solvation dynamics. *J. Phys. Chem.* **1996**, *100*, 11944–11953. DOI: 10.1021/jp9601983.
- (57) Barthel, E. R.; Martini, I. B.; Schwartz, B. J. How does the solvent control electron transfer? Experimental and theoretical studies of the simplest charge transfer reaction. *J. Phys. Chem. B* **2001**, *105*, 12230–12241. DOI: 10.1021/jp011150e.
- (58) Nilsson, L.; Halle, B. Molecular origin of time-dependent fluorescence shifts in proteins. *Proc. Natl. Acad. Sci. U.S.A.* **2005**, *102*, 13867-13872. DOI: 10.1073/pnas.0504181102.
- (59) Stratt, R. M.; Cho, M. The short-time dynamics of solvation. *J. Chem. Phys.* **1994**, *100*, 6700–6708. DOI: 10.1063/1.467030.
- (60) Stratt, R. M. The instantaneous normal modes of liquids. *Acc. Chem. Res.* **1995**, *28*, 201–207. DOI: 10.1021/ar00053a001.
- (61) Jimenez, R.; Fleming, G. R.; Kumar, P. V.; Maroncelli, M. Femtosecond solvation dynamics of water. *Nature* **1994**, *369*, 471–473. DOI: 10.1038/369471a0.
- (62) Maroncelli, M.; MacInnis, J.; Fleming, G. R. Polar solvent dynamics and electron-transfer reactions. *Science* **1989**, *243*, 1674–1681. DOI: 10.1126/science.243.4899.1674.
- (63) Rosenthal, S. J.; Xie, X.; Du, M.; Fleming, G. R. Femtosecond solvation dynamics in acetonitrile: observation of the inertial contribution to the solvent response. *J. Chem. Phys.* **1991**, *95*, 4715–4718. DOI: 10.1063/1.461742.
- (64) Vanderkooi, J. M. The protein state of matter. *Biochim. Biophys. Acta* **1998**, *1386*, 241–253.
- (65) Bashkin, J. S.; McLendon, G.; Mukamel, S.; Marohn, J. Influence of medium dynamics on solvation and charge separation reactions: comparison of a simple alcohol and a protein "solvent." *J. Phys. Chem.* **1990**, *94*, 4757-4761. DOI: 10.1021/j100375a001.
- (66) Pierce, D. W.; Boxer, S. G. Dielectric relaxation in a protein matrix. *J. Phys. Chem.* **1992**, *96*, 5560–5566. DOI: 10.1021/j100192a069.
- (67) Bushnell, G. W.; Louie, G. V.; Brayer, G. D. High-resolution three-dimensional structure of horse heart cytochrome *c. J. Mol. Biol.* **1990**, *214*, 585–595. DOI: 10.1016/0022-2836(90)90200-6.

- (68) Moog, R. S.; Kuki, A.; Fayer, M. D.; Boxer, S. G. Excitation transport and trapping in a synthetic chlorophyllide substituted hemoglobin: orientation of the chlorophyll S₁ transition dipole. *Biochemistry* **1984**, *23*, 1564–1571.
- (69) Vanderkooi, J. M.; Landesberg, R.; Hayden, G. W.; Owen, C. S. Metal-free and metal-substituted cytochromes *c*. Use in characterization of the cytochrome *c* binding site. *Eur. J. Biochem.* **1977**, *81*, 339–347. DOI: 10.1111/j.1432-1033.1977.tb11957.x.
- (70) Vanderkooi, J. M.; Glatz, P.; Casadei, J.; Woodrow, G. V. I. Cytochrome c interaction with yeast cytochrome b_2 . *Eur. J. Biochem.* **1980**, *110*, 189–196.
- (71) Dixit, B. P. S. N.; Waring, A. J.; Wells, K. O. I.; Wong, P. S.; Woodrow, G. V. I.; Vanderkooi, J. M. Rotational motion of cytochrome c derivatives bound to membrane measured by fluorescence and phosphorescence anisotropy. *Eur. J. Biochem.* **1982**, *126*, 1–9.
- (72) Anni, H.; Vanderkooi, J. M.; Mayne, L. Structure of zinc-substituted cytochrome c: nuclear magnetic resonance and optical spectroscopic studies. *Biochemistry* **1995**, *34*, 5744–5753. DOI: 10.1021/bi00017a006.
- (73) Qian, C.; Yao, Y.; Tong, Y.; Wang, J.; Tang, W. Structural analysis of zinc-substituted cytochrome c. *J. Biol. Inorg. Chem.* **2003**, *8*, 394–400. DOI: 10.1007/s00775-002-0428-1.
- (74) Teczan, F. A.; Crane, B. R.; Winkler, J. R.; Gray, H. B. Electron tunneling in protein crystals. *Proc. Natl. Acad. Sci. U.S.A.* **2001**, *98*, 5002–5006. DOI: 10.1073/pnas.081072898.
- (75) Lampa-Pastirk, S. *Dynamic solvation of Zn(II)-cytochrome c in the native fold and the unfolding transition state.* Ph. D. Thesis, Michigan State University: 2005.
- (76) Lampa-Pastirk, S.; Lafuente, R. C.; Beck, W. F. Excited-state axial-ligand photodissociation and nonpolar protein-matrix reorganization in Zn(II)-substituted cytochrome *c. J. Phys. Chem. B* **2004**, *108*, 12602–12607. DOI: 10.1021/jp049587k.
- (77) Lampa-Pastirk, S.; Beck, W. F. Polar solvation dynamics in Zn(II)-substituted cytochrome *c:* diffusive sampling of the energy landscape in the hydrophobic core and solvent-contact layer. *J. Phys. Chem. B* **2004**, *108*, 16288–16294. DOI: 10.1021/jp0488113.

- (78) Lampa-Pastirk, S.; Beck, W. F. Intramolecular vibrational preparation of the unfolding transition state of Zn^{II} substituted cytochrome *c. J. Phys. Chem. B* **2006**, *110*, 22971–22974. DOI: 10.1021/jp0654359.
- (79) Barns, K. J.; Lampa-Pastirk, S.; Dillman, K. L.; Beck, W. F. Intramolecular vibrational excitation of unfolding reactions in Zn^{II}-substituted and metal-free cytochromes *c*: activation enthalpies from integrated fluorescence Stokes shift and lineshape excitation profiles. *J. Phys. Chem. B* **2008**, *112*, 15108–15115. DOI: 10.1021/jp803756n.
- (80) Sharp, K. A.; Vanderkooi, J. M. Water in the half shell: structure of water, focusing on angular structure and solvation. *Acc. Chem. Res.* **2010**, *43*, 231–239. DOI: 10.1021/ar900154j.
- (81) Bryngelson, J. D.; Wolynes, P. G. Spin glasses and the statistical mechanics of protein folding. *Proc. Natl. Acad. Sci. U.S.A.* **1987**, *84*, 7524–7528. DOI: 10.1073/pnas.84.21.7524.
- (82) Leopold, P. E.; Montal, M.; Onuchic, J. N. Protein folding funnels: a kinetic approach to the sequence-structure relationship. *Proc. Natl. Acad. Sci. U.S.A.* **1992**, *89*, 8721–8725. DOI: 10.1073/pnas.89.18.8721.
- (83) Ansari, A.; Berendzen, J.; Bowne, S. F.; Frauenfelder, H.; Iben, I. E.; Sauke, T. B.; Shyamsunder, E.; Young, R. D. Protein states and proteinquakes. *Proc. Natl. Acad. Sci. U.S.A.* **1985**, *82*, 5000–5004. DOI: 10.1073/pnas.82.15.5000.
- (84) Zwanzig, R. Diffusion in a rough potential. *Proc. Natl. Acad. Sci. U.S.A.* **1988**, 85, 2029–2030. DOI: 10.1073/pnas.85.7.2029.
- (85) Socci, N. D.; Onuchic, J. N.; Wolynes, P. G. Diffusive dynamics of the reaction coordinate for protein folding funnels. *J. Chem. Phys.* **1996**, *104*, 5860–5868. DOI: 10.1063/1.471317.
- (86) Goto, Y.; Calciano, L. J.; Fink, A. L. Acid-induced folding of proteins. *Proc. Natl. Acad. Sci. U.S.A.* **1990**, *87*, 573–577. DOI: 10.1073/pnas.87.2.573.
- (87) Tremain, S. M.; Kostić, N. M. Molten-globule and other conformational forms of zinc cytochrome *c*. Effect of partial and complete unfolding of the protein on its electron-transfer reactivity. *Inorg. Chem.* **2002**, *41*, 3291–3301. DOI: 10.1021/ic010893b.
- (88) Lesch, H.; Stadlbauer, H.; Friedrich, J.; Vanderkooi, J. M. Stability diagram and unfolding of a modified cytochrome *c*: what happens in the transformation regime? *Biophys. J.* **2002**, *82*, 1644–1653. DOI: 10.1016/S0006-3495(02)75515-X.

- (89) Fleming, G. R.; Cho, M. Chromophore-solvent dynamics. *Annu. Rev. Phys. Chem.* **1996**, *47*, 109–134. DOI: 10.1146/annurev.physchem.47.1.109.
- (90) García, A. E.; Hummer, G. Conformational dynamics of cytochrome *c*: correlation to hydrogen exchange. *Proteins: Struct. Funct. Genet.* **1999**, *36*, 175–191. DOI: 10.1002/(SICI)1097-0134.
- (91) Vanderkooi, J. M.; Adar, F.; Ericińska, M. Metallocytochromes *c:* characterization of electronic absorption and emission spectra of Sn⁴⁺ and Zn²⁺ cytochromes *c. Eur. J. Biochem.* **1976**, *64*, 381–387. DOI: 10.1111/j.1432-1033.1976.tb10312.x.
- (92) Elias, H.; Chou, M. H.; Winkler, J. R. Electron-transfer kinetics of Zn-substituted cytochrome c and its Ru(NH₃)₅(Histidine-33) derivative. *J. Am. Chem. Soc.* **1988**, *110*, 429–434. DOI: 10.1021/ja00210a019.
- (93) Ye, S.; Shen, C.; Cotton, T. M.; Kostić, N. M. Characterization of zinc-substituted cytochrome *c* by circular dichroism and resonance Raman spectroscopic methods. *J. Inorg. Biochem.* **1997**, *65*, 219–226. DOI: 10.1016/S0162-0134(97)00001-9.
- (94) Lakowicz, J. R. *Principles of Fluorescence Spectroscopy*, Second ed.; Kluwer Academic/Plenum Publishers: New York, 1999.
- (95) Velapoldi, R. A.; Mielenz, K. D. *A Fluorescence Standard Reference Material: Quinine Sulfate Dihydrate*; National Bureau of Standards (U. S.): 1980.
- (96) Cantor, C. R.; Schimmel, P. R. *Biophysical Chemistry. Part II: Techniques for the Study of Biological Structure and Function*; W. H. Freeman and Company: San Francisco, 1980.
- (97) Siano, D. B.; Metzler, D. E. Band shapes of the electronic spectra of complex molecules. *J. Chem. Phys.* **1969**, *51*, 1856–1861. DOI: 10.1063/1.1672270.
- (98) McHale, J. L. *Molecular Spectroscopy*; Prentice Hall: Upper Saddle River, New Jersey, 1999.
- (99) Kennis, J. T. M.; Larsen, D. S.; Ohta, K.; Facciotti, M. T.; Glaeser, R. M.; Fleming, G. R. Ultrafast protein dynamics of bacteriorhodopsin probed by photon echo and transient absorption spectroscopy. *J. Phys. Chem. B.* **2002**, *106*, 6067–6080. DOI: 10.1021/jp014681b.
- (100) Jordanides, X. J.; Lang, M. J.; Song, X.; Fleming, G. R. Solvation dynamics in protein environments studied by photon echo spectroscopy. *J. Phys. Chem. B* **1999**, *103*, 7995–8005. DOI: 10.1021/jp9910993.

- (101) Simon, J. D.; Thompson, P. A. Spectroscopy and rotational diffusion of oxazine 725 in alcohols: a test of dielectric friction theories. *J. Chem. Phys.* **1990**, *92*, 2891–2896.
- (102) Maroncelli, M.; Fleming, G. R. Picosecond solvation dynamics of coumarin 153: the importance of molecular aspects of solvation. *J. Chem. Phys.* **1987**, *86*, 6221–6239. DOI: 10.1063/1.452460.
- (103) Åkerlöf, G. Dielectric constants of some organic solvent-water mixtures at various tempeatures. *J. Am. Chem. Soc.* **1932**, *54*, 4125-4139. DOI: 10.1021/ja01350a001.
- (104) Scholte, T. G. Relation between the refractive index increment and the density increment of binary mixtures: application to the determination of partial specific volumes of polymers in solution. *J. Polymer Sci. A-2* **1972**, *10*, 519–526. DOI: 10.1002/pol.1972.160100308.
- (105) Toptygin, D.; Woolf, T. B.; Brand, L. Picosecond protein dynamics: the origin of the time-dependent spectral shift in the fluorescence of the single Trp in the protein GB1. *J. Phys. Chem. B* **2010**, *114*, 11323–11337. DOI: 10.1021/jp104425t.
- (106) Toptygin, D.; Savtchenko, R. S.; Meadow, N. D.; Brand, L. Homogeneous spectrally- and time-resolved fluorescence emission from single-tryptophan mutants of IIA^{Glc} protein. *J. Phys. Chem. B* **2001**, *105*, 2043–2055. DOI: 10.1021/jp003405e.
- (107) Vincent, M.; Gilles, A.-M.; de la Sierra, I. M. L.; Briozzo, P.; Bârzu, O.; Gallay, J. Nanosecond fluorescence dynamic Stokes shift of tryptophan in a protein matrix. *J. Phys. Chem. B* **2000**, *104*, 11286–11295. DOI: 10.1021/jp000638x.
- (108) Cho, B. M.; Carlsson, F.; Jimenez, R. Photon echo spectroscopy of porphyrins and heme proteins: effects of quasidegenerate electronic structure on the peak shift decay. *J. Chem. Phys.* **2006**, *124*, 144905. DOI: 10.1063/1.2186318.
- (109) Carter, E. A.; Hynes, J. T. Solvation dynamics for an ion pair in a polar solvent: time-dependent fluorescence and photochemical charge transfer. *J. Chem. Phys.* **1991**, *94*, 5961–5979. DOI: 10.1063/1.460431.
- (110) Maroncelli, M.; Kumar, P. V.; Papazyan, A.; Horng, M. L.; Rosenthal, S. J.; Fleming, G. R. Studies of the inertial component of polar solvation dynamics. In *Ultrafast Reaction Dynamics and Solvent Effects*; Guaduel, Y., Rossky, P. J., Eds.; AIP Press: Woodbury, NY, 1994; pp 310–333.

- (111) Ladanyi, B. M.; Stratt, R. M. Short-time dynamics of solvation: linear solvation theory for polar solvents. *J. Phys. Chem.* **1995**, *99*, 2502–2511. DOI: 10.1021/j100009a007.
- (112) Jimenez, R.; Romesberg, F. E. Excited state dynamics and heterogeneity of folded and unfolded states of cytochrome *c. J. Phys. Chem. B* **2002**, *106*, 9172–9180. DOI: 10.1021/jp0209648.
- (113) Riter, R. E.; Edington, M. D.; Beck, W. F. Inertial protein-matrix solvation of a light-harvesting chromophore. In *Ultrafast Phenomena X*; Barbara, P., Knox, W., Zinth, W., Fujimoto, J., Eds.; Springer-Verlag: Berlin, 1996; pp 324–325.
- (114) Riter, R. E.; Edington, M. D.; Beck, W. F. Protein-matrix solvation dynamics in the α subunit of *C*-phycocyanin. *J. Phys. Chem.* **1996**, *100*, 14198–14205. DOI: 10.1021/jp960453j.
- (115) Pal, S. K.; Peon, J.; Bagchi, B.; Zewail, A. H. Biological water: femtosecond dynamics of macromolecular hydration. *J. Phys. Chem. B* **2002**, *106*, 12376–12395. DOI: 10.1021/jp0213506.
- (116) Pal, S. K.; Peon, J.; Zewail, A. H. Biological water at the protein surface: dynamical solvation probed directly with femtosecond resolution. *Proc. Natl. Acad. Sci. U.S.A.* **2002**, *99*, 1763–1768. DOI: 10.1073/pnas.042697899.
- (117) Qiu, W.; Zhang, L.; Okobia, O.; Yang, Y.; Wang, L.; Zhong, D.; Zewail, A. H. Ultrafast solvation dynamics of human serum albumin: correlations with conformational transitions and site-selected recognition. *J. Phys. Chem. B* **2006**, *110*, 10540–10549. DOI: 10.1021/jp055989w.
- (118) Abbyad, P.; Shi, X.; Childs, W.; McAnaney, T. B.; Cohen, B. E.; Boxer, S. G. Measurement of solvation responses at multiple sites in a globular protein. *J. Phys. Chem. B* **2007**, *111*, 8269–8276. DOI: 10.1021/jp0709104.
- (119) Abbyad, P.; Childs, W.; Shi, X.; Boxer, S. G. Dynamic Stokes shift in green fluorescent protein variants. *Proc. Natl. Acad. Sci. U.S.A.* **2007**, *104*, 20189–20194. DOI: 10.1073/pnas.0706185104.
- (120) Halder, M.; Mukherjee, P.; Bose, S.; Hargrove, M. S.; Song, X.; Petrich, J. W. Solvation dynamics in protein environments: comparison of fluorescence upconversion measurements of coumarin 153 in monomeric hemeproteins with molecular dynamics simulations. *J. Chem. Phys.* **2007**, *127*, 055101-1-6.
- (121) Lang, M. J.; Jordanides, X. J.; Song, X.; Fleming, G. R. Aqueous solvation dynamics studied by photon echo spectroscopy. *J. Chem. Phys.* **1999**, *110*, 5884–5892. DOI: 10.1063/1.478488.

- (122) Simonson, T. Gaussian fluctuations and linear response in an electron transfer protein. *Proc. Natl. Acad. Sci. U.S.A.* **2002**, *99*, 6544–6549. DOI: 10.1073/pnas.082657099.
- (123) Bagchi, B. Water solvation dynamics in the bulk and in the hydration layer of proteins and self-assemblies. *Annu. Rep. Prog. Chem. Sect. C* **2003**, *99*, 127–175. DOI: 10.1039/b208505b.
- (124) Bagchi, B. Water dynamics in the hydration layer around proteins and micelles. *Chem. Rev.* **2003**, *105*, 3197–3219. DOI: 10.1021/cr020661+.
- (125) Li, T.; Kao, Y.-T.; Zhong, D.; Singer, S. J. Hydration dynamics and time scales of coupled water-protein fluctuations. *J. Am. Chem. Soc.* **2007**, *129*, 3376–3382. DOI: 10.1021/ja0685957.
- (126) Toptygin, D.; Gronenborn, A. M.; Brand, L. Nanosecond relaxation dynamics of protein GB1 identified by the time-dependent red shift in the fluorescence of tryptophan and 5-fluorotryptophan. *J. Phys. Chem. B.* **2006**, *110*, 26292–26302. DOI: 10.1021/jp064528n.
- (127) Cohen, B. E.; McAnaney, T. B.; Park, E. S.; Jan, Y. N.; Boxer, S. G.; Jan, L. Y. Probing protein electrostatics with a synthetic fluorescent amino acid. *Science* **2002**, *296*, 1700–1703. DOI: 10.1126/science.1069346.
- (128) Golosov, A. A.; Karplus, M. Probing polar solvation dynamics in proteins: A molecular dynamics simulation analysis. *J. Phys. Chem. B* **2007**, *111*, 1482–1490. DOI: 10.1021/jp065493u.
- (129) Beece, D.; Eisenstein, L.; Frauenfelder, H.; Good, D.; Marden, M. C.; Reinisch, L.; Reynolds, A. H.; Sorensen, L. B.; Yue, K. T. Solvent viscosity and protein dynamics. *Biochemistry* **1980**, *19*, 5147–5157. DOI: 10.1021/bi00564a001.
- (130) Ansari, A.; Jones, C. M.; Henry, E. R.; Hofrichter, J.; Eaton, W. A. The role of solvent viscosity in the dynamics of protein conformational changes. *Science* **1992**, *256*, 1796–1798. DOI: 10.1126/science.1615323.
- (131) Sahu, K.; Mondal, S. K.; Ghosh, S.; Roy, D.; Bhattacharyya, K. Temperature dependence of solvation dynamics and anisotropy decay in a protein: ANS in bovine serum albumin. *J. Chem. Phys.* **2006**, *124*, 124909. DOI: 10.1063/1.2178782.
- (132) Kumar, P. V.; Maroncelli, M. Polar solvation dynamics of polyatomic solutes: simulation studies in acetonitrile and methanol. *J. Chem. Phys.* **1995**, *103*, 3038–3060. DOI: 10.1063/1.470493.

- (133) Berry, R. S.; Rice, S. A.; Ross, J. *Physical Chemistry*; John Wiley & Sons: New York, 1980.
- (134) McQuarrie, D. A. *Statistical Mechanics*; HarperCollins Publishers: New York, 1976.
- (135) Frauenfelder, H.; Chen, G.; Berendzen, J.; Fenimore, P. W.; Jansson, H.; McMahon, B. H.; Stroe, I. R.; Swenson, J.; Young, R. D. A unified model of protein dynamics. *Proc. Natl. Acad. Sci. U.S.A.* **2009**, *106*, 5129–5134. DOI: 10.1073/pnas.0900336106.
- (136) Chen, H.; Rhoades, E.; Butler, J. S.; Loh, S. N.; Webb, W. W. Dynamics of equilibrium structural fluctuations of apomyoglobin measured by fluorescence correlation spectroscopy. *Proc. Natl. Acad. Sci. U.S.A.* **2007**, *104*, 10459–10464. DOI: 10.1073/pnas.0704073104.
- (137) Bai, Y.; Sosnice, T. R.; Mayne, L.; Englander, S. W. Protein folding intermediates: native-state hydrogen exchange. *Science* **1995**, *269*, 192–197. DOI: 10.1126/science.7618079.
- (138) Carlini, P.; Bizzarri, A. R.; Cannistraro, S. Temporal fluctuations in the potential energy of proteins: $1/f^{\alpha}$ noise and diffusion. *Physica D* **2002**, *165*, 242–250. DOI: 10.1016/S0167-2789(02)00426-8.
- (139) Nettels, D.; Gopich, I. V.; Hoffmann, A.; Schuler, B. Ultrafast dynamics of protein collapse from single-molecule photon statistics. *Proc. Natl. Acad. Sci. U.S.A.* **2007**, *104*, 2655–2660. DOI: 10.1073/pnas.0611093104.
- (140) Cellmer, T.; Henry, E. R.; Hofrichter, J.; Eaton, W. A. Measuring internal friction of an ultrafast-folding protein. *Proc. Natl. Acad. Sci. U.S.A.* **2008**, *105*, 18320–18325. DOI: 10.1073/pnas.0806154105.
- (141) Best, R. B.; Hummer, G. Coordinate-dependent diffusion in protein folding. *Proc. Natl. Acad. Sci. U.S.A.* **2010**, *107*, 1088–1093. DOI: 10.1073/pnas.0910390107.
- (142) Henzler-Wildman, K. A.; Lei, M.; Thai, V.; Kerns, S. J.; Karplus, M.; Kern, D. A hierarchy of timescales in protein dynamics is linked to enzyme catalysis. *Nature* **2007**, *450*, 913–916. DOI: 10.1038/nature06407.
- (143) Creighton, T. E. *Proteins*; W. H. Freeman: New York, 1992.
- (144) Tripathy, J.; Beck, W. F. Nanosecond-regime correlation timescales for equilibrium protein structural fluctuations of metal-free cytochrome *c* from picosecond time-resolved fluorescence spectroscopy and the dynamic Stokes shift. *J. Phys. Chem. B* **2010**, *114*, 15958–15968. DOI: 10.1021/jp1044964.

- (145) Bhuyan, A. K. Off-pathway status for the alkali molten globule of horse ferricy-tochrome *c. Biochemistry* **2010**, *49*, 7764–7773. DOI: 10.1021/bi100880d.
- (146) Hamada, D.; Kuroda, Y.; Kataoka, M.; Aimoto, S.; Yoshimura, T.; Goto, Y. Role of heme axial ligands in the conformational stability of the native and molten globule states of horse cytochrome *c. J. Mol. Biol.* **1996**, *256*, 172–186. DOI: 10.1006/jmbi.1996.0075.
- (147) Yu, H. -Z.; Baskin, J. S.; Zewail, A. H. Ultrafast dynamics of porphyrins in the condensed phase: II. Zinc tetraphenylporphyrin. *J. Phys. Chem. A.* **2002**, *106*, 9845–9854. DOI: 10.1021/jp0203999.
- (148) Enescu, M.; Steenkeste, K.; Tfibel, F.; Fontaine-Aupart, M. -P. Femtosecond relaxation processes from upper excited states of tetrakis(N-methyl-4-pyridyl)porphyrins studied by transient absorption spectroscopy. *Phys. Chem. Chem. Phys.* **2002**, *4*, 6092–6099. DOI: 10.1039/b207421d.
- (149) Kawato, S.; Kinosita, K. Time-dependent absorption anisotropy and rotational diffusion of proteins in membranes. *Biophys. J.* **1981**, *36*, 277–296. DOI: 10.1016/S0006-3495(81)84728-5.
- (150) Kinosita, K.; Ikegami, A.; Kawato, S. On the wobbling-in-cone analysis of fluorescence anisotropy decay. *Biophys. J.* **1982**, *37*, 461–464. DOI: 10.1016/S0006-3495(82)84692-4.
- (151) Guest, C. R.; Hochstrasser, R. A.; Sowers, L. C.; Millar, D. P. Dynamics of mismatched base pairs in DNA. *Biochemistry* **1991**, *30*, 3271–3279. DOI: 10.1021/bi00227a015.
- (152) Hess, S. T.; Sheets, E. D.; Wagenknecht-Wiesner, A.; Heikal, A. A. Quantitative analysis of the fluorescence properties of intrinsically fluorescent proteins in living cells. *Biophys. J.* **2003**, *85*, 2566–2580. DOI: 10.1016/S0006-3495(03)74679-7.
- (153) Otosu, T.; Nishimoto, E.; Yamashita, S. Multiple conformational state of human serum albumin around single tryptophan residue at various pH revealed by time-resolved fluorescence spectroscopy. *J. Biochem.* **2010**, *147*, 191–200. DOI: 10.1093/jb/mvp175.
- (154) Lipari, G.; Szabo, A. Effect of librational motion on fluorescence depolarization and nuclear magnetic resonance relaxation in macromolecules and membranes. *Biophys. J.* **1980**, *30*, 489–506. DOI: 10.1016/S0006-3495(80)85109-5.
- (155) Lakowicz, J. R. *Principles of Fluorescence Spectroscopy*; Plenum Press: New York, 1983.

- (156) Vos, K.; Laane, C.; Weijers, S. R.; Van Hoek, A.; Veeger, C.; Visser, A. J. Timeresolved fluorescence and circular dichroism of porphyrin cytochrome *c* and Zn-porphyrin cytochrome *c* incorporated in reversed micelles. *Eur J Biochem* **1987**, *169*, 259–268. DOI: 10.1111/j.1432-1033.1987.tb13606.x.
- (157) Tanford, C.; Nozaki, Y.; Reynolds, J. A.; Makino, S. Molecular characterization of proteins in detergent solutions. *Biochemistry* **1974**, *13*, 2369–2376. DOI: bi00708a021.
- (158) Pal, S.; Maiti, P. K.; Bagchi, B.; Hynes, J. T. Multiple time scales in solvation dynamics of DNA in aqueous solution: the role of water, counterions, and cross-correlations. *J. Phys. Chem. B* **2006**, *110*, 26396–26402. DOI: 10.1021/jp065690t.
- (159) Morar, A. S.; Olteanu, A.; Young, G. B.; Pielak, G. J. Solvent-induced collapse of α -synuclein and acid-denatured cytochrome *c. Protein Sci.* **2001**, *10*, 2195–2199. DOI: 10.1110/ps.24301.
- (160) Tao, T. Time-dependent fluorescence depolarization and Brownian rotational diffusion coefficients of macromolecules. *Biopolymers* **1969**, *8*, 609–632. DOI: 10.1002/bip.1969.360080505.
- (161) Roder, H.; Elöve, G. A.; Englander, S. W. Structural characterization of folding intermediates in cytochrome c by H-exchange labelling and proton NMR. *Nature* **1988**, *335*, 700–704. DOI: 10.1038/335700a0.
- (162) Englander, S. W.; Sosnick, T. R.; Mayne, L. C.; Shtilerman, M.; Qi, P. X.; Bai, Y. W. Fast and slow folding in cytochrome c. *Acc. Chem. Res.* **1998**, *31*, 737–744. DOI: 10.1021/ar970085h.
- (163) Shastry, M. C. R.; Roder, H. Evidence for barrier-limited protein folding kinetics on the microsecond time scale. *Nat. Struct. Biol.* **1998**, *5*, 385–392. DOI: 10.1038/nsb0598-385.
- (164) Yeh, S. -R.; Takahashi, S.; Fan, B.; Rousseau, D. L. Ligand exchange during cytochrome *c* folding. *Nature Struct. Biol.* **1997**, *4*, 51–56. DOI: 10.1038/nsb0197-51.
- (165) Yeh, S. -R.; Rousseau, D. L. Folding intermediates in cytochrome *c. Nat. Struct. Biol.* **1998**, *5*, 222–228. DOI: 10.1038/nsb0398-222.
- (166) Yeh, S.; Han, S.; Rousseau, D. L. Cytochrome *c* folding and unfolding: a biphasic model. *Acc. Chem. Res.* **1998**, *31*, 727–736. DOI: 10.1021/ar970084p.

- (167) Myer, Y. P. Ferricytochrome *c*: refolding and the methionine 80-sulfur-iron linkage. *J. Biol. Chem.* **1984**, *259*, 6127–6133.
- (168) Kawahara, K.; Tanford, C. Viscosity and density of aqueous solutions of urea and guanidine hydrochloride. *J. Biol. Chem.* **1966**, *241*, 3228–3232.
- (169) Brayer, G. D.; Murphy, M. E. Structural studies of eukaryotic cytochromes *c*. In *Cytochrome* c: *A Multidisciplinary Approach*; Scott, R. A., Mauk, A. G., Eds.; University Science Books: Sausalito, California, 1996; pp 103–166.
- (170) Mayne, L.; Englander, S. W. Two-state *vs.* multistate protein unfolding studied by optical melting and hydrogen exchange. *Protein. Sci.* **2000**, *9*, 1873–1877.
- (171) Maity, H.; Maity, M.; Englander, S. W. How cytochrome *c* folds, and why: submolecular foldon units and their stepwise sequential stabilization. *J. Mol. Biol.* **2004**, *343*, 223–233. DOI: 10.1016/j.jmb.2004.08.005.
- (172) Maity, H.; Maity, M.; Krishna, M. M. G.; Mayne, L.; Englander, S. W. Protein folding: the stepwise assembly of foldon units. *Proc. Natl. Acad. Sci. U.S.A.* **2005**, *102*, 4741–4746. DOI: 10.1073/pnas.0501043102.
- (173) Yeh, S. -R.; Rousseau, D. L. Ligand exchange during unfolding of cytochrome *c. J. Biol. Chem.* **1999**, *274*, 17853–17859. DOI: 10.1074/jbc.274.25.17853.